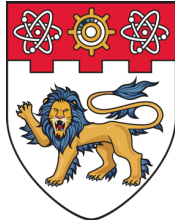

Holistic optimization framework for the operation of urban energy systems



**NANYANG
TECHNOLOGICAL
UNIVERSITY
SINGAPORE**

Chiam Zhonglin

School of Computer Science & Engineering

A thesis submitted to the Nanyang Technological University
in partial fulfillment of the requirements for the degree of
Doctor of Philosophy

2019

Statement of Originality

I hereby certify that the work embodied in this thesis is the result of original research, is free of plagiarised materials, and has not been submitted for a higher degree to any other University or Institution.

10/12/2019

.....

Date

Chiam Zhonglin



.....

Supervisor Declaration Statement

I have reviewed the content and presentation style of this thesis and declare it is free of plagiarism and of sufficient grammatical clarity to be examined. To the best of my knowledge, the research and writing are those of the candidate except as acknowledged in the Author Attribution Statement. I confirm that the investigations were conducted in accord with the ethics policies and integrity standards of Nanyang Technological University and that the research data are presented honestly and without prejudice.

10/12/2019

.....

Date



.....

Assoc. Prof. Arvind EASWARAN

Authorship Attribution Statement

This thesis contains material from three papers published in the following peer-reviewed journals / from papers accepted at conferences in which I am listed as an author.

Chapter 4 is submitted as Z. Chiam, I. Papas, A. Easwaran, C. Alonso and B. Estibals. Holistic optimization of the operation of a ground-source heat pump system: A case study on the ADREAM building in Toulouse, France. *Energy and Buildings*, currently under review.

The contributions of the co-authors are as follows:

- I. Papas assisted with the modeling, processing of data and manuscript drafts.
- Assoc. Prof. A. Easwaran provided the initial project direction, feedback on methodology and edited the manuscript drafts.
- Assoc. Prof. C. Alonso facilitated the initialization of the project.
- Assoc. Prof. B. Estibals assisted with the interpretation of the raw data.
- I chose the models, decided on the optimization strategy, generated the results and wrote the manuscript.

Chapter 5 is published as Z. Chiam, A. Easwaran, D. Mouquet, S. Fazlollahi and J. M. Villás. A hierarchical framework for holistic optimization of the operations of district cooling systems. *Applied Energy*, 239, 23-40 (2019).

The contributions of the co-authors are as follows:

- Assoc. Prof. A. Easwaran provided the initial project direction, feedback on methodology and edited the manuscript drafts.
- Dr. D. Mouquet provided input on the models and interpretation of the results.
- Dr. S. Fazlollahi provided feedback on the use of optimization methodologies.
- J. M. Villás assisted with the interpretation of the raw data.
- I chose the models, decided on the optimization strategy, generated the results and wrote the manuscript.

Chapter 7 is submitted as Z. Chiam, A. Easwaran, D. Mouquet, and M. Gupta. Holistic, real-time optimization of the operations of district cooling systems via deep reinforcement learning and mixed integer linear programming. *Proceedings of the 11th International Conference on Applied Energy*, 2019-8-12/2019-8-15, Västerås, Sweden.

The contributions of the co-authors are as follows:

- Assoc. Prof. A. Easwaran provided the initial project direction, feedback on methodology and edited the manuscript drafts.
- Dr. D. Mouquet provided input on the models and interpretation of the results.
- M. Gupta assisted with the implementation of the algorithms.
- I chose the models, decided on the optimization strategy, generated the results and wrote the manuscript.

10/12/2019



.....

Date

.....

Chiam Zhonglin

Acknowledgements

First and foremost, I would like to express my utmost gratitude to my advisor Arvind Easwaran for his unwavering support throughout the course of these four years. His methodical approach to problem-solving elucidated the art of conducting independent research to me. The discussions we had were always insightful and highly enjoyable. This extends beyond academics - well into general topics, especially during our travels. I am extremely thankful to him for empowering me with space and freedom to develop intellectually. It has simply been an honor and a pleasure to work with him. Words alone do no justice.

Besides, I would also like to thank my co-supervisor Claude Guet for his guidance, facilitating this Ph.D. programme and inviting me to participate in summer schools. Not only have these events been enriching, in addition, collaborations of high significance to this thesis also have been forged.

In addition to my thesis supervisors, I would also like to thank my thesis advisory committee members for the valuable suggestions and encouragement that I received.

I would like to thank Veolia City Modeling Center (VECMC) for the financial support, in particular, Samira Fazlollahi, David Mouquet, Nicolas Marèchal-Abram, and Jiayi Ng, for the invaluable feedback, facilitating the acquisition of case studies and hospitality during my countless travels. I will always be indebted to Samira for giving me the chance to pursue my doctorate.

Special thanks to Ilias and Corinne for the fruitful collaboration. The advice and validation of the models were integral to the improvement of the optimization methodology.

It has been a great pleasure to spend four years at Nanyang Technological University. I take this opportunity to thank all members of the Cyber-Physical Systems

research group, for which I have thoroughly enjoyed the banter and learn a lot from - Saravanan, Siram, Ankita, Jean, Zahra, Daniel, and Vijay. Also, a huge thank you to all my school mates - Andhita, Tanjung, Siew Wei, Kaushik, Weiliang and Adrian, for the unforgettable badminton games and company.

Last but not least, I would like to express my heartfelt gratitude to my parents, brother and my girlfriend, Xiaojun for their unconditional love and support especially during the most trying periods of this endeavor. They are my motivation to persevere and persist against the odds.

“In the end, its all a question of balance.”

—Rohinton, Mistry

To my dear family

Abstract

The push for greater sustainability in urban energy use has led to increasingly complex systems - favoring greater extents of centralization and integration. Centralization of energy systems offers unrivaled levels of energy efficiencies and cost-effectiveness, a consequence of economies of scale. Shared infrastructures from centralized systems, further act as an enabler for facilitating the integration of alternative energy sources. These sources include renewable energy and the harvest of waste energy.

The incongruity between the design and operating conditions of these complex energy systems will always persist; it is inevitable to make assumptions given data limitations. When these conditions differ too vastly, the expected gains could easily be negated. Measures to improve the operation of urban energy systems could be explored through mathematical optimization on the appropriate models. The fundamental difference between operations, as opposed to design optimization problems, lies in the necessity for real-time performance, hence computationally efficient techniques must be sought for this undertaking.

Components of urban energy systems are often operated at predefined setpoints or independently optimized - a repercussion of complexity. Localized control strategies inhibit the ability to adapt well under less-than-ideal scenarios, through the disregard of cascading effects on the system. Formulation of optimization problems that concurrently express these systems in its tuneable variables and captures the tight-coupling between the numerous components, i.e., holistically, usually results in a mixed integer non-linear program which is large and difficult to solve, prohibiting its potential use for real-time operational applications. To address this issue, abstraction techniques of judiciously selected models enabled the accompanying optimization problem to be formulated as a mixed-integer linear program. However, this technique has limited applications as it is highly reliant on case-study specific information.

For generic purposes, a hierarchical optimization framework for the operation of urban energy systems is introduced in the current work. In this framework, model abstraction techniques are first applied so that the resultant problem could be solved using a combination of a genetic algorithm and a mixed-integer linear program solver. The metaheuristic is introduced to handle important decision variables that cannot be linearized. Using the mixed-integer linear program in tandem with the genetic algorithm effectively alleviates the computational effort, by reducing the search space of the latter. Since the reliance on the metaheuristic is reduced, the likelihood of achieving global optimality is increased.

The existence of energy storage systems, sanctions for energy to be stored in more favorable periods to be available later, thus enhancing cost-effectiveness and/or energy efficiency. Multi-period considerations demand optimization across several periods, burgeoning the size of the problem. Thus, the sliding-window technique is used in tandem with the hierarchical framework. This technique permits the trade-off between solution accuracy and problem size, hence resolution time and solvability. When the case-specific, size of the window (number of periods) is suitably chosen, the sacrifice in accuracy becomes justifiable, for the above-mentioned reasons.

Genetic algorithms are population-based metaheuristics and can require a considerable amount of iterations to converge. This issue is further exacerbated in the framework where a mixed-integer linear program has to be solved in each iteration. For online applications, the genetic algorithm was substituted with a reinforcement learner. Implementation of the reinforcement learner allows part of the optimization load (learning) to be shifted offline, hugely speeding up the resolution time, when deployed online. Once trained, the framework only requires a single iteration to generate close-to-optimal solutions.

Finally, the three versions of the optimization framework were applied to case studies for illustration purposes. These case studies were based on an existing district cooling system and ground-coupled heat pump system serving a building. Results generated suggest substantial energy savings of up to 31% for the district cooling system, when the operations were optimized for a given cooling demand. As for the ground-coupled heat pump system, potential cost and energy savings of up to 12.7% and 35% respectively could be achieved.

Contents

Acknowledgements	ix
Abstract	xiii
List of Figures	xxi
List of Tables	xxv
Symbols and Acronyms	xxvii
1 Introduction	1
1.1 Context	1
1.2 Urban energy systems	3
1.2.1 Centralization of energy systems	3
1.2.2 Integrated energy systems	4
1.3 Motivation and problem statements	6
1.4 Contributions and thesis organization	9
2 Literature review	13
2.1 Overview	13
2.2 Evolution of urban energy systems	13
2.2.1 History of urban energy systems	14
2.2.2 Current state of urban energy systems	14
2.2.2.1 Integration with sustainable sources	15
2.2.2.2 Process integration	16
2.2.2.3 Role of storage systems	16
2.2.2.4 Losses in large-scale energy systems	17
2.2.2.5 Future trends	17
2.3 Optimization of urban energy systems	18
2.3.1 Design optimization	18
2.3.1.1 Mono-objective optimization	19
2.3.1.2 Multi-objective optimization	20
2.3.2 Operation optimization	20
2.3.2.1 Mono-objective optimization	21

2.4	Review summary	22
3	Model selection and abstraction	25
3.1	Overview	25
3.2	Component-level models from the literature	25
3.2.0.1	Heat pumps / chillers	26
3.2.0.2	Cooling towers	27
3.2.0.3	Pump and network	27
3.2.0.4	Heat exchangers	28
3.2.0.5	Building integrated photovoltaics	28
3.2.0.6	Electricity storage systems	29
3.2.0.7	Thermal energy storage	29
3.3	Model selection and abstraction	29
3.3.1	Electric heat pumps	30
3.3.1.1	Description	30
3.3.1.2	Selected model	30
3.3.1.3	Model abstraction	32
3.3.1.4	Error analysis	35
3.3.2	Cooling tower	37
3.3.2.1	Description	37
3.3.2.2	Selected model	37
3.3.2.3	Model abstraction	39
3.3.2.4	Error analysis	41
3.3.3	Pump and network	42
3.3.3.1	Description	42
3.3.3.2	Selected models	43
3.3.3.3	Model abstraction	47
3.3.3.4	Parallel-pumps network configuration	49
3.3.3.5	Single-pump-parallel network configuration	50
3.3.3.6	Error analysis	53
3.3.4	Water-to-air heat exchanger	55
3.3.4.1	Description	55
3.3.4.2	Selected model	56
3.3.4.3	Model abstraction	56
3.3.4.4	Error analysis	57
3.3.5	Other models	58
3.3.5.1	Building integrated photovoltaics	59
3.3.5.2	Electricity storage system	60
3.3.5.3	Ground heat exchangers	61
3.3.5.4	Thermal energy storage	63
3.3.6	Summary	66
4	Holistic optimization using mixed integer linear programming	67

4.1	Overview	67
4.2	Introduction	68
4.2.1	Ground-coupled heat pump (GCHP) system	69
4.2.2	Objectives	70
4.2.3	Literature review	71
4.3	Description of the chosen case study	72
4.3.1	Description of the chosen case-study scenarios	73
4.3.2	Management of input data	75
4.3.3	Model selection and abstraction	76
4.4	Problem formulation	76
4.4.1	Parameters and variables	77
4.4.2	Mathematical formulation	77
4.4.3	Modeling error and base case definition	80
4.5	Results and discussion	80
4.5.1	Case-study scenario 1: Energy optimization of the hydronic network	81
4.5.2	Case-study scenario 2: Operation cost optimization.	82
4.5.3	Case-study scenario 3: Energy optimization including WAHX.	83
4.5.4	Case-study scenario 4: Operation cost optimization including WAHX.	85
4.6	Conclusion	89
5	Hierarchical framework for holistic optimization using genetic algorithm and mixed integer linear program	93
5.1	Overview	93
5.2	Introduction	94
5.2.1	District cooling system	95
5.2.2	Literature review	95
5.2.3	Objectives	97
5.3	Optimization framework	98
5.3.1	Pre-optimization	98
5.3.2	Master level	100
5.3.2.1	Current implementation	102
5.3.3	Model abstraction	104
5.3.3.1	Unit definition	104
5.3.3.2	Layer definition	105
5.3.3.3	Constraint definition	106
5.3.4	Slave level	107
5.3.5	Post processing	107
5.3.6	Summary	108
5.4	Problem formulation	109
5.4.1	Model selection and abstraction	110
5.4.2	Implementation of optimization framework	111

5.4.2.1	Mathematical formulation	112
5.4.2.2	Modeling error	115
5.4.2.3	Definition of base-cases and algorithm parameters .	116
5.5	Results and discussion	117
5.5.1	Comparison of approaches: GA-only and the optimization framework	117
5.5.2	Case study results	119
5.6	Conclusion	125
6	Multi-period, multi-objective, holistic optimization, using the sliding-window approach	129
6.1	Overview	129
6.2	Introduction	130
6.2.1	Sliding-window technique	131
6.2.2	Literature review	131
6.2.3	Objectives	133
6.3	Problem formulation	133
6.3.1	Case study description	133
6.3.2	Sliding-window augmented hierarchical framework	134
6.3.3	Mathematical formulation	135
6.4	Results and discussion	139
6.4.1	Effect of TES on chiller operation	140
6.4.2	Effect of sliding-window size	141
6.5	Conclusion	142
7	Towards real-time holistic optimization using reinforcement learning and mixed integer linear programming	145
7.1	Overview	145
7.2	Introduction	146
7.2.1	Reinforcement learning	146
7.2.2	Literature review	147
7.3	Problem formulation	148
7.3.1	Case study description	148
7.3.2	GA-MILP approach	148
7.3.2.1	Mathematical formulation	149
7.3.3	RL-MILP approach	151
7.4	Results and discussion	153
7.4.1	Solution quality	155
7.4.2	Resolution speed	156
7.5	Conclusion	156
8	Conclusion	159
8.1	Overview	159
8.1.1	Conclusions	159

8.1.2 Suggestions for future work	162
A Hydraulically decoupled cooling system	165
B Low ΔT syndrome	167
List of Author's Publications	169
Bibliography	171

List of Figures

1.1	Reproduced graph of cumulative world energy consumption by fuel type [1].	2
1.2	Five elements of urban energy systems.	6
3.1	Schematic of a vapor compression electric heat pump.	31
3.2	Summary of the model abstraction process for the electric heat pump.	35
3.3	Black-box model of the electric heat pump.	36
3.4	Plot of \dot{E}_{hp} of the original model vs abstracted model.	37
3.5	Schematic of a general cooling tower unit.	38
3.6	Black-box model of the cooling tower.	41
3.7	Summary of the abstraction process for the cooling tower model.	41
3.8	Plot of ΔT_{ct} values of the abstracted UEM against UEM.	42
3.9	Example diagram of a pump-network system.	44
3.10	Example pump-network system curve.	44
3.11	Example pump electricity consumption curve.	45
3.12	Example of single-pump-parallel network diagram.	46
3.13	Example of converging fluid streams of different temperatures.	47
3.14	Abstracted model of the parallel-pumps network configuration.	49
3.15	Black-box model of the parallel-pumps network configuration.	50
3.16	Summary of the abstraction process for the parallel-pumps network configuration model.	50
3.17	Abstracted model of the single-pump-parallel network configuration.	51
3.18	Black box model of the single-pump-parallel network configuration.	53
3.19	Summary of the abstraction process for the single-pump-parallel network configuration model.	53
3.20	Plot of \dot{E}_{pump} of the graphical method and regression model.	54
3.21	Schematic of a general water-to-air heat exchanger.	55
3.22	Black-box model of the water-to-air heat exchanger.	58
3.23	Summary of the abstraction process for the water-to-air heat exchanger model.	58
3.24	Plot of \dot{Q}_{WAHX} of the analytical method and regression model.	59
3.25	Black-box model of the BIPV.	60
3.26	Black-box model of the ESS.	61
3.27	Black-box model of the GHX.	63
3.28	Schematic of a two-layer TES tank.	64

3.29	Black-box model of the TES.	66
4.1	Layout of a GCHP system serving a laboratory.	69
4.2	Schematic of the GCHP system serving the laboratory.	74
4.3	Schematic of a hybrid GCHP system.	74
4.4	Heat pump error plots.	80
4.5	Distribution pump error plots.	81
4.6	Approximate distribution pump electricity consumption under three operating strategies.	82
4.7	Comparison of distribution pump pressure setting between <i>bc2</i> and <i>opt3</i> for a typical day in July.	83
4.8	Comparison of average operating cost between two battery operating strategies.	84
4.9	Difference in battery operation across a 24 hour period in June.	84
4.10	Comparison of average monthly electricity consumption between current operating practices and optimization with WAHX.	86
4.11	Plot of electrical consumption and ground temperatures between <i>bc3</i> and <i>opt3</i> for a typical day in July.	86
4.12	Comparison of <i>COP</i> and ground temperatures between <i>bc3</i> and <i>opt3</i> for a typical day in July.	87
4.13	Comparison of monthly average operating cost amongst <i>bc3</i> , <i>opt3</i> and <i>opt4</i>	88
4.14	Comparison of battery operation between <i>opt3</i> and <i>opt4</i> for a typical day in July.	89
4.15	Comparison of operating strategies among <i>bc3</i> , <i>opt3</i> and <i>opt4</i> for a typical day in July.	90
4.16	Comparison of system <i>COP</i> between <i>opt3</i> and <i>opt4</i>	90
4.17	Plot of electricity annual electricity consumption across all seven cases.	91
5.1	Overview of the components of a typical DCS.	95
5.2	Overview of the optimization framework.	99
5.3	Overview of a generic genetic algorithm.	101
5.4	Crossover sites of continuous and binary implementation.	103
5.5	Complete parallelized hierarchical optimization framework	108
5.6	Schematic of DCS in case study.	110
5.7	Customer demand profiles of the three chosen periods.	111
5.8	Ambient condition profiles of the three chosen periods.	111
5.9	Error plots of the chosen models used in the case study.	116
5.10	Performance comparison between the direct application of GA and the optimization framework.	118
5.11	Result comparison of the three optimization cases over the three representative periods.	119
5.12	Comparison of chiller staging strategies between the ‘base’ and ‘holistically optimized’ cases.	122

5.13 Comparison of $\dot{m}_{dist,nwk}$ in the distribution network between the ‘base’ and ‘holistically optimized’ cases.	123
5.14 Impact of lowering chilled water temperatures at various points of the part-load curve.	124
5.15 Comparison of $\Delta P_{dist,nwk}$ between the ‘base’ and ‘holistically optimized’ cases.	126
5.16 Comparison of customer substation ΔT between the ‘base’ and ‘holistically optimized’ cases.	127
6.1 The sliding-window technique.	131
6.2 Schematic of the case study DCS with a theoretical two-layer storage tank.	134
6.3 Overview of the sliding-window augmented hierarchical framework. .	135
6.4 Comparison of cold energy stored across 24-hours, when optimized for different objectives.	141
6.5 Comparison of cold energy supply across 24-hours, when optimized for different objectives.	141
6.6 Pareto frontier evolution with sliding-window size, for large TES. .	142
6.7 Pareto frontier evolution with sliding-window size, for small TES. .	143
7.1 Typical implementation of a RL.	147
7.2 Schematic of the scaled-down DCS.	149
7.3 Neural network architectures.	154
7.4 Summary of the RL-MILP approach.	155
7.5 Plots of \dot{E}_{DCS} for the ‘base’-case, GA-MILP and RL-MILP (after 3000 episodes) approaches.	157
A.1 A typical primary-secondary hydronic system, for chilled water distribution.	166

List of Tables

3.1	Component-level models required in each case study.	26
3.2	Independent variables, dependent variables and parameters related to the electric heat pump model.	31
3.3	Percentage error incurred with different number of linear pieces, n	36
3.4	Percentage error incurred with different number of linear pieces, m while $n = 4$	36
3.5	Independent variables, dependent variables and parameters related to the cooling tower model.	38
3.6	Independent variables, dependent variables and parameters related to the WAHX model.	55
3.7	Independent variables, dependent variables and parameters related to the BIPV model.	60
3.8	Independent variables, dependent variables and parameters related to the ESS model.	61
3.9	Independent variables, dependent variables and parameters related to the GHX model.	62
3.10	Independent variables, dependent variables and parameters related to the TES model.	64
4.1	Base and optimization cases used in case studies.	75
4.2	Description of the case-study scenarios.	75
4.3	Component-level models required for this case study.	76
4.4	Treatment of temporary parameters in the selected component models.	77
4.5	Variables and parameters of the optimization problem.	78
4.6	Comparison of average electricity savings in the distribution pumps across different operating strategies.	82
4.7	Comparison of average cost savings across different operating strategies of the GCHP system.	89
5.1	A general unit description	105
5.2	Layers description	106
5.3	Component-level models required for the DCS case study.	112
5.4	Parameters and variables associated with the case study.	112
5.5	Decision variable settings of the DCS in the three optimization cases defined.	117
5.6	GA hyperparameters for both approaches.	118

5.7	Percentage change in electricity consumption across the representative periods.	120
5.8	Working hours of chillers in DCS.	121
6.1	Parameters and variables associated with the storage scheduling phase.	136
7.1	Parameters and variables associated with the case study based on the scaled-down DCS.	150
7.2	Definition of the MDP in the RL-MILP approach.	153
7.3	Comparison of differences in \dot{E}_{DCS} between the ‘base’-case, GA-MILP and RL-MILP approach over 3000 episodes.	156

Symbols and Acronyms

Symbols

$\%$	fraction, percentage
Δ	difference
a	actor neural network
A	area (m^2)
c	critic neural network
C	monetary costs (ϵ)
Cf	correction factor
Cp	specific heat capacity (kJ/kgK)
CO_2	carbon dioxide
COP	coefficient of performance
\dot{E}	electrical energy (kWh)
F	capacity constraint variable
Gi	global inclined irradiance arriving at a surface
k	TES loss coefficient
K_{temp}	PV temperature coefficient
$loss$	system loss coefficient
\dot{m}	fluid flowrate (m^3/h)
$NTU - \epsilon$	effectiveness number of transfer units
\mathcal{N}	normal distribution
P	pressure (mH_2O)
$Pump$	hydraulic pump
pwl	piecewise linear segments
\dot{Q}	thermal energy (kWh)
R^2	coefficient of determination
st	stream variable

T	temperature (K)
u, v	RLT variables
U	overall heat transfer coefficient (W/m^2K)
V	volume of thermal storage system (m^3)
W	linear weights
X	neural network
Y	binary on-off variable
$p, n, m, k, j, r, x, ..$	generic variables

greek letters

$\alpha, \beta, \gamma, \nu$	regression-derived constants
ϵ	effectiveness
η	efficiency
ω	angle ($^\circ$)
Θ	excess temperature, $T_{g,t} - T_{ginit}$ (K)
μ	mean
σ	standard deviation
δ	error
θ	neural network weights

superscripts

in	flow entering
out	flow exiting
n	generic number
min	lower bound
max	upper bound

subscripts

a	air
act	actor
amb	ambient
app	approach

<i>br</i>	branch
<i>c</i>	condenser
<i>cm</i>	cooling mode
<i>ch</i>	chiller
<i>cp</i>	common pipe
<i>cri</i>	critic
<i>ct</i>	cooling tower
<i>cold</i>	cold water
<i>d</i>	demand
<i>dist</i>	distribution
<i>e</i>	evaporator
<i>ele_rate</i>	electricity rate ($\text{€}/\text{kWh}$)
<i>exc_solar</i>	excess solar
\dot{E}	electrical energy (kWh)
<i>ESS</i>	electricity storage system
<i>g</i>	ground
<i>grid</i>	grid
<i>hm</i>	heating mode
<i>hp</i>	heat pump
<i>hot</i>	hot water
<i>init</i>	initial
<i>INV</i>	inverter
<i>li</i>	linear interval
<i>limit</i>	limit
<i>loss</i>	losses
<i>mu</i>	make-up
<i>nwk</i>	network
<i>op</i>	operating
<i>OHM</i>	ohmic
<i>pump</i>	pump
<i>pv</i>	photovoltaic
<i>rq</i>	required
<i>s</i>	stored
<i>scm</i>	storage charging mode
<i>sdm</i>	storage discharging mode

<i>sel</i>	selected
<i>sf</i>	surface
<i>ss</i>	substation
<i>sw</i>	sliding window
<i>sys</i>	system
<i>t</i>	time-period
u, v	RLT variables
<i>unit</i>	collective, group, unit
<i>w</i>	water
<i>wd</i>	window index within sliding window
<i>WAHX</i>	water-to-air heat exchanger
<i>wb</i>	thermodynamic wet-bulb
x_1, x_2, x_3	generic variables
<i>z</i>	zone
$0, 1, \dots, i, j, k, m, n$	generic labels
/	or
//	parallel

Acronyms

Adam	adaptive moment estimation
ADREAM	<i>architectures dynamiques reconfigurables pour systèmes embarqués autonomes mobiles</i>
ANN	artificial neural network
BIPV	building integrated photovoltaics
CP	condenser pump
COP	coefficient of performance
CCHP	combined cooling, heating and power
CNRS	<i>centre national de la recherche scientifique</i>
DCS	district cooling system
DPG	deterministic policy gradient
DDPG	deep deterministic policy gradient
DP	distribution pump
DHC	district heating and cooling
DHS	district heating system

DHW	domestic hot water
EP	evaporator pump
ELD	equal load distribution
ESS	electrical storage system
GA	genetic algorithm
GCHP	ground-coupled heat pump
GHE	ground heat exchanger
GNU	gordon-ng universal
GP	geometric programming
GSO	group-search optimizer
HVAC	heating, ventilation and air conditioning
IEA	international energy agency
IoT	internet of things
LAAS	<i>laboratoire d'analyse et d'architecture des systèmes</i>
LMTD	log-mean-temperature-difference
MAE	mean-average-error
MDP	markov decision process
MILP	mixed-integer linear program
MINLP	mixed-integer non-linear program
MIQCP	mixed-integer quadratically-constrained program
MPC	model predictive control
Mtoe	million tonnes of oil equivalent
NLP	non-linear program
NN	neural network
NSGA-II	non-dominated sorting genetic algorithm, version two
OCL	optimal chiller loading
OF	objective function
PV	photovoltaic
QP	quadratic program
RL	reinforcement learning
RLT	reformulation-linearization-technique
RPM	revolutions per minute
SFEE	steady-flow-energy equation
SOC	state-of charge
TES	thermal energy storage

TRNSYS	transient system simulation tool
UEM	universal engineering model
WAHX	water-to-air heat exchanger
ZEB	zero energy buildings

Chapter 1

Introduction

1.1 Context

Current energy use in the urban context has a consequential role in environmental degradation - motivating a spectrum of initiatives spanning from the development of alternative fuels, including renewables to techniques for efficiency improvements. As of 2018, the world's total consumption of energy stood at approximately 14 000 Mtoe, a rise of above 50% from a decade ago (*Figure 1.1*) [1]. Of which, above 85% of this consumption was derived from non-renewable sources such as coal, oil and gas. This has contributed to unprecedented levels of CO_2 emissions which threaten to accelerate climate change at an alarming rate [2].

Buildings are responsible for up to 36% of global final energy use and 40% of CO_2 emissions with space conditioning and electricity usage as chief contributors [3]. Estimates from the international energy agency (IEA) highlighted the potential for buildings to be up to 40% more efficient than the current state. Improvements to these statistics must be made for urbanization to continue sustainably.

In 2019, renewable energies have not yet sufficiently matured to fully supplement global energy requirements, hence the necessity for integration with existing systems [4]. Centralization of urban energy systems offers unrivaled levels of energy efficiencies and cost-effectiveness - a direct consequence of economies of scale. Shared infrastructure from centralized systems, further function as a platform for facilitating the integration of alternative energy sources, which comprise renewables and

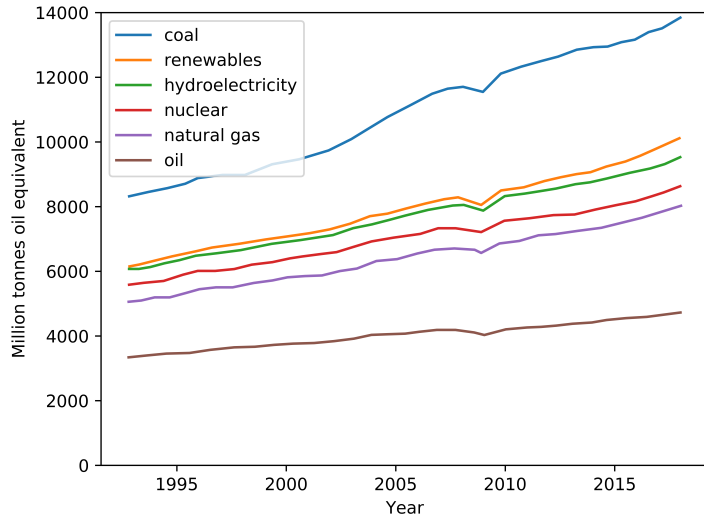


FIGURE 1.1: Reproduced graph of cumulative world energy consumption by fuel type [1].

waste energy harvest. Increasingly complex systems that emerge from the multiplex of energy sources and consumers, calls for equivalently capable management strategies to realize their potential for energy efficiencies.

The incongruity between the design and operating conditions of the complex urban energy systems will persist indefinitely; it is inevitable to make assumptions given data limitations [5]. When these conditions vastly differ, the expected gains from centralization could easily be negated. Measures to improve the operations of these systems could be explored through mathematical optimization of the appropriate models. Optimization of operations, demands the algorithm to deliver results in real-time, which can be achieved using an amalgamation of model abstraction and optimization techniques to increase computational efficiency.

Components of these systems are often operated at predefined setpoints or independently optimized - a repercussion of complexity [6, 7]. Inefficiency is further compounded by such control strategies; localized control inhibits the ability for systems to adapt appropriately under less ideal scenarios, by disregarding the cascading effect on the system. Formulation of optimization problems that both incorporate models with sufficient fidelity and captures the interdependencies amongst them usually results in a mixed-integer non-linear program (MINLP) which is large and difficult to solve. Hence, the primary focus of this thesis is to develop an optimization framework which is not only able to perform holistic optimization of

the operations of complex energy systems but also has the potential to be utilized in real-time. This framework is meant to function as a decision support tool for system operators.

1.2 Urban energy systems

Urban areas currently house more than 50% of the world's population, with this figure expected to approach 70% by 2050 [8, 9]. Improved economic and social opportunities that cities offer serve as explanations for this observed trend [10, 11]. Consequently, as significant energy resources are channeled for the sustenance of the urban populations, cities account for much of the environmental pollution. In this thesis, 'energy systems' refers to an umbrella term for electricity, heating and cooling supply for buildings. The principal existence of such systems is to facilitate the conversion and transportation of energy for eventual consumption.

1.2.1 Centralization of energy systems

Centralization of energy systems has been the common theme for the past century where energy efficiency is concerned [12]. With varying degrees, centralization could occur at the building up to the district level. These systems offer many advantages over their decentralized counterparts in terms of economies of scale. By their sheer magnitude, they enjoy substantial economies of scale. The main benefits are summarized as follows:

- **Higher quality equipment.** The supply of energy becomes a utility that is delivered by a provider (state-owned or private company). Profit margins inevitably become paramount for competitiveness, necessitating the investment in energy-efficient equipment. Better resource utilization will result, hence, in alleviating the burden on the environment. District cooling systems (DCS), an example of a centralized energy system, reported electricity savings of up to 20% over decentralized counterparts in Hong Kong [13]. The above-mentioned reasons also promote the reliability of energy supply.

- **Distribution infrastructure.** Whether in the form of cables or a network of pipes, they enable vastly greater flexibility in the selection of primary fuels to generate the required energy supply. Decentralized counterparts typically only have singular choices. Centralized systems, thus have the flexibility to appropriate the right fuel type (renewables, etc.) for the purpose, without major infrastructural changes. This shared infrastructure also serves as a platform for the integration of alternative fuels in the future.
- **Demand aggregation.** Having a large system alleviates the need for smaller individual equipment from part-load operation - a commonplace scenario for decentralized systems. Operating efficiencies often peak at nominal loads, and greatly deteriorates otherwise. Opportunities for better design and control to further improve resource efficiency is also made possible with information derived from global monitoring systems
- **Consumer savings.** Maintenance of privately owned equipment becomes redundant as energy becomes a utility to be purchased.

1.2.2 Integrated energy systems

The logical step which follows centralization is the integration of alternative energy sources to further the cause of energy efficiency. As it stands, energy generated from renewable sources is still intermittent, thus fossil fuels still play an important role [14]. The integration of renewables not only has the benefit of relieving environmental burden but also an opportunity for engineers to build familiarity with operational know-how.

A classic example of an integrated energy system is that of a combined cooling, heating and power (CCHP) plant. Waste heat from power generation is used to fire up boilers and absorption chillers, for space conditioning purposes. Combining these processes, primary fuel efficiencies could be improved by two-fold - from a mediocre 40% to up to 80% [15, 16]. For urban systems, the complexity of integrated systems transcends that of mere process integration. Sporadic contribution from renewables and stochastic demand compounds the challenge of designing capable control strategies.

Permeation of the internet of things (IoT) into urban energy systems unveils a myriad of opportunities for improved design and operation [13]. Voluminous data generated by the deployed sensors reveal trends that challenge conventional wisdom. This is made possible by the rapidly increasing computational capacities and the abundance of functional algorithms. However, despite these technological advances, conservative design and operating procedures are still practiced. Given that urban energy systems are categorized as critical infrastructures, malfunctioning is a costly catastrophe which can never be contemplated.

Nevertheless, research work exists to challenge the status quo. To accommodate the lack of experimental studies, virtual modeling is often resorted to, for testing and development of applicable solutions [17]. These methods, very often are targeted at efficient design and operation of an energy system such that electrical consumption is reduced. The primary objectives of design and operation studies are to select and schedule the various equipment (chillers, pumps, etc.), respectively, such that energy consumption and/or cost is reduced while meeting system constraints and satisfying end-user demands [18].

Independent operation of subdivisions of urban energy systems is a paradigm that should be shifted, given the current state of data availability and computing prowess. Although complex, there exists enormous potential to increase efficiency and reduce primary energy usage by integrating these processes. *Figure 1.2* summarized the five key aspects of urban energy systems [8]. The confluence of electricity and thermal energy from all sources, working in synergy and managed by advanced control systems for maximizing efficiency in meeting demand is archetypal of an ideal urban energy system. The result should be the following:

- Adaptable to changes in fuel, i.e., toggling between renewables and fossil fuels when required.
- Harvest of waste energy through process integration (e.g. waste heat harvest).
- Appropriate response to consumer demands, such that operational efficiency is maximized.
- Utilization of storage systems to reduce peak load.

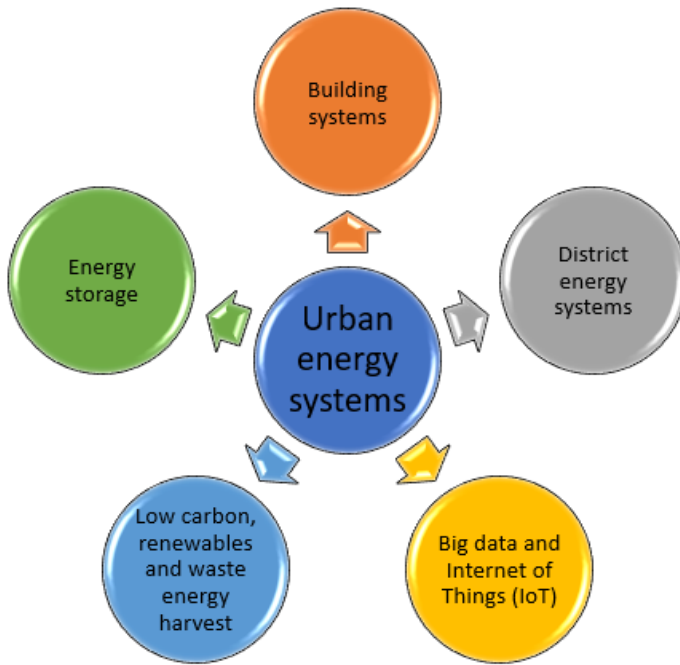


FIGURE 1.2: Five elements of urban energy systems.

1.3 Motivation and problem statements

Despite the availability of data, estimates are inevitable during the design phase of urban energy systems. The deviation between design and operating conditions could be detrimental to varying degrees - depending on the type of equipment involved. A poorly designed system runs the risk of performing worse than even decentralized options. To further complicate matters, such infrastructures involve large capital investments and time to establish, thereby resistant to changes in design. Hence, methods to improve operation for a given system should be explored to ease the banes brought about by these discrepancies.

The vast majority of the work on the operation of urban energy systems fall into one of the two following categories - simulation-based or optimization with highly abstract models. The benefits of conducting simulation lie in the ability to incorporate models of high fidelity, resulting in higher confidence for the results generated. However, highly detailed models are also more complex (non-convex), making options for optimization very limited, explaining why simulation is often conducted instead. The converse is true for the latter - while it is easy to perform optimization on highly abstract models, the results generated offer very little for operational improvement. To address this issue, this thesis focuses on the development of a

framework that balances modeling fidelity with optimization compatibility to promote computational efficiency - a critical requirement for the real-time application on urban energy systems. The three fundamental issues addressed are as follows:

1. **Given an existing energy system, what is the best mode of operation to satisfy end-user demands while meeting system constraints?**

The existence of numerous decision variables, non-convexities, and tight-coupling amongst components, makes the determination of the optimal operating strategy a highly challenging task. For simplicity, existing work tend to focus on component-level optimization [19, 20] or utilize highly abstract models [21, 22]. While the solvability of the resulting optimization problem is indeed improved, such techniques unnecessarily prune solution space which is already restricted by the system design.

For the results of the optimization problem to be useful, two criteria must first be met. Firstly, the tuneable variables of the system need to be expressed as decision variables. The same demand could be satisfied with various combinations of decision variables, each with a different impact on system efficiency. This is especially true for thermal systems where a load can be fulfilled with many combinations of flowrate and temperature setpoints. Secondly, it is cardinal to capture the interdependencies amongst the system components and holistically optimize the system. Since a myriad of non-linearities exist in and amongst the models of system components, component-level optimization becomes overly naive.

The judicious choice of component models and the subsequent application of abstraction techniques enable the formulation of the resulting optimization problem as a mixed-integer linear program (MILP). However, this has limited applications and is hugely dependent on case-study specific information and objectives. For generalized applications, abstracted models are used with the introduced hierarchical optimization framework for optimizing the operations of urban energy systems. This approach decomposes the accompanying problem into its linear and non-linear segments and solves them, with the aid of a genetic algorithm (GA) and MILP - the GA iterates on the parameters of the MILP, until a convergence criteria is met. Doing so maintains the solvability of the problem and gives a higher chance of globally optimal solutions

while enabling the model-related intricacies such as non-linearities, etc. to be factored. This framework is formally introduced in *Chapter 5* of this thesis.

2. How to balance between the resolution speed of the algorithm and the solution accuracy for multi-period optimization problems involving energy storage systems?

Energy storage systems complicate optimization problems as they require multi-period and multi-objective considerations. Although burgeoning problem sizes are a consequence, formulations across time-periods enable the solvers to sanction for energy to be stored in more favorable periods to be available later. Doing so can potentially enhance cost-effectiveness and/or energy efficiencies. Similarly, the extent of abstraction made in the related work while they offer relevant solutions to design-related issues are not suitable for the optimization of system operations [23, 24].

For solving such problems, the sliding-window technique is deployed in tandem with the hierarchical optimization framework [25]. Depending on the factors such as electricity pricing, energy demand, and size of the thermal storage, selection of the appropriate window size (number of periods), despite reducing the size of the concomitant optimization problem, still, delivers close-to-optimal results. This approach is discussed in greater detail in *Chapter 6*.

3. How to increase real-time applicability of the optimization framework?

Owing to the sheer number of conflicting decision variables and the non-convex nature of the problem, the holistic optimization of urban energy systems is a computationally intensive undertaking. This is the likely reason which inhibits the real-time deployment of algorithms for the optimization of operations. Where real-time control is concerned, model predictive control (MPC) techniques are often deployed for performance optimization [25]. While MPCs have the benefit of localized optimization through the use of simplified empirical models, significant cost and energy savings are disregarded by not performing optimization at the system-level.

Reinforcement learning (RL) as a technique for optimal control is rapidly gaining traction for the closely related building systems [26]. However, system-level optimization is still shunned due to its complexity; only a small set of

tunable variables are chosen as decision variables [27]. Such techniques while they give insight into the applicability of RL algorithms, effectively disregard large segments of the solution space by ignoring the possibility of optimizing the remaining tunable variables.

To address the issue of slow resolution speed associated with the hierarchical optimization framework, the GA is replaced with a RL. When coupled with the MILP in the hierarchical framework, the RL could be trained offline using data traces obtained from historical data. When the training is deemed sufficient and deployed in real-time, only one iteration of MILP is needed for generating the close-to-optimal solution. Although solution quality tends to be inferior to the GA, deployment of the RL enables the heavy computation (learning process) to be shifted offline, vastly speeding up real-time deployment, as will be presented in *Chapter 7*.

1.4 Contributions and thesis organization

The main contributions of this thesis are summarized by chapter in the following.

1. *Chapter 2* presents the literature review done on fields related to the focus of this thesis - the evolution of urban energy systems, modeling of associated system components, associated simulation and optimization techniques. Finally, the gaps in the literature which motivate the current work are discussed.
2. *Chapter 3* documents component models which are required for the case studies in the ensuing chapters. The choice of models and complexity of the models are discussed.
3. *Chapter 4* highlights the benefits of abstracting the chosen models, as they permit the optimization problem to be formulated as a MILP. Several approaches to abstract the required models are discussed and subsequently applied to a case study based on an existing building-level ground-coupled heat pump (GCHP) system, which is integrated with solar photovoltaics and energy storage system. Multi-period and multi-objective considerations are

essential to effectively model the electricity storage system and residual thermal energy from the ground. The abstraction of models enabled the system to be modeled with reasonable fidelity whilst maintaining compatibility with MILP solvers. Additionally, interdependencies amongst components could also be captured, giving useful insights into the bottlenecks of the system. These insights prompted the addition of a theoretical water-to-air heat exchanger (WAHX) to function as an alternative to the ground for thermal exchange. Cost and electricity savings up to 12.7% and 35% was achievable, suggesting that the additional investment cost is recoverable within five years.

4. **Chapter 5** introduces the hierarchical optimization framework, which is to be used with abstracted component models, for the optimization of the operations of urban energy systems. This framework is introduced to handle decision variables that could not be managed by the abstraction techniques alone. The key feature of this framework lies in the ability to holistically optimize MINLP problems by decomposing them into their linear and non-linear counterparts and sequentially solving them with the use of a GA and MILP solver. Indiscriminate use of metaheuristics on complex models is a common practice as evidenced by related work. Using a case study on an existing district cooling system (DCS) as an example, the benefits of the decomposed approach is highlighted by comparison against the sole use of the GA. For the predefined periods, the former always converged to a superior solution. Finally, the benefits of holistic optimization are highlighted through the counter-intuitive results generated by the framework for the given demand profiles. The energy efficiencies of a few major components in the DCS were compromised for the benefit of the entire system. Results from the case study indicated that an additional 18.9% of electricity could be saved when the DCS was optimized holistically as opposed to at the component level. This re-emphasizes the importance of modeling the non-linearities which are inherent to components and interdependencies amongst them, before performing optimization.
5. **Chapter 6** discusses the adaptation of the proposed optimization framework for compatibility with energy storage systems. Multi-period and multi-objective optimizations are required because of storage systems. Existing

work, while they emphasize the importance of storage systems from the design perspective, offers little insight into the operation of system components, due to the use of models that are too abstract. The sliding-window technique was subsequently added to the proposed optimization framework for this undertaking. This technique performs optimization over a predefined number of periods (window size), but only uses the result for the first period. This is successively done until all the required periods in the optimization problem are resolved. Doing so greatly reduces the size of the accompanying optimization problem and hence the resolution time. While the result is an approximation of the global optimal, the difference is justifiable when compared to the improvement in solvability and resolution time. This technique was implemented in a case study based on a DCS. Results affirm the applicability of the technique and indicate that the window size is dependent on several factors, such as fluctuations in electricity price and capacity of the thermal storage system, for instance.

6. **Chapter 7** proposes the replacement of the GA in the optimization framework with a RL. This effectively increased the feasibility of the optimization framework to be deployed in real-time. Through the use of the RL, the heavy computation which is required to determine the relationship between the non-linear variables and the optimal solution could be determined (learned) offline, vastly speeding up the resolution time of the algorithm in real-time. As opposed to the original implementation involving the GA, the RL-MILP framework, when trained, just required a single iteration to deliver optimal solutions. Recently, RL is often suggested as a potential solution to some of the control-related optimization problems in energy systems. However, a highly limited number of variables are considered in the studies conducted. The training process for the neural network (NN) in the RL is an arduous task, especially when the output layer is larger than the input layer.

The combination of the RL with the MILP mitigates these issues, by having the MILP solve the bulk of the optimization problem. In doing so, the RL has to only determine the relationship between a handful of decision variables and the optimal solution. This not only reduces the size of the NN required and the training time but increases the likelihood of the solution quality. The capabilities of the RL-MILP approach is demonstrated using the same case

study based on the DCS. Results generated, when compared against the GA-MILP approach showed only a 7.52% compromise in the optimal solution for a vast improvement in the resolution time.

7. ***Chapter 8*** provides a summary of this thesis and discusses some directions for future work.

Chapter 2

Literature review

2.1 Overview

This chapter presents the latest work relevant to the optimization of urban energy systems. ‘Urban energy systems’ is generally used as an umbrella term for electricity, heating and cooling supply for buildings [28]. Both district and building-level studies are considered in this review as they are closely related. The literature review is structured into three main sections as listed below.

1. Evolution of urban energy systems
2. Optimization of urban energy systems
3. Review summary

2.2 Evolution of urban energy systems

The purpose of this section is to present a brief history of urban energy systems, discuss its current state and future trends. This information is an important consideration for positioning the work of this thesis and deciding on its future relevance.

2.2.1 History of urban energy systems

Centralized thermal energy systems began way before the advent of electricity - the first district heating system (DHS) was established in the 14th century, in Chaudes-Aigues, France [29]. The heating system was established to collectively draw geothermal heat for the small village. Electricity generation followed suit in the 1870s when the Edison Electric Company established the first integrated power and lighting system in the streets of London and New York [30]. Towards the end of the same decade, DCSs emerged [31]. Common to all three systems, which the modern urban energy system is typically comprised of, centralization was undertaken to take advantage of economies of scale. The economy of scale which was traditionally derived from the transportation of energy supply has since evolved to also encompass operating efficiencies and control of complex equipment [32]. These systems are generally deployed for the sectors (industrial, commercial, etc.) with stable and highly predictable demand. Over the years (1870 - 2019), urban energy systems have also seen greater inclusion of sustainable energy sources, improvements in system design (storages, management systems, control algorithms, equipment, etc.) and a wider variety of sectors. In the current era of accelerated urbanization, urban energy systems are expected to be increasingly relevant, as inferred from the attention which they receive in the contemporary research [12].

2.2.2 Current state of urban energy systems

Electrical and thermal energy systems appear to be moving in opposite directions in terms of centralization, albeit at differing rates. For electrical systems, solar photovoltaics are increasingly being touted as a viable supplement to the power grid - a move away from centralization. The current share of building integrated photovoltaic (BIPV) systems account for 2.5% of the photovoltaic (PV) market and is expected to rise to 13% by 2022 [33, 34]. For thermal systems, however, district-level systems are gaining in popularity, especially in newer urban establishments [12, 35]. In general, these systems are progressing away from fossil fuels and towards taking greater advantage of the environment sustainably and utilize energy more efficiently (waste energy harvest). Storage systems are also often utilized for the improvement of operating efficiencies.

2.2.2.1 Integration with sustainable sources

Integration with water bodies (sea, ocean, lake, etc.) to district thermal systems is an attractive option, as they offer thermal exchange with the environment at more favorable temperatures as compared to ambient air. This is especially true where cooling systems are concerned. Depending on the temperature of the water body in the region, chillers could even be done away with, resulting in very significant energy savings [36].

For regions with seasonal demands for cooling and heating, heat pumps are often used to harvest the thermal energy from the sea. The sea alternates its role as a heat sink and source during the summer and winter, respectively [37, 38].

Integration with geothermal sources in this context refers to the naturally occurring heat sources and aquifers. Aquifers are underground layers of water-bearing permeable rocks that contain groundwater [39]. Due to the low thermal conductivity of soil and rocks, the temperature of the water remains invariant to ambient conditions; therefore it is relatively cooler in the summer and vice-versa in the winter as compared to ambient air [40]. When coupled with heat pumps, thermal energy could be harvested for both cooling and heating purposes. Aquifers are commonly used in one of the two ways - direct use of water for cooling or heating purposes or as a thermal storage facility. The benefits of using aquifers are discussed in [41, 42].

Borehole heat exchangers are usually deployed for thermal exchange with the ground [43]. In the absence of water, with the right type of composition and depth, the thermal inertia in the ground could be used for similar purposes. These systems are known as ground-coupled heat pumps.

Solar energy could power thermal collectors, absorption chillers and photovoltaics to fulfill heating, cooling and electricity demands respectively. These systems tend to be lower in efficiencies than their traditional counterparts, however, not having to draw current from the grid meant lower emissions and operating costs. That, however, is only possible with a higher initial capital outlay for the appropriate equipment (PV panels, absorption chillers, etc.) [44, 45].

2.2.2.2 Process integration

Intergation of heat, power, and cooling into combined heating, cooling, and power plants could potentially offer unparallel efficiencies for the production of all three utilities. In these facilities, residual heat from the generation of electricity is used to fire up boiler and absorption chillers for heating and cooling respectively. Doing so can easily double the primary fuel efficiency [46]. The design of these CCHP systems are naturally more complicated than traditional power plants. There is much research the combination of variables such as steam pressures and temperatures to maximize the overall plant performance [21, 47–57].

Waste heat recovery from various processes (municipal solid water [58], electricity production [59–61], etc.) are commonly extracted and fire up heat pumps and chillers in district energy systems. Pinch analyses were often used to determine possibilities for such integration. The literature reviewed reported a reduction in fuel usage and CO_2 emissions of up to 41% and 60% respectively. Percentage savings, however, were highly influenced by the electricity price [62]. Especially where heating systems are concerned, the embracing of infrastructure for low-temperature networks, presents a highly viable option of integrating waste heat[63].

Integration with waste cold recovery is also a possible option, should there be a cooling system located in the vicinity of such processes. Natural gas and nitrogen, typically are imported in large cylinders and regasified into the network, releasing substantial amounts of cold energy [64, 65].

2.2.2.3 Role of storage systems

Energy storage systems permit the shifting of electrical and thermal load from peak to non-peak periods [66–68]. Both consumers and producers stand to benefit in terms of the improved energy performance of the energy systems which in turn translates into cost savings. Where thermal storages are concerned, water and ice are the preferred options. While water is the cheaper option, in certain scenarios, space-efficiency issues result in the preference for ice. Phase change materials have since been explored for the use with large scale thermal systems, however, they have yet to be feasible due to the loss of cost-effectiveness [69, 70]. For electrical systems, options for storage range from pumped hydro systems to lithium batteries

depending on scale [71]. Due to the advancement in battery technologies, the efficiency and cost of production of lithium batteries have dropped, hence it is becoming an increasingly popular option for building-level PV systems.

2.2.2.4 Losses in large-scale energy systems

Losses in electricity transmission are much lower than that of thermal pipelines [72, 73]. While there is currently not an easily available alternative for grid electricity in urban areas, there exist many decentralized options with the low capital cost for thermal systems, making urban thermal systems more price elastic. Therefore, there is a greater imperative to minimize distribution losses in the thermal network.

The majority of the losses occurring in district heating and cooling systems occur in the distribution network. The two main sources of thermal losses (temperature degradation) are to the environment and pumps. These losses are much more pronounced than in decentralized systems, due to the need to pump water over large distances to reach the consumers who are connected to the network. These large distances also incur considerable head losses, requiring the pumps to work even harder.

Surfactants could be introduced to reduce the viscous losses at the fluid-pipe interface. Drag coefficients reduction of up to 80% has been reported in the state-of-the-art, significantly reducing the power required for pumping [74]. Considerable research was invested in the attempt to reduce thermal losses to the environment by working with fluid temperature which is closer to ground temperatures. That resulted in the widely popular low-temperature district heating networks [63, 75]. In cooling networks, however, the temperature difference is small, leaving little room for adjustments. Hence guidelines for design, such as the maximum radius of the network, etc., are adhered to [12].

2.2.2.5 Future trends

In the absence of revolutionary technologies that could radically improve energy efficiencies and cost-effectiveness where the production of heating, cooling, and electricity are concerned, researchers have unanimously agreed that higher levels of integration with sustainable sources should be pursued [76]. This, however,

implies that the design and control measures that govern these systems must correspondingly evolve [12, 77].

The residential sector represents a large untapped potential for urban energy systems due to the unpredictability of demands. Electricity, for instance, is usually priced similarly throughout the day, unlike their commercial and industrial counterparts. As the demand increases, due to the impending introduction of newer technologies (electric cars, etc.), control measures need to improve in tandem to reduce inefficient operation due to unnecessarily high peak loads. The control of thermal systems should also mirror that of the electrical grids, enabling bi-directional purchase and sale of energy whenever appropriate [78].

2.3 Optimization of urban energy systems

This section reviews the existing optimization work related to urban energy systems. The objective of this review is to identify how such problems are approached in the state-of-the-art, i.e., determination of objectives, variables, simplifications and choosing algorithms to solve them. The literature on both district and building level problems are included in this review.

2.3.1 Design optimization

Optimization pertaining to the design of urban energy systems attempt to determine the best configuration of equipment type, primary resource, distribution route and variability of consumer profiles, which would result in the highest possible efficiency. Such formulations typically employ highly abstract models, which tend to regard many otherwise tuneable variables as constants. Owing to the complexity performing optimization holistically, i.e., at the system-level, an overwhelming majority of the case studies reviewed performed optimization on components locally (heat pumps, network, etc.). The popular objective functions are investment cost, electricity consumption and to a much lower extent, CO_2 emissions.

2.3.1.1 Mono-objective optimization

Building-mix. The ‘optimal’ combination of consumers (type, demand profile, etc.) heavily impacts the resulting efficiency of the energy system. Components belonging to these systems typically have small operating ranges where efficiency values are at their highest. Large fluctuations in demand are extremely detrimental as they are solely responsible for dips in efficiency which propagates through the system, causing poor performance of ancillary components too. Metaheuristics have been used during the design phase to minimize the stochasticity of the cumulative demand profile through the lens of the centralized system by selecting the best mix of consumers [79].

Network design optimization attempts to determine the best placement of nodes (central station, substations, transformers, etc.) and edges (transmission lines) for the minimization of a certain objective function. For thermal systems, some case studies even consider the sizing of pipelines.

For highly simplified problems, the network design could be modeled as a set of nodes and edges, with fixed/linear weights attached to each edge. Such formulations could be solved using Dijkstra’s algorithm [80], linear weights, on the other hand, are formulated into MILPs [81, 82]. These problems were formulated with estimated demand profiles as hard constraints that cannot be violated. However, the treatment of non-linearities (temperature, pressure, etc.) as constants may adversely impact the feasibility of suggested solutions.

Where the non-linear variables are considered, metaheuristics are commonly deployed. For greater accuracy, analytical equations were used to estimate the required pumping power and hence the investment cost of pumps [80, 83, 84]. Metaheuristics are hugely popular because of their ease of implementation and relatively decent performance in the search for an ‘improved’ solution.

System-level design pertains to the sizing of equipment in the central plant and the transmission/distribution network to most efficiently fulfill the demands of consumers. Often, the sizing of the major system components receives the greatest attention as they are perceived to have the largest impact on the system. Furthermore, due to the complexity, models used are usually highly minimalistic. Black-box modes with constant efficiencies regardless of load factor is one such

example, used in many CCHP optimization studies [21]. Through simplification, the inclusion of a wider array of components (alternative sources, solar, etc.) was still possible whilst still maintaining the problem's MILP feasibility. Simplifications, inevitably neglect some tuneable variables which may have the objective function may be sensitive to, should conditions deviate from the presumed state [48]. A technique known as the ‘reformulation-linearization-technique’ (RLT) could be used to linearize bilinear variables in optimization problems [85]. This enabled more variables to be optimized by MILP solvers.

Uncertainties such as the impact of improper maintenance, malfunction, reduced performance, weather, design, construction, and outdoor conditions could be considered with the aid of techniques such as the Markov method [86] and minimax regret theory [87, 88] in optimization problems. Through sensitivity analyses, it was deemed that the objective function was most sensitive to the design of buildings, above the other considered factors.

2.3.1.2 Multi-objective optimization

Evolutionary algorithms are often used to generate solution sets for multi-objective optimization problems concerning urban energy systems. Total investment cost and CO_2 emissions are the most commonly chosen objectives. The Pareto frontiers of these two objectives are usually discontinuous with many points of local optima [89, 90].

To incorporate more decision variables into the problem formulation, a decomposed optimization approach was used by Fazlollahi et al. for the optimization of district heating systems [91–93]. In this approach, the non-linear and linear aspects of the optimization problem are first separated and solved sequentially with the use of evolutionary algorithms and MILP solvers. To further improve the resolution speed of the approach, load clustering algorithms were used to reduce the size of the input data.

2.3.2 Operation optimization

Estimations are inevitable during the design phase of urban energy systems due to the lack of information. Consequently, the performance of the resulting energy

system when operational tends to be lower than expected. Optimization of control measures could be used to reduce this deficit.

Given the design of an urban energy system as an input parameter, the purpose of such optimization problems is to determine modes of operation so that the energy demands are met in the most efficient manner. Thus, the task involves finding the combination of component-level variables such as flowrate, temperature, pressures, loading-factors, etc., to fulfill the given objective. This calls for component-level models that reflect a much higher level of fidelity than design level problems. Such models involve highly complex governing equations which make solving the resultant optimization problem a challenge. Complexity is further compounded at the system-level, thus, for simplicity, these systems are often operated by only tuning a small subset of these variables, disregarding substantial energy-saving potential.

2.3.2.1 Mono-objective optimization

District level optimization problems are formulated with the focus of maximizing the energy efficiency of pre-selected components. These components are prioritized as they are often the most energy-consuming [94]. The need for detailed models, results in complex optimization problems, making the application of metaheuristics in this domain a hugely popular choice. Operation cost is often defined as the objective function with energy demands from consumers as binding constraints [95–98]. Operators of energy systems, although contractually obligated to fulfill the energy demands of consumers can sometimes choose to violate the agreement and pay a penalty instead; such considerations enable the relaxation of binding constraints, widening the solution space and gaining insights into counter-intuitive measures [99].

With the use of appropriate equation-based models of components, the complex MINLP could be broken down into smaller quadratic programs (QP) and solved dynamically [19]. Doing so improved both the quality of the solution and resolution speed. Simplifications such as the removal of binary variables and load aggregation were however still necessary.

Building-level optimization problems tend to place greater emphasis on the major components of the energy systems [100, 101]. For instance, the ‘optimal chiller loading’ problem was often the primary focus in cooling systems. Building systems,

unlike district-level systems, have significantly lower energy expenditure on distribution, hence justifying the lack of focus on ancillary components. Metaheuristics are often used on these highly detailed models to solve the economic dispatch problem. In some cases, convex optimization methods were used, after simplifying the governing equations using regression [102]. Although there were little differences in the quality of the final solutions in either method, the latter had a strong guarantee of achieving the global optimum.

Component-level optimization using MPCs are also often deployed. Such controls typically use polynomial approximations to simplify complex models for computational efficiency [25, 103]. While they work well for individual components, polynomial approximations are too simplistic to capture system-level dynamics, making MPCs not yet suitable for holistic optimization.

As a technique for optimal control, RL is rapidly gaining traction in the field of building energy control [27]. RL hinges on the capabilities of NNs, hence enabling complex relationships inherent to the system to be incorporated without the explicit use of models. Training stability and convergence, however, are major issues that are not yet adequately addressed. Hence, as a compromise, optimization involving RL often only deals with a small subset of decision variables, which implies localized optimization.

2.4 Review summary

Urban energy systems trend towards heightened levels of centralization and energy integration for increased efficiencies and reduced emissions. This makes control measures of such systems increasingly challenging, due to the sheer number of variables to tune, while considering interdependencies of these components. Given the inherent non-linearities in, and amongst component models, it is thus paramount to factor in these considerations in the formulation optimization problems. Modeling such intricacies, although they result in better solutions through a wider solution space, are often not computationally feasible to solve. The following are some gaps in the literature which pertains to the global optimization of the operations of these systems

1. Component models of energy systems are typically highly simplified; while they are applicable for design-based problems, they have very little value in tuning for the optimum performance in operation. Often, only quantities of energy flows are considered, without indicating how to achieve that quantity - thermal systems could easily deliver the same quantity of thermal energy with an infinite combination of flowrates and temperatures, each affecting efficiency very differently. Assumptions such as fixed operating efficiencies regardless of equipment part-load condition eliminate much of the already restricted solution space which could otherwise have been explored.
2. There are no perceivable differences in the models used for building and district-level optimization problems. There appears to be an appreciable quantity of energy expended in delivering the utilities over considerable distances, through the distribution/transmission network. Besides, losses in that process are also likely to be relatively pronounced, as evidenced by the work identified in the literature. Including the transmission, thus is highly likely to have a profound impact on the objective function.
3. Optimization studies pertaining to the operation of energy systems are largely focused only on major components. Besides, these components are optimized independently from each other. This is likely due to the complexity of system-level optimization. While it is generally true that such practices may give results that are close-to-optimal in smaller systems, the impact of ancillaries should not be ignored especially in larger, more integrated systems. It is not inconceivable to operate some major components inefficiently for improved system-level performance, due to the more pronounced roles of ancillaries in highly integrated, interdependent, district-level systems.
4. The optimal performance of the operating energy storage systems in the related work is often determined over an arbitrarily defined time-period, ranging from a day to a week. While the optimal results certainly suggest the benefits of including storage systems in these studies, the computation of the results could be done more efficiently. Arbitrarily choosing the time-period assumes that the energy demands that the system is optimized for remains invariant throughout, which may not be the case, in reality. This results in the methodology being less adaptable to fluctuations. Besides, the consideration of storage systems requires optimization across several time-periods, easily

burgeoning the size of the problem, especially for formulations involving detailed models. Therefore, methods to improve the computational efficiency of these problems are required.

5. Literature on the real-time optimization of urban energy systems only involves component-level optimization due to computational infeasibility. However, if it is possible to optimize a system holistically in real-time, the likelihood of better adaptability under less ideal situations will be improved. Since the use of MILP is widespread and has quick resolution speeds, the combination of RL and MILP could be explored for this purpose.

This thesis is positioned to address the above-mentioned gaps in the literature. Firstly, abstraction techniques were applied to carefully chosen models which reflect the suitable level of detail to the problem formulation. These techniques balanced modeling fidelity with optimization compatibility. Where model abstraction alone is insufficient, a hierarchical framework was introduced to be used in tandem with these abstracted models. This combination provides a systematic approach for optimizing complex energy systems, holistically. Finally, to handle the demands of energy storage systems and real-time optimization, the sliding-window technique and RL were also incorporated in the developed framework.

Chapter 3

Model selection and abstraction

3.1 Overview

The selection of component-level models of energy systems used for case studies in this thesis is presented. Firstly, a brief survey of compatible component models is conducted before justifying the final choice. The selected model is then abstracted as much as possible so that it is compatible for formulation as a MILP. These two aspects are discussed in greater detail in the ensuing subsections. The purpose of this chapter is to provide a background of the abstracted models which will be repeatedly used throughout this thesis.

Two case studies based on existing urban energy systems are used for illustration in this thesis - the first is based on a building-level GCHP system and the second, a district-level cooling system. *Table 3.1* summarizes the list of component-level models required for each of the case studies. Complete formulations require the proposed optimization frameworks, which will be discussed in detail, in the later chapters (*Chapters 4 to 7*).

3.2 Component-level models from the literature

Component-level models, from existing literature, which are required by the case studies in this thesis are reviewed in this subsection (*Table 3.1*). The understanding of these models is crucial to the formulation of optimization problems and the

	<i>Chapter 4 : GCHP system</i>	<i>Chapter 5 and 7 : DCS</i>	<i>Chapter 6 : DCS + thermal storage</i>
Component	Heat pump/chiller	✓	✓
	Cooling tower	✓	✓
	Pump + network	✓	✓
	Heat exchanger	✓	✓
	BIPV	✓	
	Ground heat exchanger (GHE)	✓	
	Electricity storage system (ESS)	✓	
	WAHX	✓	
	Thermal energy storage (TES)		✓

TABLE 3.1: Component-level models required in each case study.

development of the corresponding strategies for solving them. Models that are considered here extend beyond those already used in the related work on similar problems, as they are usually too simplified. The purpose is to first identify these models before abstracting them into black-box models that are compatible with optimization algorithms. Models complexity also has a direct impact on the range of compatible optimization techniques.

3.2.0.1 Heat pumps / chillers

Chillers are just heat pumps operated in reverse, thus they could be represented by the same model. They represent one of the more efficient methods of cold and hot energy production in urban energy systems. Black-box models of heat pumps must accurately predict the coefficient of performance (*COP*, a metric of efficiency) over a range of operating conditions (load, temperatures, etc.). The heat pump models are categorized into four groups - iterative, regression, thermodynamic and machine-learning-based models.

The ‘elemental $NTU - \epsilon$ ’ and the simultaneous equation models are two iterative models of heat pumps [104, 105]. Both models attempt to simultaneously solve for the governing equations for each subcomponent of the heat pump (compressor, evaporating-valve, evaporator and condenser).

Several regression-based models have also since been developed [106–111]. The complexities of the models range from linear to multi-variate polynomial. Although these models have no physical significance, they perform well in the working range for which they were used.

Thermodynamic models are based on the linear relationship between the reciprocal of COP and thermal load and the irreversibilities of thermal transfer [112]. Based on this observation, three models were developed [110, 112–119]. Each of the three models was developed for differing purposes, evidenced by the difference in variables considered. Since they are based on analytical formulae, they exhibit the best extrapolative properties, performing well with very limited training datasets [106, 111].

Machine-learning techniques have also been used to model heat pumps, and they exhibited the best predictive capabilities, within the training dataset [120].

3.2.0.2 Cooling towers

Cooling towers are often used to dissipate heat from the condenser side of the heat pumps when used for cooling (chillers). This is primarily done by taking advantage of the cooling effect from evaporating water. The evaporation of water thus, involves differential heat and mass transfer equations, making these models mathematically involved. Thus, iterative methods are employed to solve such equations [121]. A simpler model proposed by Lu et al. used Taylor’s series expansion to make polynomial approximations of these differential equations [122]. That resulted in a regression-based model.

3.2.0.3 Pump and network

The pump and network need to be modeled simultaneously due to their high degree of dependence. The Darcy-Weisbach equation is often used to describe the pressure-flowrate relationship of fluid motion in pipes. Pump models used in related problems are often regression-based, relating power consumption directly to the flowrate [80, 83, 84]. This implicitly implies that the pressure requirements for any given flowrate are always satisfied.

3.2.0.4 Heat exchangers

All types of heat exchangers are either modeled using the effectiveness-NTU ($\epsilon - NTU$) or log-mean-temperature-difference (LMTD) method [123]. The $\epsilon - NTU$ method is easier to deploy when there is limited information about the operating temperatures of the heat exchanger. Correction factors may have to be added if the configurations deviate from the classical ones.

The modeling of ground heat exchangers (GHE) requires additional considerations such as variation in the ground temperatures, which is typically ignored [124]. The fluctuation of ground temperatures has a significant impact on heat pump based systems. Not considering that will result in a gross over-estimation of operating efficiencies. A ground heat exchanger model, considering the dynamic variation in temperature was formulated for solving with a hybrid differential evolution algorithm [125]. This model takes into consideration the thermal resistance model of the ground, by incorporating soil properties. As evidenced by the results obtained, the variation in ground temperatures had a very pronounced role in the optimal operation plan. A closely related study validated this effect experimentally. Through these results, an empirical ground temperature model was developed [126].

3.2.0.5 Building integrated photovoltaics

The accurate modeling of solar photovoltaics depends on the consideration of several variables - such as the surface area, angle of irradiance, working temperatures, etc. As such, tools from Matlab's Simulink toolboxes are often favored for modeling the individual components in which the solar panel is comprised [127, 128]. The governing equations of each subcomponent are then solved using iterative methods. Where accurate black-box models are required, neural networks were employed [129]. In a bid to develop a simplified empirical model for estimating the usable electricity produced by a solar panel, Neuhaus et al., combined several empirical equations from previous work in literature. That resulted in a multivariate single equation photovoltaic model with prediction accuracies comparable to simulations from commercial programs [130].

3.2.0.6 Electricity storage systems

Accurate modeling of electricity storage systems (batteries), require variables such as current, voltage and the state-of-charge (SOC) to compute the percentage of usable electricity stored in the battery. Typically, equation-based models encompassing these variables are utilized [131]. Battery losses occur due as a result of internal resistance, which correspondingly increases as a function of the SOC. These losses are significant and can amount up to 50% when the battery is near its maximum charge capacity [132]. Most optimization studies deploy battery models with constant charge efficiencies and only consider the input and outputs of usable electricity, measured in kilowatt-hours (kWh) [133].

3.2.0.7 Thermal energy storage

Thermal energy storage (TES) systems can come in many forms, however, in this thesis, only water storage tanks are required for the case study. The inclusion of TES systems into optimization problems requires consideration over several time-periods, making the resulting formulation quite sizable. Often, assumptions such as fully-mixed, singular temperature layers are considered for simplification purposes [134]. To make models more realistic, upper and lower bounds of temperature ranges were considered in an MINLP formulation [135]. In an era where MINLP is still not tractable for reasonably sized problems, a MILP formulation for water storage tanks, considering thermal stratification was developed [136]. This model discretizes the thermal stratification in the tank. and expresses both the temperature and volume of water stored as decision variables. The bilinear relationship between these variables was linearized using Taylor's approximation. The reduction of the formulation into a MILP greatly increases the solvability of the problem.

3.3 Model selection and abstraction

Models that are chosen to represent the components of energy systems in the two case studies are discussed in this section. Equation-based models are preferred as they give a clear insight into the ‘class’ which the resultant optimization problem might fall into. Manipulation and/or simplification of these equations allow the

deployment of well-known techniques (convex, MILP, etc.) and solvers that have a good estimate of the optimum. These models are formulated such that they contribute directly to the primary objective function, which is defined to be electricity consumption.

The abstraction of the selected models to suit a MILP formulation is discussed in the following subsections. MILP was chosen due to the availability of solvers and its widespread use in related problems [18]. In each of the following subsections, justification of the chosen model is first provided, followed by the abstraction process and finally, discussion on the error incurred. Discussions of the error incurred are only presented for models that are based on existing equipment and have been calibrated with raw data.

3.3.1 Electric heat pumps

3.3.1.1 Description

Electric heat pumps are a central component of the two case studies. They produce heating/cooling by extracting and rejecting heat at the evaporator and condenser respectively. *Figure 3.1* illustrates the schematic of a generic electric heat pump. The primary objective of this model is to express the *COP* in terms of the independent (tunable) variables listed in *Table 3.2*. *COP* is essential in the determination of electricity consumption and exhibits a highly non-linear relationship with these variables; hence a model is required.

3.3.1.2 Selected model

Gordon-Ng universal chiller model (GNU) is selected to represent the generic heat pump [118]. The model is based-off analytical equations and can be calibrated with raw data. It is a grey-box model that incorporated laws of thermodynamics and energy balances at heat exchangers with some assumptions of internal and external energy losses. As a result, it displays relatively good predictive capabilities (including extrapolation) despite limited data points [106, 111]. The describing equation for this heat pump model is as follows,

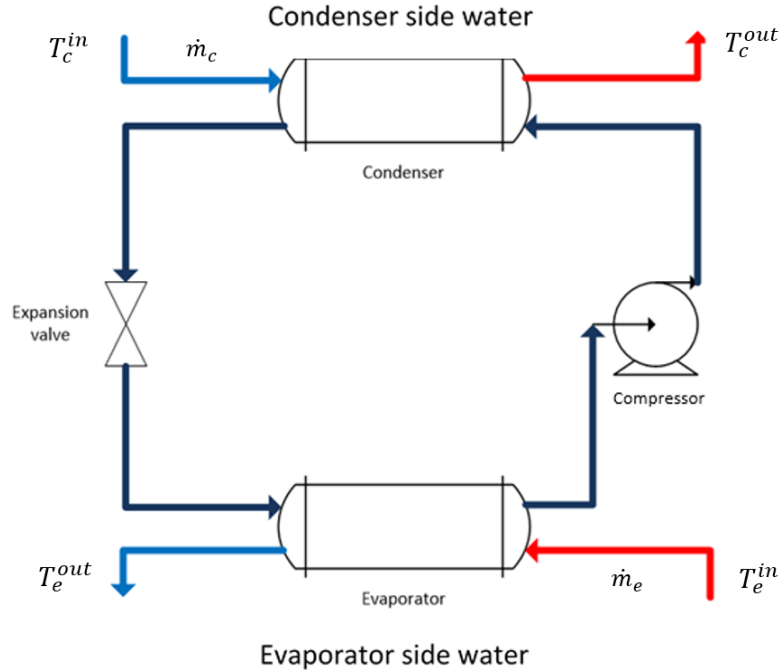


FIGURE 3.1: Schematic of a vapor compression electric heat pump.

	Units	Description
Independent variables		
T_e^{out}	K	evaporator outlet temperature
T_e^{in}	K	evaporator inlet temperature
\dot{m}_e	m^3/h	evaporator flowrate
T_c^{in}	K	condenser inlet temperature
T_c^{out}	K	condenser outlet temperature
\dot{m}_c	m^3/h	condenser flowrate
Dependent variables		
COP		coefficient of performance
\dot{Q}_e	kWh	thermal exchange at the evaporator
\dot{Q}_c	kWh	thermal exchange at the condenser
E_{hp}	kWh	electricity consumed by the heat pump
Parameters		
Cp_w	kJ/kgK	specific heat of water

TABLE 3.2: Independent variables, dependent variables and parameters related to the electric heat pump model.

$$\frac{T_e^{in}}{T_c^{in}} \left(1 + \frac{1}{COP}\right) = \beta_0 \frac{T_e^{in}}{\dot{Q}_e} + \beta_1 \frac{T_c^{in} - T_e^{in}}{T_c^{in} \dot{Q}_e} + \beta_2 \frac{\dot{Q}_e}{T_c^{in}} \left(1 + \frac{1}{COP}\right) \quad (3.1)$$

where β_0 , β_1 and β_2 are derived using regression with raw data.

The steady flow energy equation (SFEE) is invoked [137] to relate \dot{Q}_e and \dot{Q}_c

to their respective fluid flowrates.

$$\dot{Q}_e = \dot{m}_e \times Cp_w \times (T_e^{out} - T_e^{in}) \quad (3.2)$$

$$\dot{Q}_c = \dot{m}_c \times Cp_w \times (T_c^{in} - T_c^{out}) \quad (3.3)$$

The heat rejected at the condenser side is the approximate sum of the compressor work, and the cooling effect produced at the evaporator side for steady-state operation. A constant is added so that the following equation can be calibrated with raw data. Doing so accounts for the inefficiencies in the compressor (i.e. compressor work $\leq \dot{E}_{hp}$).

$$\dot{Q}_c = \alpha_0 \times (\dot{Q}_e + \dot{E}_{hp}) \quad (3.4)$$

where α_0 is derived using regression.

Finally, the relationship between COP , \dot{Q}_e and \dot{E}_{hp} is,

$$COP = \frac{\dot{Q}_e}{\dot{E}_{hp}} \quad (3.5)$$

3.3.1.3 Model abstraction

The characteristic electric heat pump equation described by the GNU model needs to undergo a certain level of abstraction so that it can be used in a MILP. The aim is to express the dependent variable \dot{E}_{hp} in terms of its input variables as linearly as possible. The following steps illustrate how the model is simplified.

1. Use *Equation 3.5* to substitute COP terms in *Equation 3.1* with \dot{E}_{hp} .

$$\frac{T_e^{in}}{T_c^{in}}(1 + \frac{\dot{E}_{hp}}{\dot{Q}_e}) = \beta_0 \frac{T_e^{in}}{\dot{Q}_e} + \beta_1 \frac{T_c^{in} - T_e^{in}}{T_{cond}^{in} \dot{Q}_e} + \beta_2 \frac{\dot{Q}_e}{T_c^{in}}(1 + \frac{\dot{E}_{hp}}{\dot{Q}_e}) \quad (3.6)$$

2. Fixing T_e^{in} and T_c^{in} as parameters reduces *Equation 3.6* into $\dot{E}_{hp} = f(\dot{Q}_e)$.

3. Apply piecewise linearization such that \dot{E}_{hp} varies linearly with \dot{Q}_e within predefined bounds $(\dot{Q}_{e,i}^{min}, \dot{Q}_{e,i}^{max})$.

The resultant piecewise linear formulation is,

$$\dot{E}_{hp} = \sum_{i=1}^n \gamma_{0,i} \dot{Q}_{e,i} + Y_{0,i} \nu_{0,i}, \quad Y_i \in [0, 1] \quad (3.7)$$

$$Y_i \dot{Q}_{e,i}^{min} \leq \dot{Q}_{e,i} \leq Y_i \dot{Q}_{e,i}^{max}, \quad \forall i \quad (3.8)$$

$$\sum_{i=1}^n Y_i \leq 1 \quad (3.9)$$

where $\gamma_{0,i}$ and $\nu_{0,i}$ represent constants to be determined, $\dot{Q}_{e,i}^{min}$ and $\dot{Q}_{e,i}^{max}$ denote predefined bounds according to n number of linear pieces. *Equation 3.9* ensures that no more than one linear piece is activated.

4. Use *Equation 3.2* to substitute $\dot{Q}_{e,i}^{max}$ term in *Equation 3.7*.

$$\dot{E}_{hp} = \sum_{i=1}^n \gamma_{1,i} \dot{m}_e T_e^{out} + \gamma_{2,i} \dot{m}_e + Y_i \nu_{0,i}, \quad Y_i \in [0, 1] \quad (3.10)$$

where $\gamma_{1,i}$ and $\gamma_{2,i}$ are constants to be determined.

The constraint in *Equation 3.8* becomes,

$$Y_i \dot{Q}_{e,i}^{min} \leq \dot{m}_e C p_w (T_e^{out} - T_e^{in}) \leq Y_i \dot{Q}_{e,i}^{max}, \quad \forall i \quad (3.11)$$

5. *Equation 3.10* consists of a bilinear term $(\dot{m}_e T_e^{out})$ which could be linearized using RLT introduced by Sherali et al. [137]. This involved the introduction of additional variables.

- (a) Introduce u and v as variables such that,

$$u = \dot{m}_e + T_e^{out} \quad (3.12)$$

$$v = \dot{m}_e - T_e^{out} \quad (3.13)$$

thus,

$$\dot{m}_e T_e^{out} = \frac{u^2 - v^2}{4} \quad (3.14)$$

- (b) *Equation 3.10* can be expressed entirely in terms of u and v . However it would contain quadratic terms. Piecewise linearization is hence, required again. The following illustrates the final formulation of $\dot{E}_{hp,i}$ in terms of u and v .

$$\begin{aligned} \dot{E}_{hp} = \sum_{i=1}^n \gamma_{3,i} & \left\{ \left[\sum_{j=1}^m \gamma_{4,j} u_j + \nu_{1,j} Y_{u,j} \right] + \left[\sum_{k=1}^m \gamma_{5,k} v_k + \nu_{2,k} Y_{v,k} \right] \right\} + \\ & \left[Y_i \nu_{0,i} \right], \quad Y_i, Y_{u,j}, Y_{v,k} \in [0, 1] \end{aligned} \quad (3.15)$$

$$Y_i \dot{Q}_{e,i}^{min} \leq \left[\sum_{j=1}^m \gamma_{6,j} u_j + \nu_{3,j} Y_{u,j} \right] + \left[\sum_{k=1}^m \gamma_{7,k} v_k + \nu_{4,k} Y_{v,k} \right] \leq Y_i \dot{Q}_{e,i}^{max}, \quad \forall i \quad (3.16)$$

$$Y_{u,j} u_j^{min} \leq u_j \leq Y_{u,j} u_j^{max}, \quad \forall j \quad (3.17)$$

$$Y_{v,k} v_k^{min} \leq v_k \leq Y_{v,k} v_k^{max}, \quad \forall k \quad (3.18)$$

$$\sum_{i=1}^n Y_i \leq 1, \quad \sum_{j=1}^m Y_{u,j} \leq 1, \quad \sum_{k=1}^m Y_{v,k} \leq 1 \quad (3.19)$$

$$\left[\sum_{j=1}^m Y_{u,j} \right] + \left[\sum_{j=1}^m Y_{u,j} \right] - 2 \left[\sum_{i=1}^n Y_i \right] = 0 \quad (3.20)$$

where all γ s, ν s, and bounds (min, max) are constants to be determined. m and n represent the number of linear pieces defined in each stage. *Equation 3.20* ensures that both u and v will be activated and deactivated in tandem.

6. \dot{E}_{hp} could thus be minimized in terms of u and v . Obtained values will be then used to determine \dot{m}_e and T_e^{out} . A similar approach was used on the condenser side to express $\dot{E}_{hp} = f(\dot{m}_c, T_c^{out})$ linearly. \dot{m}_c however, is kept

as a constant as the original model (*Equation 3.1*) is incapable of handling variations in this variable. Further improvements to the heat pump model is required if this feature is needed.

Figure 3.2 summarizes the abstraction process for the electric heat pump model. The process allows the use of MILP to solve the following problem type with T_e^{in} and T_c^{in} kept as parameters.

$$\begin{aligned} \text{minimize} \quad & \dot{E}_{hp} = f(\dot{m}_e, T_e^{out}) \\ \text{subject to} \quad & \dot{Q}_{e/c} = \dot{Q}_d \end{aligned}$$

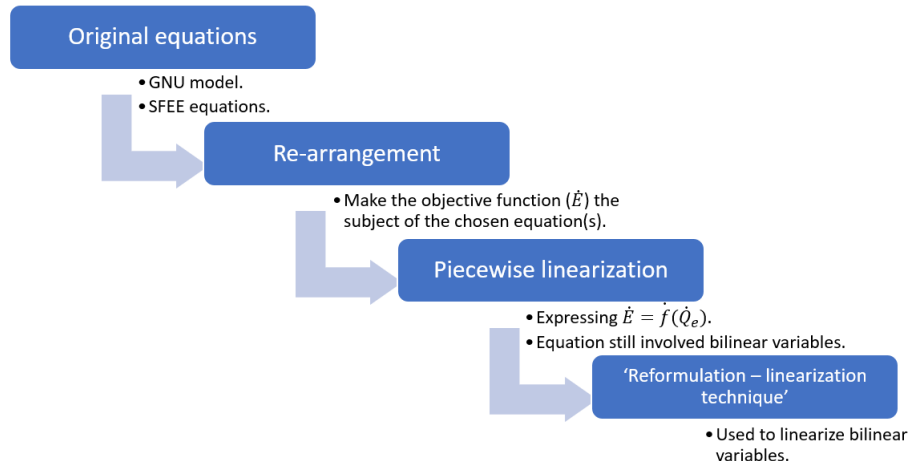


FIGURE 3.2: Summary of the model abstraction process for the electric heat pump.

where \dot{Q}_d represents the thermal demand to be met by the heat pump, and $\dot{Q}_e = f(\dot{m}_e, T_e^{out})$. The black-box model of the electric heat pump is illustrated in *Figure 3.3*. Additional parameters (m, n etc.) are required to be defined separately.

3.3.1.4 Error analysis

Piecewise linearization is used twice in the abstraction process. The mean-squared-error (MAE) incurred as a result of each linearization step is documented in this section. n and m refers to the number of pieces used to for the linearization of *equation 3.7* and *equation 3.14* respectively. The error is computed through comparison of the model outputs (\dot{E}_{hp}) of the original model (*equation 3.1*). The

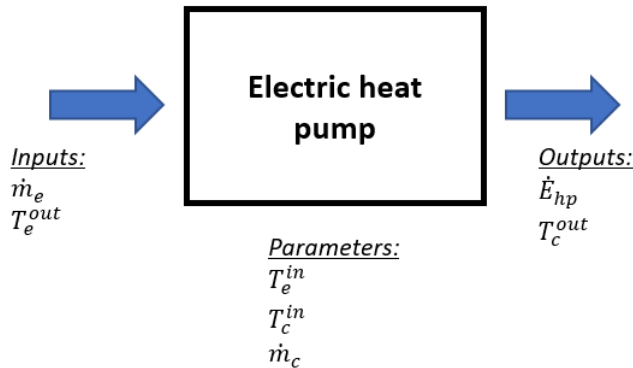


FIGURE 3.3: Black-box model of the electric heat pump.

models are trained using data from a centrifugal chiller (reverse heat pump, from the case study discussed in *Chapter 5*) for the following illustration. The data contains records of the chiller's electricity consumption and all temperatures and flowrates at the evaporator and condenser.

$n =$	Error ($\Delta\dot{E}_{hp}$, %)
2	5.029
4	0.625
6	0.624

TABLE 3.3: Percentage error incurred with different number of linear pieces, n .

Since there is little improvement in percentage error for $n \geq 4$, *Table 3.4* varied m while $n = 4$.

$n = 4, m =$	Error ($\Delta\dot{E}_{hp}$, %)
4	0.753
8	0.490
12	0.422

TABLE 3.4: Percentage error incurred with different number of linear pieces, m while $n = 4$.

Marginal improvement in the output values was observed beyond $m \geq 8$, and the comparison of performances between the GNU and abstracted model is shown in *Figure 3.4*. The MAE incurred is approximately 0.049% despite applying piecewise linearization twice. It is an indication that the integrity of the original model is preserved.

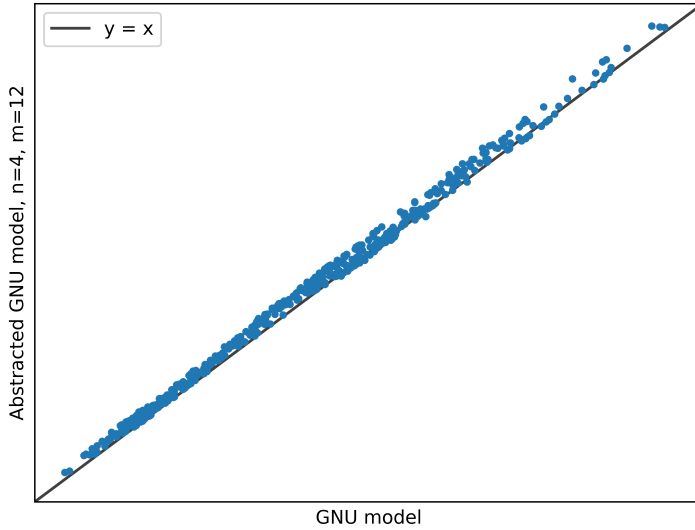


FIGURE 3.4: Plot of \dot{E}_{hp} of the original model vs abstracted model.

3.3.2 Cooling tower

3.3.2.1 Description

Cooling towers are often used for heat rejection in cooling systems. They represent the most economical mode of rejecting heat should there be no natural options (water-bodies etc.). *Figure 3.5* shows the schematic of a general cooling tower unit. The objective of this model is to use the variables listed in *Table 3.5* to predict the outlet temperature, make-up water and electricity consumed.

3.3.2.2 Selected model

The universal engineering model (UEM) for cooling towers was selected. The model was built using a polynomial approximation of the fundamental laws of mass and energy balance. The model illustrated good performance when compared to the often used of Braun's model [122]. The describing equation for the model is as follows,

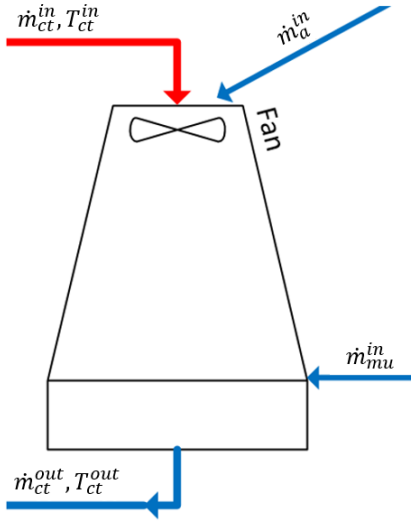


FIGURE 3.5: Schematic of a general cooling tower unit.

	Units	Description
Independent variables		
\dot{m}_{ct}^{in} T_{ct}^{in} \dot{m}_a^{in}	m^3/h K m^3/h	inlet water flowrate inlet temperature inlet air flowrate
Dependent variables		
T_{ct}^{out} \dot{m}_{mu}^{in} \dot{Q}_{ct} \dot{E}_{ct}	K m^3/h kWh kWh	outlet temperature make-up water flowrate heat dissipated electricity consumed by the cooling tower
Parameters		
T_{wb} Cp_w Cp_a T_{mu}^{in}	K kJ/kgK kJ/kgK K	thermodynamic wet-bulb temperature specific heat of water specific heat of air make-up water temperature

TABLE 3.5: Independent variables, dependent variables and parameters related to the cooling tower model.

$$\varepsilon = \beta_0 + \beta_1 \left[\frac{\dot{m}_a^{in}}{\dot{m}_{ct}^{in}} \right] + \beta_2 \left[T_{ct}^{in} - T_{wb} \right] + \beta_3 \left[\frac{\dot{m}_a^{in}}{\dot{m}_{ct}^{in}} \right]^2 + \beta_4 \left[T_{ct}^{in} - T_{wb} \right]^2 + \beta_5 \left[\frac{\dot{m}_a^{in}}{\dot{m}_{ct}^{in}} \right] \left[T_{ct}^{in} - T_{wb} \right] \quad (3.21)$$

where ε is,

$$\varepsilon = \frac{\dot{m}_{ct}^{in} Cp T_{ct}^{in} + \dot{m}_{mu}^{in} Cp T_{mu}^{in} - \dot{m}_{ct}^{out} Cp T_{ct}^{out}}{\dot{m}_{ct}^{out} Cp (T_{ct}^{in} - T_{wb})} \quad (3.22)$$

and β s are derived using regression.

To estimate the make-up water required, it is estimated that 1% of the circulating water is evaporated for a 5.6 K change in temperature [138]. An additional 0.27% is added to account for drift and other forms of water losses according to the manufacturer's specifications. Additionally, a calibration constant is added so that this formula can be calibrated with raw data. The resulting formula was,

$$\dot{m}_{mu}^{in} = \alpha \left\{ \left[0.0027 + \left(0.01 \times \frac{T_{ct}^{in} - T_{ct}^{out}}{5.6} \right) \right] \times \dot{m}_{ct}^{in} \right\} \quad (3.23)$$

Finally, the only component which consumes electricity in the cooling tower unit is the fan. A linear relationship between the flowrate and electricity consumed is assumed. The impact of this assumption on the final objective is small as cooling towers tend to represent a small percentage of electricity consumption of the systems they serve.

$$\dot{E}_{ct} = \gamma \dot{m}_{ct}^{in} \quad (3.24)$$

where γ is a constant to be determined.

3.3.2.3 Model abstraction

Cooling tower models are often complex as they involve heat and mass transfer equations. The following measures are taken to simplify the equations listed in the preceding subsection.

1. Since the value of make-up water is usually very small, it is difficult to get high quality data on its flowrate and temperature. Thus, the assumption that $\dot{m}_{ct}^{in} \approx \dot{m}_{ct}^{out}$ is used for the simplification of *Equation 3.22*.

$$\varepsilon = \frac{T_{ct}^{in} - T_{ct}^{out}}{T_{ct}^{in} - T_{wb}} \quad (3.25)$$

and

$$\frac{T_{ct}^{in} - T_{ct}^{out}}{T_{ct}^{in} - T_{wb}} = \beta_0 + \beta_1 \left[\frac{\dot{m}_a^{in}}{\dot{m}_{ct}^{in}} \right] + \beta_2 \left[T_{ct}^{in} - T_{wb} \right] + \beta_3 \left[\frac{\dot{m}_a^{in}}{\dot{m}_{ct}^{in}} \right]^2 + \beta_4 \left[T_{ct}^{in} - T_{wb} \right]^2 + \beta_5 \left[\frac{\dot{m}_a^{in}}{\dot{m}_{ct}^{in}} \right] \left[T_{ct}^{in} - T_{wb} \right] \quad (3.26)$$

2. For a cooling tower of n individual units, it is assumed that the fluid flowrate \dot{m}_{ct}^{in} through each tower unit is equally divided. That is to maximize the cooling area to fluid ratio, and thus ‘free’ cooling. Fixing the total flowrate in the parallel-pumps network configuration, meant that the flowrate through each tower unit is fixed too.
3. *Equation 3.26* is highly non-linear. Since T_{ct}^{out} and \dot{m}_{ct}^{in} had to be fixed due to the heat pump and parallel-pumps network configuration models respectively, T_{ct}^{out} depended only on variables T_{ct}^{in} and \dot{m}_a^{in} . Regression is used to reduce the order of the equation, making it simpler for linearization.

$$\Delta T_{ct} = \nu_0 T_{ct}^{in} + \nu_1 \dot{m}_a^{in} + \nu_2 T_{ct}^{in} \dot{m}_a^{in} + \nu_3 \quad (3.27)$$

where $\Delta T_{ct} = T_{ct}^{in} - T_{ct}^{out}$ and ν s represent regression constants to be determined.

The bilinear terms in *Equation 3.27* could be linearized using the RLT.

4. The determination of ΔT_{ct} is important in computing the cooling tower unit’s outlet temperature (T_{ct}^{out}) and the volume of make-up water needed (\dot{m}_{mu}^{in}).

Make-up water is not yet considered in the objective function, due to data limitations. Therefore, the above discussed steps enabled the MILP formulation of the following problem.

$$\begin{aligned} & \text{minimize} && \dot{E} = f(\dot{m}_a^{in}, T_{ct}^{in}) \\ & \text{subject to} && T_{ct}^{out} \leq T_{rq}^{out}, \quad T_{ct}^{out} \geq T_{wb}, \end{aligned}$$

where T_{rq}^{out} is the required outlet temperature as determined by the evaporator/-condenser side of the heat pump (constant). *Figure 3.6* illustrates the black-box

model of the cooling tower. *Figure 3.7* summarizes the abstraction process for the cooling tower model.

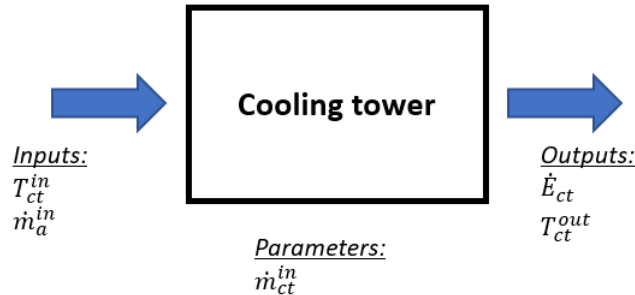


FIGURE 3.6: Black-box model of the cooling tower.

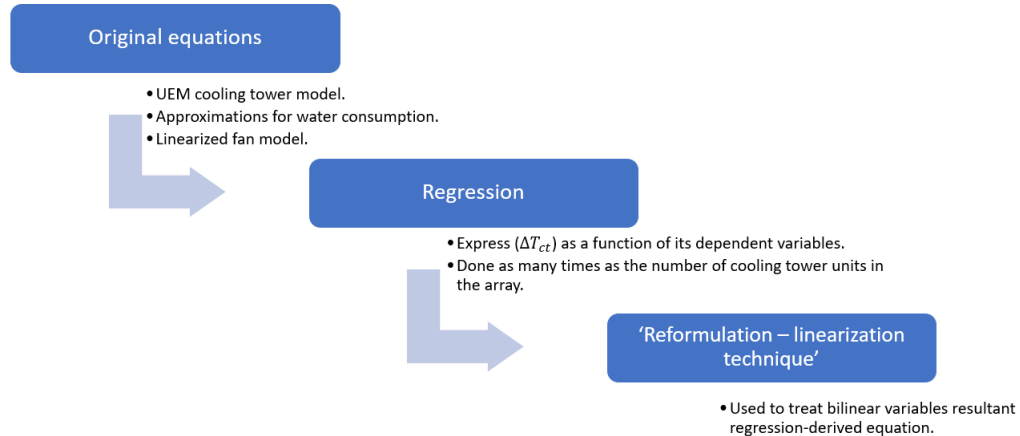


FIGURE 3.7: Summary of the abstraction process for the cooling tower model.

3.3.2.4 Error analysis

Errors incurred using the RLT is not discussed as results obtained are highly similar to that of the heat pump model. The focus of this subsection is to illustrate the impact of applying regression to simplify the original model (UEM). The R^2 value obtained was about 0.8 indicating a relatively lower level of fitness. *Figure 3.8* illustrates the plot of ΔT_{ct} values using the two models. The cooling tower model was calibrated using data from the case study discussed in *Chapter 5*.

The MAE is high. However, it can be reduced to approximately 10% if regression is applied separately to datasets organized by T_{ct}^{in} into three ranges. This was so as the error was greatest at the extremes.

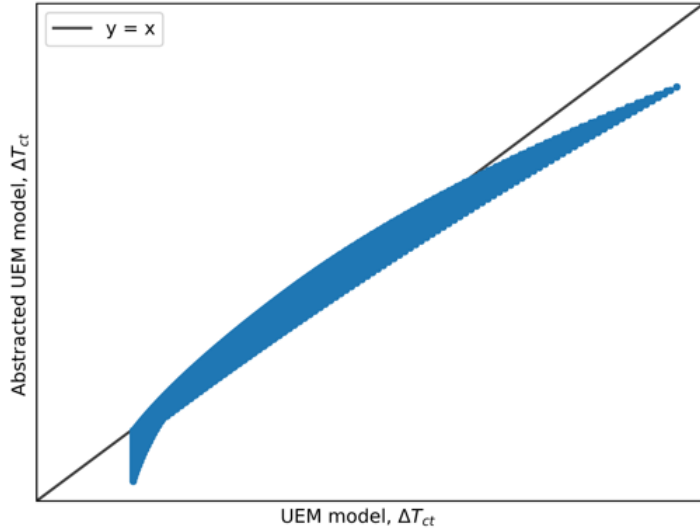


FIGURE 3.8: Plot of ΔT_{ct} values of the abstracted UEM against UEM.

However, the accuracy of this model did not impact the objective function as the contribution of electricity consumption due to cooling towers is the lowest (5-7 %). Even though the electricity output of this model has poor accuracy, the influence of temperature constraints (T_{wb} etc.) can be of value in terms of guiding the operation of cooling towers in the system.

3.3.3 Pump and network

3.3.3.1 Description

Chilled(evaporator side)/warm(condenser side) water produced by heat pumps is transported via the piping network. The pump(s) and (piping) network are modeled collectively due to their high level of dependence. Two models are developed to capture the essence of the commonly used ‘primary-secondary’ pumping scheme (*Appendix A*) which is critical to understand the cause of inefficiency in the system (‘low- ΔT ’ syndrome (*Appendix B*), etc.). These models are designed to output the electricity consumed by pumps and the return fluid temperature while respecting physical and thermodynamic principles/constraints.

The following models will describe the flowrate in two commonly utilized parallel configurations in hydronic systems for thermal energy systems - parallel-pumps and single-pump-parallel network configuration. For the latter, a partial heat exchanger model is embedded; the consumer side of the heat exchanger is not modeled because it is out of the scope of the case studies.

3.3.3.2 Selected models

Problem formulations in the literature reviewed are highly simplified, neglecting the pressure and temperature considerations in networks. Hence, the network models used in this section are formulated using analytical models [139]. Consideration of these factors is essential for addressing operation related problems. The following are the four main principles used to build the models.

1. Pump-network system pressure versus flowrate relationship

The flowrate-pressure relationship is illustrated in this part. *Figure 3.9* represents an example of a pump connected to a network system. A network system refers to any combination of network components (pipes, heat exchangers, valves, etc.) which impedes (pressure drop) fluid flow. Generally, the more complex the system is, the higher the pressure drop penalty incurred. Hence, more pumping power is required to move the fluid.

Figure 3.10 illustrates the pressure-flowrate relationship between the pump and the network system. The operating point of the pump-network system will always be the intersection of the two characteristic curves. Adjusting operating parameters (lowering pump speed, closing valve, etc.) will shift both curves, hence the possible operating points are bounded by the solid blue curve (lowest pressure drop case (fully open valves, etc.) for network system curve), solid red curve (pump operating at maximum speed) and the y-axis.

Any pump curve could be represented by a quadratic equation. The general formula,

$$\Delta P_{sys} = \alpha \dot{m}_{sys}^{1.852} \quad (3.28)$$

where ΔP_{sys} , \dot{m}_{sys} , α represent pressure, system flowrate and network coefficient respectively, was used to model the network system curve.

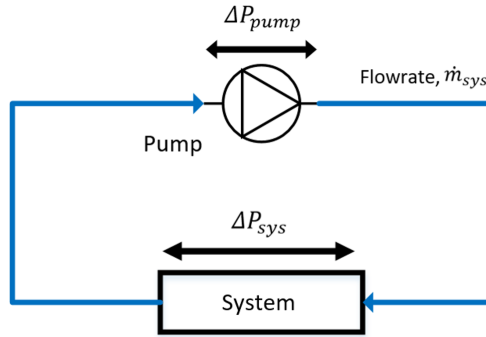


FIGURE 3.9: Example diagram of a pump-network system.

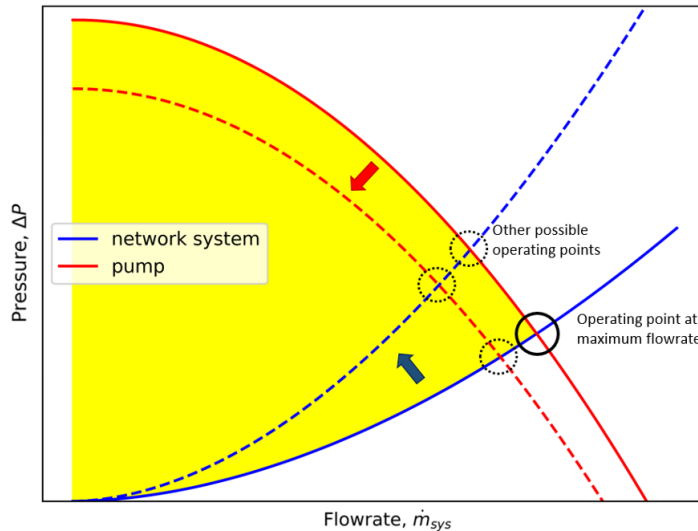


FIGURE 3.10: Example pump-network system curve.

2. Pump electricity consumption for a given network.

Manufacturers of pumps often include the plot of electricity consumption versus flowrate of pumps when they operate at their nominal/maximum speeds. This graph is meant to be used alongside with the pressure versus flowrate graph (*Figure 3.10*). To determine the electricity versus flowrate relationship when the speed of the pump is reduced, the efficiency formula recommended

by Marchi et al. is used [140]. *Figure 3.11* depicts the curves at maximum RPM (bold) and minimum RPM (dotted) for the lowest pressure requirement of a particular pump-network system configuration.

Estimating the electricity consumed by the pump (\dot{E}_{pump}) requires the knowledge of the operating point of the pump-network system configuration. For a given flowrate (\dot{m}_{sys}), the electricity consumed by the pump could be approximated as follows,

$$\dot{E}_{pump} = \frac{\Delta P_{op}}{\Delta P_{max} - \Delta P_{min}} \times (\dot{E}_{pump}^{max} - \dot{E}_{pump}^{min}) \quad (3.29)$$

where the maximum and minimum pressures and pump electricity consumption can be determined by the bounded areas shown in *Figures 3.10* and *3.11*.

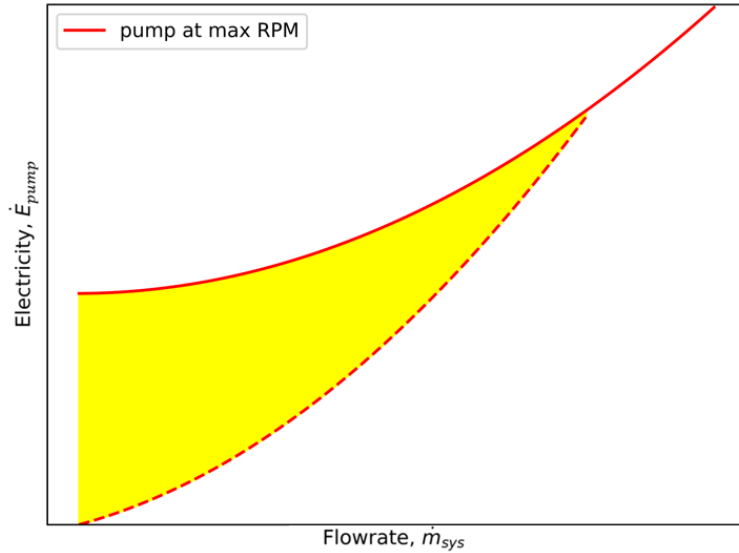


FIGURE 3.11: Example pump electricity consumption curve.

3. Flowrate in parallel networks

The single-pump-parallel network configuration is commonplace in thermal energy systems, especially for distribution. The physics of such a configuration dictates that the pressure in each member of the parallel assembly needs to be identical (*Figure 3.12*). Application of *Equation 3.28* to the depicted setup will reveal that changing the flowrate to any single member (closing a

valve etc.) will affect the flowrates in the rest of the branches and the overall system pressure ($\Delta P_1 = \dots = \Delta P_n$).

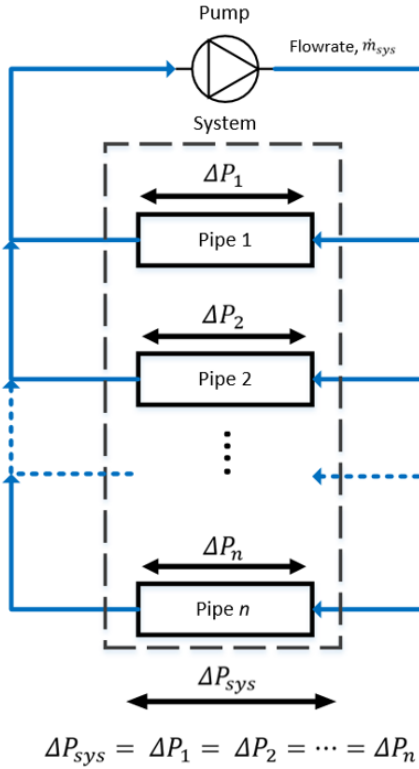


FIGURE 3.12: Example of single-pump-parallel network diagram.

4. Temperature mixing of streams

When multiple fluid streams of different temperatures mix, it is important to determine the temperature of the resultant stream. *Figure 3.13* illustrates three converging streams of different flowrates and temperatures. The objective is to determine the resultant flowrate and temperature of the converged fluid stream. Energy and continuity equations formulae are used to derive *Equations 3.30* and *3.31* [139].

$$\dot{m}^{out} = \dot{m}_1 + \dot{m}_2 + \dots + \dot{m}_n \quad (3.30)$$

$$T^{out} = \frac{\dot{m}_1 T_1 + \dot{m}_2 T_2 + \dots + \dot{m}_n T_n}{\dot{m}^{out}} \quad (3.31)$$

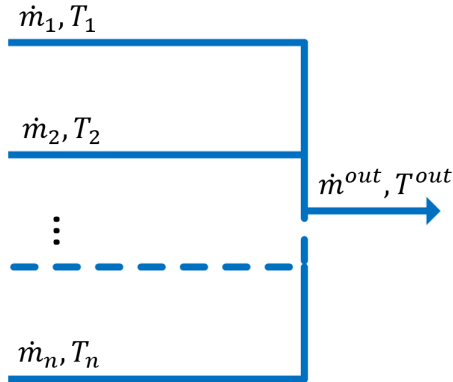


FIGURE 3.13: Example of converging fluid streams of different temperatures.

3.3.3.3 Model abstraction

For simplicity, thermal losses in the networks are not considered as a feature. The methods of determining the electricity consumption of the pump's return/outlet temperatures are common to both types of parallel network configurations.

Network electricity linearization

The objective is to map the shaded areas shown in *Figures 3.10 and 3.11* on to each other. Thus, the goal is to represent $\dot{E}_{pump} = f(\Delta P, \dot{m}_{sys})$ as a single equation. Multi-variate regression is performed, and the following equation ($R^2 \geq 0.98$) was derived.

$$\dot{E}_{pump} = \beta_0 \Delta P_{op} + \beta_1 \dot{m}_{sys} + \beta_2 \quad (3.32)$$

where β s were regression derived constants.

Since the bounds for pressures are defined by the solid blue and red curves (*Figure 3.10*), formulation of the constraints required the application of piecewise linearization on the pump and network system curves.

Piecewise linearization of the network system curve.

$$\Delta P_{sys} = \sum_{i=1}^n \gamma_{0,i} \dot{m}_{sys,i} + \gamma_{1,i} Y_i \quad (3.33)$$

Piecewise linearization of the pump curve at maximum speed.

$$\Delta P_{limit} = \sum_{i=1}^n \nu_{0,i} \dot{m}_{sys,i} + \nu_{1,i} Y_i \quad (3.34)$$

Additional constraints involved.

$$\dot{m}_{sys,i}^{min} \leq \dot{m}_{sys,i} \leq \dot{m}_{sys,i}^{max} \quad \forall i \quad (3.35)$$

$$\sum_{i=1}^n Y_i = 1 \quad (3.36)$$

where γ s, ν s, $\dot{m}_{sys,min,i}$ s, $\dot{m}_{sys,max,i}$ s and Y i's represent constants, linear limits and binary variables respectively.

Network temperature

Equation 3.31 consists of a fraction and bilinear terms. RLT is used to linearize the equation [137]. The following steps detail the process. The objective is to determine the resultant temperature of mixing streams of differing flowrates and temperatures.

1. Fix the total flowrate $\dot{m}^{out} = \sum_{j=1}^m \dot{m}_j$ as a parameter, so that the equation becomes purely the sum of bilinear terms as follows,

$$T_{out} = \dot{m}^{out} \left[\sum_{j=1}^m \alpha_j T_j \right] \quad (3.37)$$

where $\sum_{j=1}^m \alpha_j = 1$.

2. Thus, RLT can be applied. Details are not shown as the process is identical to the heat pump example.

Due to the limitations of *Equation 3.31*, the total flowrate through both the parallel configurations have to be treated as a parameters for the models to be linearized.

3.3.3.4 Parallel-pumps network configuration

Figure 3.14 illustrates the pressure and temperature layers of the parallel-pumps network configuration. The method in *Section 3.3.3.3* is used n times to individually determine the electricity consumption of each pump. Since the total flowrate is a constant, ΔP_{cp} is just a constant to be added on to each of the individual network system curves. This system is not representative of the example shown in *Figure 3.12*. The existence of a pump in each branch means that the pressure difference can be different. However, the pressure difference in the common exit pipe (ΔP_{cp}) is a common addition to all branches.

Determining the resultant outlet temperature of the evaporator network, just requires the application of the method found in *Section 3.3.3.3*. The resultant black-box model of the evaporator network is shown in *Figure 3.15*. *Figure 3.16* summarizes the abstraction process for the parallel-pumps network configuration model.

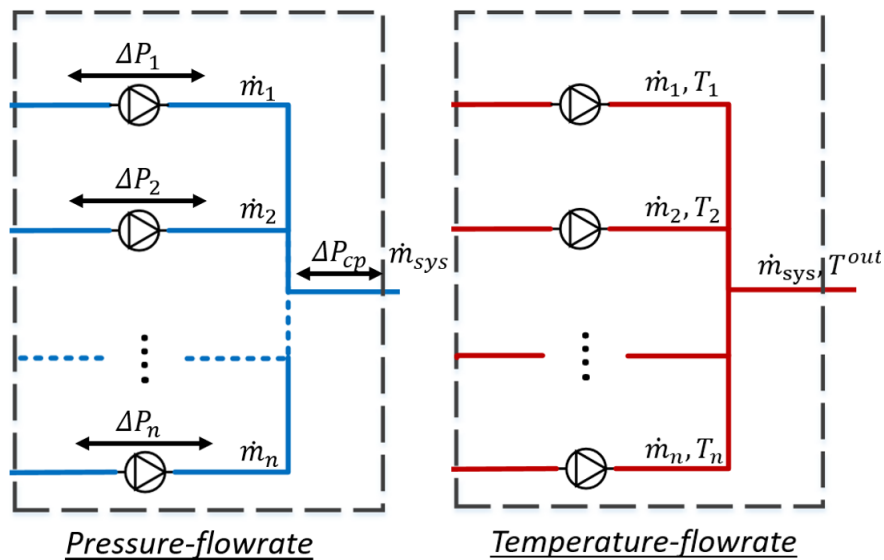


FIGURE 3.14: Abstracted model of the parallel-pumps network configuration.

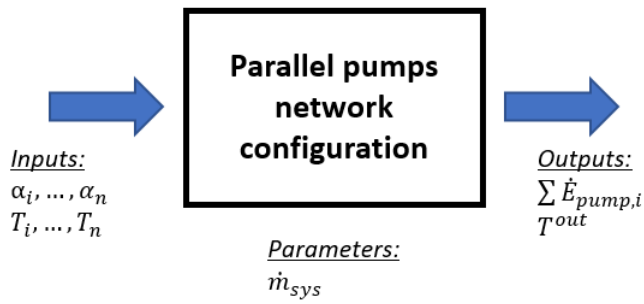


FIGURE 3.15: Black-box model of the parallel-pumps network configuration.

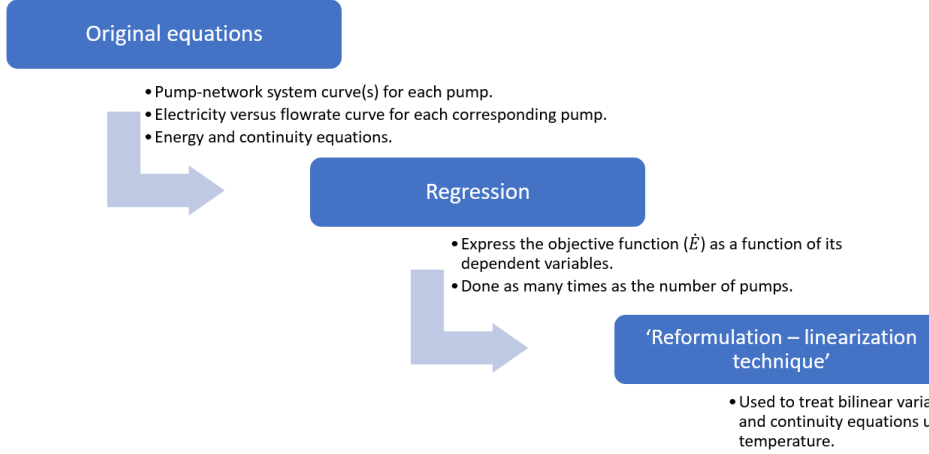


FIGURE 3.16: Summary of the abstraction process for the parallel-pumps network configuration model.

3.3.3.5 Single-pump-parallel network configuration

Figure 3.17 illustrates the pressure and temperature layers of the single-pump-parallel network configuration model. The following lists three additional simplifications that are made for this model.

1. If there exist several pumps, every combination is simplified to a single equivalent pump. Pumps working in parallel or series can be represented by a single characteristic pump curve. This curve is then used to estimate the electricity consumed. For example, if there are n pumps in the unit, there are as many equivalent pumps as their series and parallel combinations. The characteristic curves (pressure and electricity versus flowrate respectively) have to be predetermined. One of the many equivalent pumps has to be selected

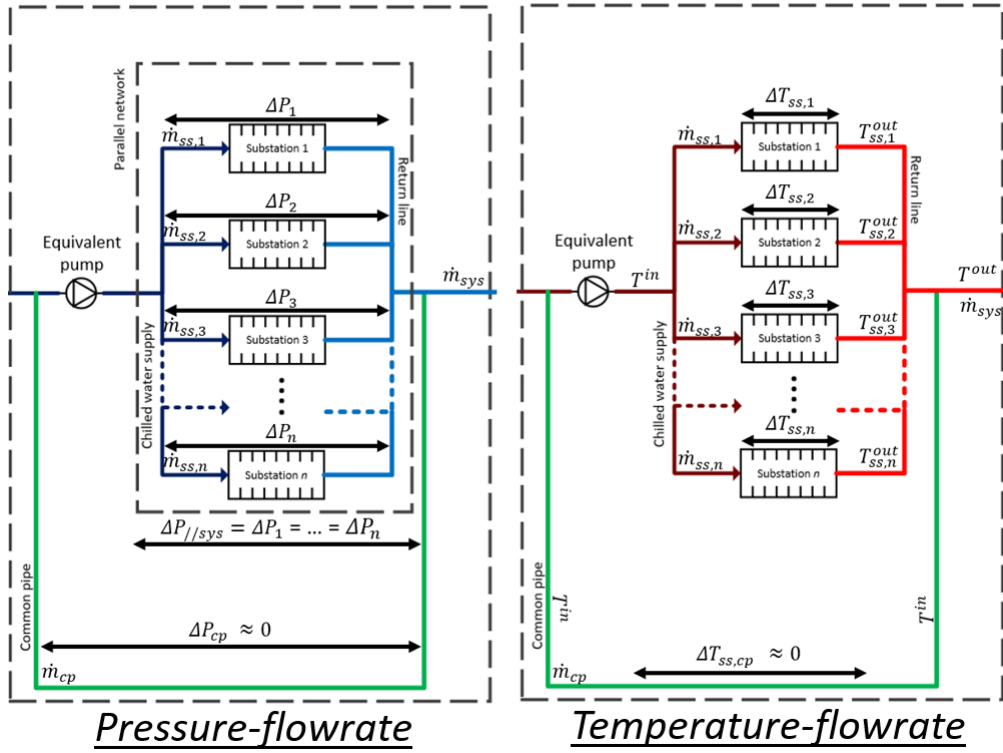


FIGURE 3.17: Abstracted model of the single-pump-parallel network configuration.

and treated as a parameter before the equations of the distribution network model can be determined.

2. The substation (*ss*) model is not yet developed. Hence, with *i*th cooling demand ($\dot{Q}_{d,i}$) given as an input parameter, the temperature difference at the *i*th substation ($\Delta T_{ss,i}$) is dependent on the flowrate through the *i*th substation ($\dot{m}_{ss,i}$) as shown by the following formula.

$$\Delta T_{ss,i} = \frac{\dot{Q}_{d,i}}{\dot{m}_{ss,i} C p_w} \quad (3.38)$$

where Cp is the specific heat of the working fluid.

$$T_{ss,i}^{out} = \frac{\dot{Q}_{d,i}}{\dot{m}_{ss,i} C p_w} + T^{in} \quad (3.39)$$

Based on *Equation 3.37*, the summation of $\alpha_i T_i$ is needed to compute the exit temperature T^{out} (*Figure 3.17*) of the single-pump-parallel network configuration model. Fixing the total flowrate (\dot{m}_{sys}) as a constant will result in the following expression for exit temperature.

$$T^{out} = \sum_{i=1}^m \frac{\dot{Q}_{d,i}}{Cp_w} + \alpha_i T_{ss,i}^{in} \quad (3.40)$$

As such, the RLT could be applied for linearization.

To compensate for the lack of substation models, a constraint was imposed on the $\Delta T_{ss,i}$ so that the ‘optimal’ results generated will be fairly realistic. The constant value $\Delta T_{limit,i}$ was determined manually by considering the specifications of the involved heat exchangers.

$$\frac{\dot{m}_{ss,i} Cp_w}{\dot{Q}_{d,i}} \geq \frac{1}{\Delta T_{limit,i}} \quad (3.41)$$

3. In reality, there is at least a valve installed at every substation. The valves are used to control flowrates (and hence, cooling supply, etc.) into the substations. Partially closed valves limit flowrates by increasing the pressure difference at the substation ($\Delta T_{ss,i}$). Allowing the flowrate in each parallel member (*Figure 3.17*) to be independent will violate the equation in *Figure 3.12*. However, if valves are to be considered, they could implicitly compensate for the difference in pressure as long as the following inequalities are satisfied. Additionally, the difference between ΔP_i and $\Delta P_{//sys}$ can be used to calculate the extent to which the implied valve is open.

$$\begin{aligned} \Delta P_{//sys} &\geq \Delta P_1 \\ \Delta P_{//sys} &\geq \Delta P_2 \\ &\vdots \\ \Delta P_{//sys} &\geq \Delta P_n \end{aligned} \quad (3.42)$$

Since the objective is to minimize electricity consumed by the pumps, minimization of $\Delta P_{//sys}$ will occur naturally. *Figure 3.18* illustrates the black-box model of the single-pump-parallel network configuration. The abstraction process for this model is summarized in *Figure 3.19*.

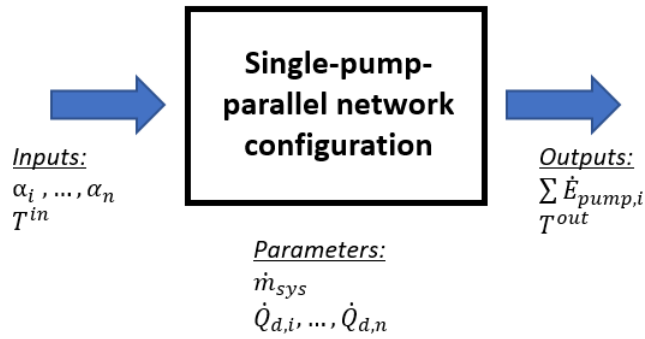


FIGURE 3.18: Black box model of the single-pump-parallel network configuration.

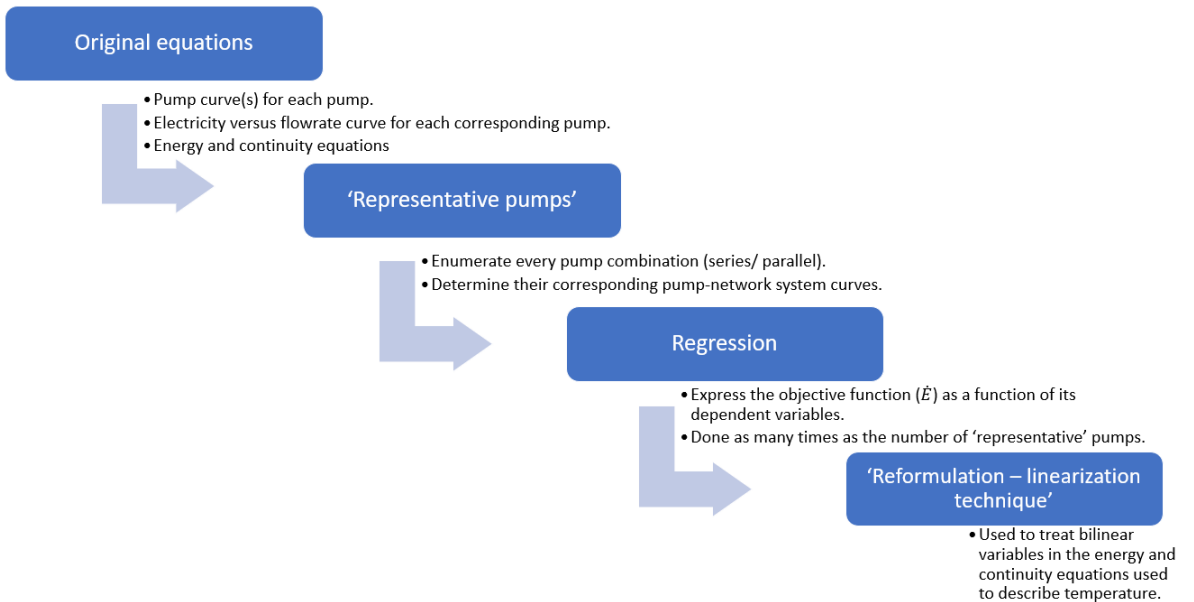


FIGURE 3.19: Summary of the abstraction process for the single-pump-parallel network configuration model.

The objective of the network models is to reflect the feasibility of selected flowrate combinations to each substation. Its contribution to the objective function (electricity consumption of pumps) can influence the selection of variables in other models (heat pumps, cooling tower, etc.).

3.3.3.6 Error analysis

First, the relationship between pressure, flowrate, and electricity consumption data of the pump-network system in the district cooling system (DCS) are simplified to

a regression model as shown by *Equation 3.32*. 75% and 25% of the data were used for training and validation respectively. The R^2 value for the regression is always greater than 0.98 for all the models evaluated. The average MAE error is under 10% if a single regression is performed. Using the parallel pumps network configuration model as an example, pump electricity consumption values obtained using the graphical method and the simplified regression methods are plotted in *Figure 3.20*. From the plot, it could be seen that the error is highest at low electricity consumption. When regression is done separately for high and low flow ranges, the error can be kept under 5% for all models.

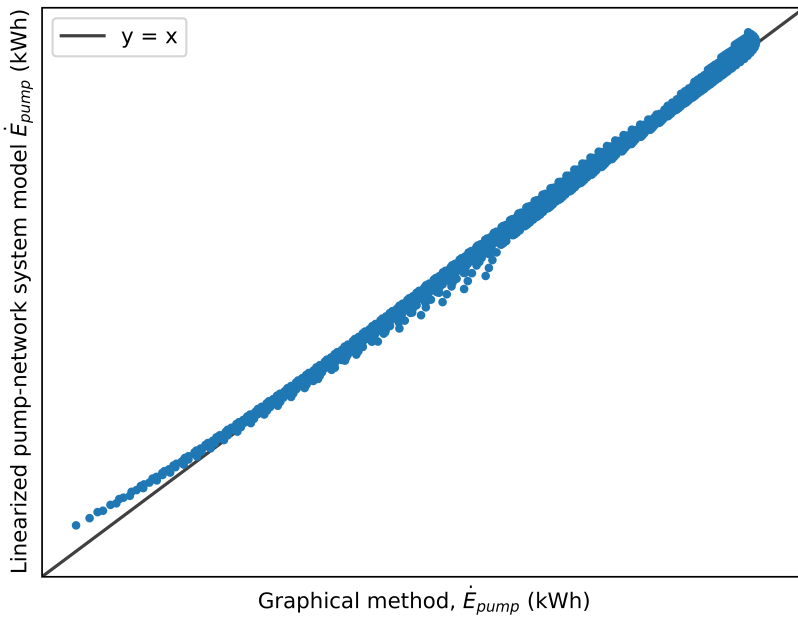


FIGURE 3.20: Plot of \dot{E}_{pump} of the graphical method and regression model.

The next source of error is attributed to the temperature estimation using RLT. For the ease of coding, the number of piecewise linear steps used are the same as the value used for the heat pump model. The average MAE is found to be under 1%.

3.3.4 Water-to-air heat exchanger

3.3.4.1 Description

Water-to-air heat exchangers (WAHX) are typically known as air towers, used for heat rejection/absorption from the environment in thermal energy systems. They are much simpler compared to cooling towers as only sensible heat transfer is involved. *Figure 3.21* shows the schematic of a typical WAHX unit. The objective of this model is to use the variables listed in *Table 3.6* to predict the outlet water temperature and electricity consumed.

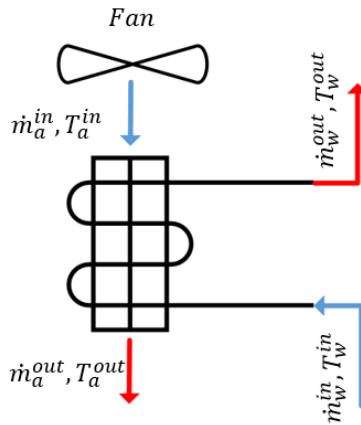


FIGURE 3.21: Schematic of a general water-to-air heat exchanger.

	Units	Description
Independent variables		
\dot{m}_a	m^3/h	air flowrate
\dot{m}_w	m^3/h	water flowrate
T_w^{in}	K	inlet water temperature
Dependent variables		
\dot{E}_{WAHX}	kWh	electricity consumed by the water-to-air heat exchanger
T_w^{out}	K	outlet water temperature
T_a^{out}	K	outlet air temperature
Parameters		
T_a^{in}	K	inlet air temperature

TABLE 3.6: Independent variables, dependent variables and parameters related to the WAHX model.

3.3.4.2 Selected model

To model the WAHX, the LMTD equation that governs counterflow heat exchangers is used alongside SFEEs [141]. This is a theoretical model, not based on any existing hardware, hence only utilizes analytical equations. With the addition of a correction factor (Cf), the LMTD equation can be used to model various cross-flow heat exchangers accurately. For illustration purposes, we assume that the WAHX functions as an air-cooled condenser for a heat pump in cooling mode. The equations used for modeling are as follows,

$$\dot{Q}_{WAHX} = Cf \times UA \left[\frac{(T_a^{in} - T_w^{out}) - (T_a^{out} - T_w^{in})}{\ln \frac{(T_a^{in} - T_w^{out})}{(T_a^{out} - T_w^{in})}} \right] \quad (3.43)$$

$$\dot{Q}_{WAHX} = \dot{m}_w \times Cp_w \times (T_w^{in} - T_w^{out}) \quad (3.44)$$

$$\dot{Q}_{WAHX} = \dot{m}_a \times Cp_a \times (T_a^{out} - T_{amb}) \quad (3.45)$$

where \dot{Q}_{WAHX} is the heat rejected into the environment by the WAHX. To estimate the electricity consumed by the fans, the following linear equation is assumed. The impact of this assumption on the final objective function is small as fans make up for only a very small percentage of the electricity consumption of the systems they serve.

$$\dot{E}_{WAHX} = \alpha_0 \dot{m}_a \quad (3.46)$$

where α_0 is a constant to be determined.

3.3.4.3 Model abstraction

The LMTD equation is relatively complex as it involves logarithmic and fractional terms. The following measures are taken to simplify the equations listed in the preceding subsection.

1. \dot{Q}_{WAHX} can be expressed directly in terms of T_w^{out} , \dot{m}_w and \dot{m}_a through the manipulation of Equations 3.43 to 3.45. Since $T_a^{in} = T_{amb}$, T_a^{in} also becomes a parameter.
2. For all manufacturer's documentation on similar WAHXS, there always exists a nominal approach temperature (T_{app}) between the cold and hot streams passing through the heat exchanger. This minimum temperature value exists to ensure that there is always a temperature gradient for thermal exchange. For simplification purposes, this value is treated as a constant.

$$T_{app} = T_{amb} - T_w^{out} \quad (3.47)$$

3. Discretizing \dot{m}_w , permits \dot{Q} to be a single-valued function of \dot{m}_a . Regression can then be used to linearize this relationship. This also enables \dot{E}_{WAHX} to be directly related to \dot{Q}_{WAHX} through equating Equations 3.46 and 3.48.

$$\dot{Q}_{WAHX} = \beta_0 \dot{m}_a \quad (3.48)$$

where β_0 is a constant to be determined.

The purpose of the abstraction process for the WAHX is to use it in a MILP in the following manner,

$$\begin{aligned} & \text{minimize} && \dot{E}_{WAHX} = f(\dot{m}_a) \\ & \text{subject to} && \dot{Q}_{WAHX} \geq \dot{Q}_{rq}, \end{aligned}$$

where \dot{Q}_{rq} is the required heat to be rejected by the heat pump into the environment. Figure 3.22 illustrates the black-box model of the WAHX. The abstraction process for the WAHX is summarized in Figure 3.23.

3.3.4.4 Error analysis

Figure 3.24 shows the plots of the predicted \dot{Q}_{WAHX} values of the abstracted WAHX and analytical-equation-based models. The R^2 values obtained were consistently very high (≥ 0.98) for the predefined WAHX parameters set for the case

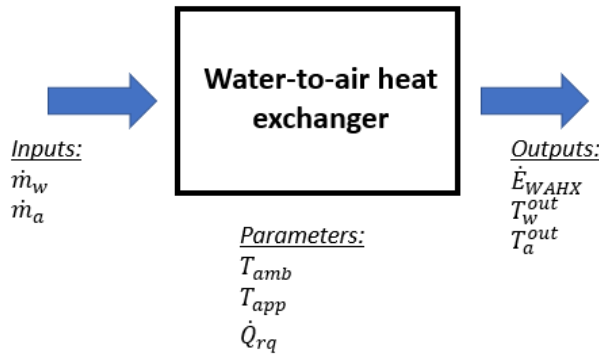


FIGURE 3.22: Black-box model of the water-to-air heat exchanger.

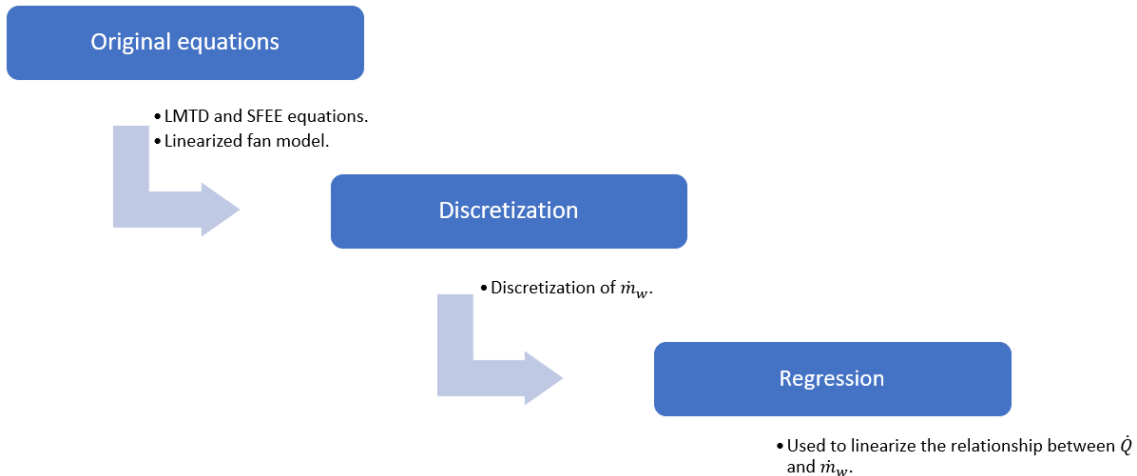


FIGURE 3.23: Summary of the abstraction process for the water-to-air heat exchanger model.

study presented in [Chapter 4](#). The MAE obtained is slightly under 10%. This is indicative of a good approximation made by the linear equation.

3.3.5 Other models

This subsection details the remaining models that are required for the case studies. Models listed need little to no abstraction - they are either extracted directly from literature or just discretized, hence not discussed in as much detail as those above.

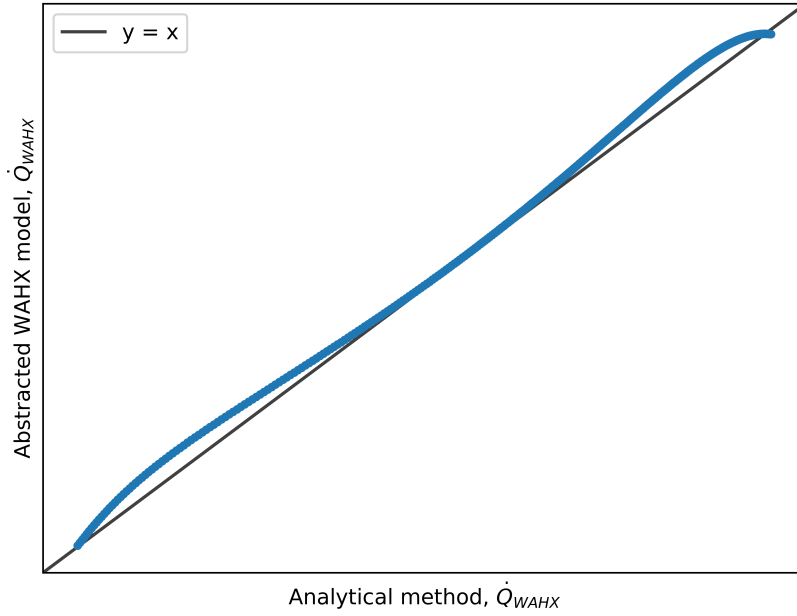


FIGURE 3.24: Plot of \dot{Q}_{WAHX} of the analytical method and regression model.

3.3.5.1 Building integrated photovoltaics

BIPVs are solar PVs which are integrated onto the building, in the form of roofs and facades. They function as an alternative source of electrical power from the grid. The objective of this model is to use ambient conditions to determine the useful electrical energy generated. *Table 3.7* documents the variables and constants related to this model.

The usable electricity (\dot{E}_{PV}) produced by the BIPVs is essentially not tuneable as the independent variables of this model is only represented by ambient conditions (parameters). Hence, there is no need for model abstraction. The equation-based BIPV model proposed by Neuhaus et al. is used in this thesis [130]. Finally, the case study (*Chapter 4*) in this thesis uses the same dataset as in the paper, hence, the errors incurred are identical, averaging about 6.2%. *Equation 3.49* describes the BIPV model, which was selected. The black-box model of the BIPV model is shown in *Figure 3.25*.

	Units	Description
Independent variables Gi_{ω} T_{amb}		global inclined irradiance arriving at a surface ambient temperature
Dependent variables \dot{E}_{PV} T_{PV}		electricity produced temperature of the photovoltaic surface
Parameters PV_{sf} $\eta_{PV,i}$ $\eta_{INV,i}$ $loss_{mm}$ $loss_{OHM}$ $Ktemp$		surface area of the photovoltaic cells efficiency of the i^{th} surface efficiency of the inverter mismatch losses ohmic losses photovoltaic temperature coefficient

TABLE 3.7: Independent variables, dependent variables and parameters related to the BIPV model.

$$\dot{E}_{PV} = \left[PV_{sf} Gi_{\omega} \eta_{PV} \eta_{INV} \times (1 - loss_{mm}) \times (1 - loss_{OHM}) \right] \times (1 + (T_{PV} - T_{amb} \times Ktemp)) \quad (3.49)$$

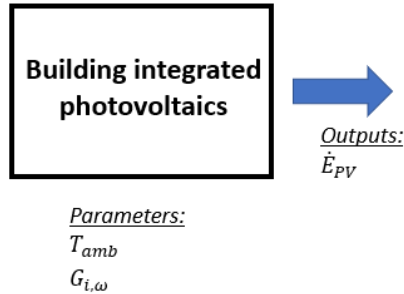


FIGURE 3.25: Black-box model of the BIPV.

3.3.5.2 Electricity storage system

Due to lack of data, a simple battery model is assumed for use as an electricity storage system (ESS) for estimating the potential cost savings from storing electricity when the unit cost is favorable [133]. An efficiency term (η_{ESS}) is used to penalize the SOC (\dot{E}_{ESS}) each time the ESS is charged. This means that the input electrical energy in the previous time-period (t) is always more than required in the current time-period ($t+1$). To incorporate the effect of diminishing efficiencies as the SOC increases, values of η_{ESS} in *Equation 3.50* is discretized. The variables

and parameters of the ESS model is documented in *Table 3.8* and *Figure 3.26* summarizes the corresponding black-box model.

	Units	Description
Independent variables $\dot{E}_{ESS,t}^{in}$	kWh	inflow charge from the current time-period
Dependent variables $\dot{E}_{ESS,t+1}^{out}$	kWh	outflow charge in the next time-period
Parameters η_{ESS}		storage efficiency

TABLE 3.8: Independent variables, dependent variables and parameters related to the ESS model.

$$\dot{E}_{ESS,t+1}^{out} = \eta_{ESS} \dot{E}_{ESS,t}^{in} \quad (3.50)$$

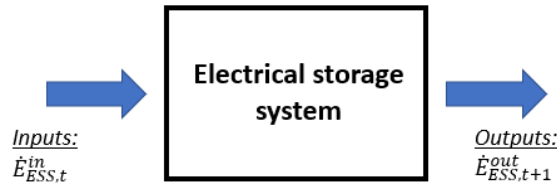


FIGURE 3.26: Black-box model of the ESS.

3.3.5.3 Ground heat exchangers

Ground heat exchangers at the building-level typically exist as borehole heat exchangers. These heat exchangers facilitate thermal exchange between the working fluid of heat pumps and the ground. The working fluid used is typically water. Two models are addressed in this subsection - the heat exchanger model and the ground temperature model. *Table 3.9* shows the variables and constants of the GHX model. For illustration purposes, only the case where the working fluid has to be cooled down by the ground, i.e., a heat pump in cooling mode, is considered.

Heat exchanger model

Similar to the WAHX model, the LMTD equation is used to model the thermal interactions in the heat exchanger, with the only difference being the assumption

	Units	Description
Independent variables		
$\dot{m}_{w,t}$ $T_{w,t}^{in}$	m^3/h K	water flowrate in the current time-period inlet temperature in the current time-period
Dependent variables		
$T_{g,t}$	K	ground temperature in the current time-period
Parameters		
$T_{g,t+1}$ $T_{w,t}^{out}$	K K	ground temperature in the next time-period outlet water temperature in the current time-period

TABLE 3.9: Independent variables, dependent variables and parameters related to the GHX model.

that for every time-period (t), the ground temperature remains invariant (T_g) [141]. T_g is only allowed to vary between time-periods. Through this assumption, it is possible to model the GHE as though the fluid stream is having thermal exchange with a surface of constant temperature.

Equation 3.51 details the LMTD formula used for the GHE. Using *Equations 3.51* and *3.52*, \dot{Q}_t can be expressed as a single-valued function of $T_{w,t}^{out}$ for fixed values of $\dot{m}_{w,t}$ and $T_{g,t}$. This enables the estimation of the return temperature value to the heat pump, which is essential for the calculation of the *COP*.

$$\dot{Q}_t = C_f \times U A \left[\frac{(T_{g,t} - T_{w,t}^{out}) - (T_{g,t} - T_{w,t}^{in})}{\ln \frac{(T_{g,t} - T_{w,t}^{out})}{(T_{g,t} - T_{w,t}^{in})}} \right] \quad (3.51)$$

$$\dot{Q}_t = \dot{m}_{w,t} \times C p_{w,t} \times (T_{w,t}^{in} - T_{w,t}^{out}) \quad (3.52)$$

Ground temperature model

To approximate the variation of T_g with the amount of thermal energy rejected, curve fitting methods are used. The equations used are deducted from the shape of the plots which are obtained from the initial testing data, performed when the system was first installed. The shape of the curves is consistent with those found in [126]. There are two modes to this model - active and passive, where there is ongoing thermal exchange with the heat pumps and left to recover to its original temperature respectively. *Equation 3.53* describes the gradual heating of the ground when heat is rejected. *Equation 3.54* describes the cooling of the

ground when it is not involved in any thermal exchange over a predefined time-period, t . Similar equations but reflected over the abscissa are used to describe the temperature variation of the ground when it is used as a heat source.

$$T_{g,t} = \alpha_0 \ln \left[\left(\sum_{t=1}^m \dot{Q}_t \right) + 1 \right] + T_{g,init} \quad (3.53)$$

$$\Theta_{t+1} = \alpha_0 e^{(T_{g,t} - T_{g,init})^{\alpha_1}} + \alpha_2 \quad (3.54)$$

where $\Theta_t = T_{g,t} - T_{g,init}$.

Combining both the sub-models

To ensure compatibility with MILP, $T_{g,t}$ is discretized for each cumulative range of $\sum_{t=1}^m \dot{Q}_t$. This provisions for the temperature of the ground to vary in accordance with the total amount of thermal exchange which has already occurred. Hence, for each range of $\sum_{t=1}^m \dot{Q}_t$, $T_{g,t}$ is a constant value which is used to calculate for $T_{w,t}^{in}$. Naturally, with more discretized values, the accuracy of the model is increased correspondingly. *Figure 3.27* summarizes the GHX black-box model.

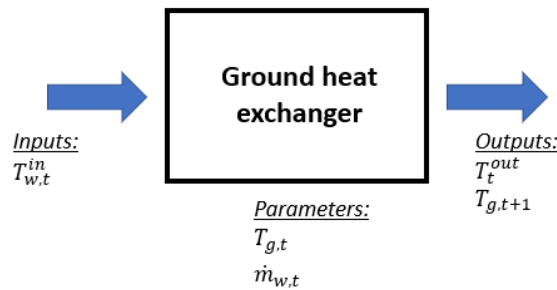


FIGURE 3.27: Black-box model of the GHX.

3.3.5.4 Thermal energy storage

A two-layer water tank with fully mixed layers is assumed for this TES model. A loss coefficient, k_{loss} is incorporated to estimate the amount of usable stored thermal energy for the subsequent time-period ($t + 1$). The schematic of a two-layer TES tank is shown in *Figure 3.28*, and the corresponding variables and parameters are detailed in *Figure 3.10*.

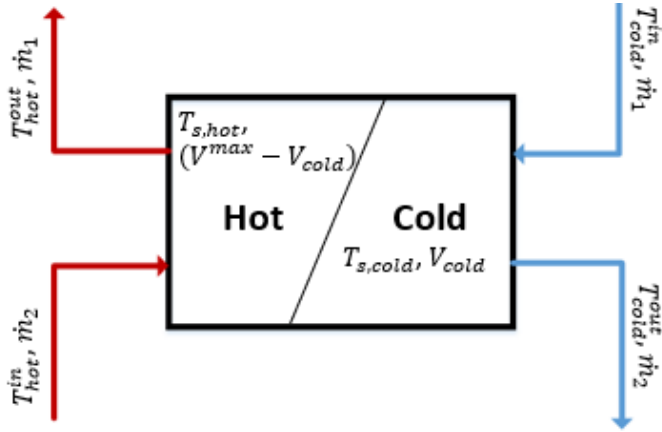


FIGURE 3.28: Schematic of a two-layer TES tank.

	Units	Description
Independent variables		
\$T_{hot}^{in}\$	K	inlet temperature to the hot layer
\$T_{cold}^{in}\$	K	inlet temperature to the cold layer
\$\dot{m}_1\$	\$m^3/h\$	inlet flowrate to hot layer/ outlet flowrate from cold layer
\$\dot{m}_2\$	\$m^3/h\$	inlet flowrate to cold layer/ outlet flowrate from hot layer
Dependent variables		
\$T_{s,hot}\$	K	hot layer temperature
\$T_{s,cold}\$	K	cold layer temperature
\$V_{cold}\$	\$m^3\$	cold layer volume
\$T_{cold}^{out}\$	K	outlet temperature of the cold layer
\$T_{hot}^{out}\$	K	outlet temperature of the hot layer
Parameters		
\$V^{max}\$	\$m^3\$	maximum volume of the tank

TABLE 3.10: Independent variables, dependent variables and parameters related to the TES model.

For simplicity, the TES model can only operate in either charging or discharging mode only. For illustration purposes, only equations relating to cold water charging and discharging are considered in the following equations. Hot water charging only involves exchanging the corresponding hot and cold variables and is not discussed. The subscripts denote the corresponding time-periods (t) they represent. The cold water charging or hot water discharging mode equations are as follows.

$$T_{s,cold,t+1} = (1 + k_{loss}) \times \frac{T_{cold,t}^{in} \dot{m}_{1,t} + T_{s,cold,t} V_{cold,t}}{\dot{m}_{1,t} + V_{cold,t}} \quad (3.55)$$

$$V_{cold,t+1} = \dot{m}_{1,t} + V_{cold,t} \quad (3.56)$$

$$\dot{m}_{2,t} = 0 \quad (3.57)$$

$$T_{hot,t}^{out} = T_{s,hot,t} \quad (3.58)$$

$$T_{s,hot,t+1} = k_{loss} \times T_{s,hot,t} \quad (3.59)$$

A simplified TES model used by Schütz et al. is deployed to verify the optimization approach which will be introduced in *Chapter 6* [136]. Instead of fixing the volume in each layer as parameters, the temperature is discretized. Additionally, by fixing the value of T_{hot}^{in} as a parameter and letting $T_{hot}^{in} = T_{hot}^{out}$ reduced calculations on the hot-side of the TES. Consequently, the above equations can be simplified as follows,

1. Cold water charging mode

$$\dot{Q}_{cold,t}^{in} = \dot{m}_{1,t} \times Cp_w \times (T_{hot}^{out} - T_{cold,t}^{in}) \quad (3.60)$$

$$\dot{Q}_{s,cold,t+1} = \dot{Q}_{cold,t}^{in} + \dot{Q}_{s,cold,t} \quad (3.61)$$

$$\dot{m}_{2,t} = 0 \quad (3.62)$$

2. Cold water discharging mode

$$\dot{Q}_{cold,t}^{out} = \dot{m}_{2,t} \times Cp_w \times (T_{hot}^{out} - T_{cold,t}^{out}) \quad (3.63)$$

$$\dot{Q}_{s,cold,t+1} = \dot{Q}_{cold,t}^{out} - \dot{Q}_{s,cold,t} \quad (3.64)$$

$$\dot{m}_{1,t} = 0 \quad (3.65)$$

Hence, by discretizing the values which T_{cold} can assume, \dot{Q}_{cold} can be expressed solely as a function of \dot{m}_{cold} , making the equation linear and compatible with the MILP format. The black-box model of the TES is shown in *Figure 3.29*.

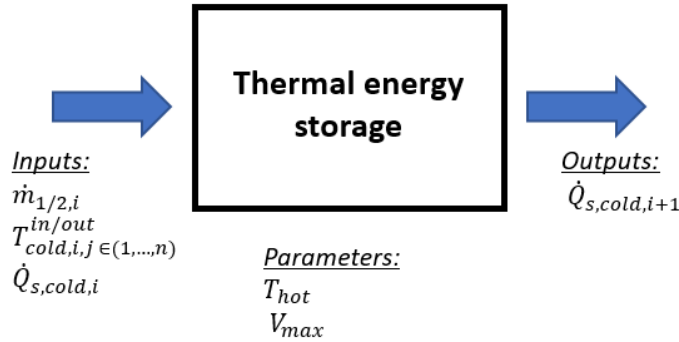


FIGURE 3.29: Black-box model of the TES.

3.3.6 Summary

The abstraction process is critical in increasing the solvability of the optimization problem. It enabled models of higher complexity to be optimized with more realistic results generated. This aspect has been missing from optimization problems related to urban energy systems. The benefit of model abstraction is clearly highlighted in *Chapter 4*.

Despite various attempts to linearize the models, however, there are certain variables that had to be left out (treated as parameters) in the abstraction process. Thus, there is a need for other means of dealing with such variables, if required (*Chapter 5*). Errors incurred in the abstraction process are generally low, thereby indicating the preservation of the integrity of the original models.

Chapter 4

Holistic optimization using mixed integer linear programming

4.1 Overview

Two essential criteria have to be met for the results of optimization studies on the operation of urban energy systems to be useful - the expression of decision variables which are tuneable, and the modeling of interactions among the critical components of the system. The latter criterion ensures that the solution space of the problem is thoroughly explored, i.e, optimized holistically. Holistic optimization is paramount, given that components within the system are highly interdependent.

The judicious use of abstraction techniques on carefully selected component-level models is used to satisfy the required criteria (*Chapter 3*). The importance of these criteria, especially for operation optimization is highlighted in this chapter through the implementation on a case study based on an existing building-level GCHP system, which is an example of an urban energy system. The limitations of the existing literature on optimizing the operations of the ground-coupled heat pump (GCHP) system is first, briefly highlighted. Subsequently, a detailed description of the case study and its associated limitations is presented. The naturally accompanying problem formulation is then, shown in *Section 4.4*, before concluding with a discussion on the insights and limitations gained from this optimization

¹The work in this chapter is under review in [142]

study. This piece of work has just been submitted to the *Energy and Buildings* journal and is currently under review [142].

4.2 Introduction

A GCHP system is an example of a centralized heating and cooling system which transfers heat to, or from the ground. Enhanced efficiency due to lower compressor-lift is the primary reason for the increasing popularity of GCHP systems [143, 144]. After a certain depth, the temperature of the ground is relatively invariant to ambient conditions, making it an ideal heat source or sink depending on heating or cooling requirements [145]. Given that space conditioning in buildings account for up to 13% of the global final energy use, any attempt to reduce this statistic could not be more welcomed [146]. The potential of GCHP systems in reality, however, is often not fully realized owing to the difference in design and operating conditions [147]. The slow dissipation of thermal energy in the ground is a consequence of the inferior thermal conductivity of the soil. The outcome is the gradual degradation of the temperature and performance of the ground as a heat source or sink, which threatens to negate the only advantage of GCHPs. These issues are much more pronounced in regions dominated by either heating or cooling, as the ground is hardly left to fallow.

Rigid control strategies based on pre-defined setpoints, or which are only concerned with maximizing efficiency at the component-level exacerbate these problems [148]. These measures disregard the cascading effect on the system level, thereby inhibiting the ability of the GCHP system to adapt appropriately under less desirable operating circumstances. Therefore, the focus of this work is to comprehensively explore the solution space mapped by tuneable variables of the GCHP system using mathematical optimization techniques. This permits insights into possible means of improving the system-level efficiency without the incurrence of high monetary costs, to be gained.

4.2.1 Ground-coupled heat pump (GCHP) system

A GCHP system leverages on thermal exchange with the ground for efficiency gains. Regardless of the season, comfortable room temperature is typically closer to the ground rather than the ambient air temperature. The smaller temperature difference reduces the mechanical load on the compressor of the heat pump, which translates into a superior efficiency when compared to traditional systems.

Figure 4.1 illustrates a GCHP system serving the *architectures dynamiques reconfigurables pour systèmes embarqués autonomes mobiles* (ADREAM) building of the *Laboratoire d'analyse et d'architecture des systèmes - Centre national de la recherche scientifique* (LAAS-CNRS) laboratory. The ADREAM building hosts an experimental platform for optimized energy networks, BIPV research, and smart grids, with the purpose of simulating zero-energy strategies according to the definitions of zero-energy buildings (ZEB) [149].

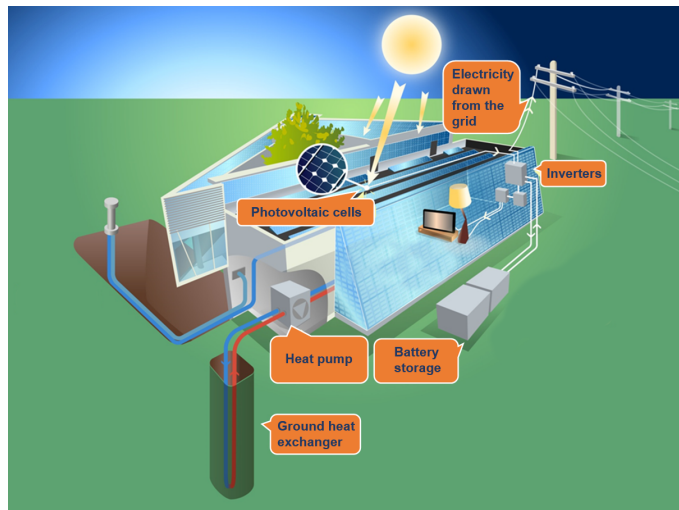


FIGURE 4.1: Layout of a GCHP system serving a laboratory.

Bore-hole heat exchangers are commonly used in systems of such scale to execute the thermal exchange with the ground. In cooling mode, hot water from the condensers of the heat pumps is circulated and cooled down by the ground. The reverse is true during heating mode. These heat exchangers are usually installed in parallel and drilled to a depth deep enough so that the ground temperature remains relatively uniform in spite of ambient conditions.

4.2.2 Objectives

Two essential criteria have to be met for the results of the optimization study to be useful - the expression of decision variables which are tuneable in reality, and the modeling of interactions between the critical components of the GCHP system. The same cooling or heating demand could be fulfilled by countless combinations of component setpoints, each with a different impact on global system-level efficiency. Non-linearities inherent within the governing equations of the component models (heat pump, pump, ground heat exchanger) further compounds the complexity of the ensuing optimization problem. Component-level optimization categorically denies the existence of scenarios whereby a compromise on the efficiencies of some components of the GCHP system could enhance the system-level performance. This effectively prunes the already restricted solution space of the problem through the introduction of unnecessary constraints, explaining why component-level optimization is less impactful than a holistic approach for operation purposes.

As a pre-requisite to the formulation of the optimization problem, models that appropriately express the workings of each component of the GCHP system as a function of tuneable variables (flowrate, temperature setpoint, pressure) are first identified. These models are then abstracted in a fashion whereby the resultant formulation is compatible with the MILP format (*Chapter 3*). That requires a prudent exploitation of case-study specific information for the balancing of model fidelity and compatibility for optimization.

This optimization strategy is then applied to several scenarios of a case study based on an existing GCHP system from the ADREAM building in Toulouse. Throughout the four scenarios defined, a single component is progressively added to the optimization problem before investigating its impact on either of the defined objective functions - total electricity consumption or operating cost. Through the results of the case study, the merits of modeling the tight-coupling amongst the GCHP components before performing optimization holistically is explicitly observed. The findings also suggest that hybridizing the GCHP system with a theoretical WAHX as an alternative to thermal exchange with the ground could result in electricity and cost savings of up to 12.7% and 35% over a year.

4.2.3 Literature review

Designing a GCHP system using the popular rule-based methods yield errors ranging anywhere from -21 % to 167%, primarily where the sizing of GHE is concerned [150, 151]. Optimization work on the design of GCHP systems attempts to bridge this gap by utilizing models with higher precision to match the required cooling or heating demands [152, 153]. Such studies try to determine the optimal configuration of equipment sizing such as the heat pump, piping network, with most of the attention paid to the design of GHEs [154, 155]. Where complex multi-energy systems involving GCHPs are concerned, meta-heuristics are often found to be deployed in tandem with simulation-based software such as TRNSYS [156–158].

The deviation between the optimal design and performance will always exist in reality; as it is inevitable to make assumptions about operating conditions [159]. Optimization of GCHP operation entails a different set of requirements - models with higher fidelity and a problem formulation that has reasonable convergence speed [25, 125]. Assumptions such as constant operating coefficients of performance (*COP*) and temperatures of the heat pumps or ground, while they greatly simplify the optimization problem, serve little purpose for operation. Polynomial approximations of complex component models coupled with more robust optimization techniques offer a rational compromise between modeling accuracy and computational efficiency, hence they are often deployed in model predictive control algorithms.

It is well established that evaporating and condensing temperatures have a strong influence on the operating *COPs* of heat pumps. Under specific scenarios, electricity savings of up to 28% could be achieved with the adjustments in space conditioning set-point temperatures [148]. Erosion of the gains in *COPs* is often observed in GCHP systems due to the degradation of ground temperatures [147]. Hybridization of GCHP systems with alternative thermal exchange options, such as cooling towers, alleviates the burden on the ground and permits temperature recovery[160]. Various control strategies ranging from rule-based to the use of artificial neural networks (ANN) methods of toggling between GHEs and the available alternatives resulted in significant *COP* improvements for these systems [161, 162].

GCHP systems, just as heating, ventilation, and air-conditioning (HVAC) systems are also comprised of several energy-consuming components such as heat pumps,

pumps, and heat exchangers, working in tandem. It is not inconceivable for ancillary components to have a significant influence on system-level energy performance. Parallels had to be drawn from studies concerning the holistic optimization of the operation of closely-related systems due to the lack thereof, on GCHP systems [125]. For chiller systems serving commercial buildings, optimization involving ancillaries enabled additional energy savings of 6.5% [94]. The uncovering of counter-intuitive operating strategies which could only have resulted through the modeling of the tight-coupling between the main components and ancillaries of the system are clearly illustrated in [162].

It becomes evident from the review that a gap exists where the optimization of the operation of GCHP systems at the system-level is concerned. The few related studies prioritized the optimal performance of heat pumps for a given thermal load, neglecting the impact of ancillaries [125]. Hence, it is natural to assume that as the complexity of systems increases, the interdependencies between components will naturally be more pronounced, further reinforcing the need for holistic optimization.

4.3 Description of the chosen case study

The case study described in this chapter is based on a functioning GCHP system serving a laboratory in Toulouse (*Figure 4.1*). This laboratory is part of the ADREAM project which focuses on the collective optimization of smart-grids, BIPV, HVAC, and ambient cyber-physical systems [149]. Simulation studies on the GCHP system of interest have since been conducted to identify areas for energy savings manually [163]. The current work is an extension of these studies through the lens of mathematical optimization performed at the system-level.

Analysis of data collected through the numerous sensors installed around the laboratory revealed two key areas to address for improving the energy performance of the GCHP system - improving the operation of the hydronic network and the ground temperatures. Inferior evaporating and condensing temperatures in the winter and summer respectively appeared to adequately explain the deviation between the theoretical and actual efficiencies of the heat pumps. This suggests that

GHEs are likely to have been undersized. Additionally, the rule-based operation inhibited the adaptability of the system for less-than-ideal scenarios. Therefore, the case-study scenarios defined in this chapter attempt to utilize potential improvements in operating practices for enhanced energy performance. The abstracted models of the system components are deployed for this undertaking (*Chapter 3*).

Figure 4.2 illustrates the GCHP system serving the laboratory. It comprises of three identical heat pumps serving a total of five zones of various usage (office, server rooms, laboratories). Depending on the season, the 18 borehole heat exchangers function as either a heat sink or source. The entire GCHP system could be powered by electricity from any combination of the three sources - grid, battery or directly from solar photovoltaics (*Figure 4.1*).

In the following subsections, the case-study scenarios are first defined, before proceeding to the discussion of management of input data. Subsequently, the required models are selected and abstracted according to the requirements of the case-studies. These lay the foundation for selecting the appropriate models and eventually formulating the optimization problem, which will be discussed in greater detail in *Section 4.4*.

4.3.1 Description of the chosen case-study scenarios

With the improvement of the hydronic network and ground temperature performances listed as primary objectives, four case-study scenarios were defined. These scenarios are chosen to progressively optimize the energy performance of the GCHP system so that the final result will be better assimilated. Optimization, when performed at the system-level, tend to lead to results that are not easily appreciable due to the amalgamation of non-linearities in, and interactions among sub-systems.

An alternative thermal exchange option had to be added to the system to reduce the degradation of the ground temperatures (*Figure 4.3*). For that, a water-to-air heat exchanger was chosen to enable the heat pumps to interact with the ambient air, thermally. Consequently, avenues were explored to justify the added monetary investment through the inclusion of battery operation and cost objectives to the optimization problem. Hence, the final model had to include heat pumps

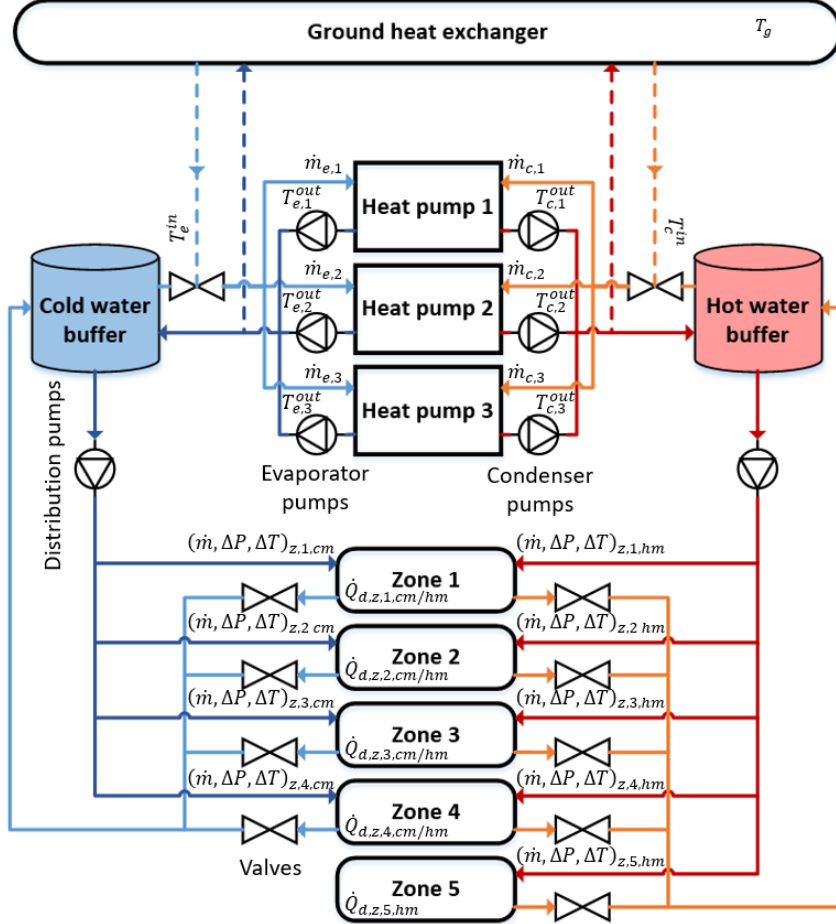


FIGURE 4.2: Schematic of the GCHP system serving the laboratory.

(HP), evaporator and condenser pumps (EP, CP), distribution pumps (DP), GHEs, WAHX, PV, grid electricity (GE) and an energy storage system (ESS).

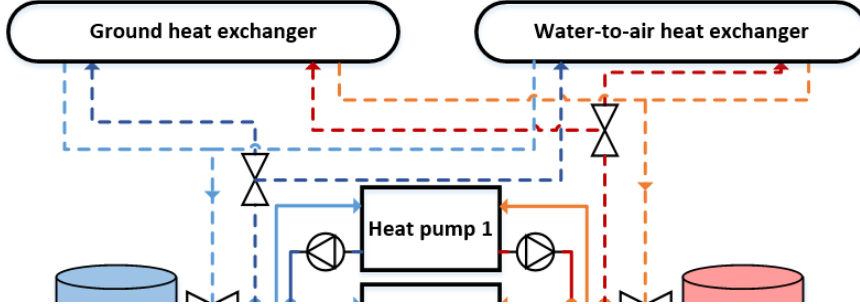


FIGURE 4.3: Schematic of a hybrid GCHP system.

Three base (*bc*) and four optimization cases (*opt*) form the basis of the case-study scenarios. *Table 4.1* documents the base and optimization cases at the component

level. *Table 4.2* describes the objective of each case-study scenario defined in this chapter.

	HP	EP	CP	DP	GHE	WAHX	ESS	OF
<i>bc1</i>	F	F	F	CS	F	NA	NA	NA
<i>bc2</i>	F	F	F	VS	F	NA	NA	NA
<i>bc3</i>	F	F	F	VS	NA	NA	ES	NA
<i>opt1</i>	F	F	F	O	F	NA	NA	\dot{E}
<i>opt2</i>	F	F	F	VS	F	NA	O	$C_{\dot{E}}$
<i>opt3</i>	O	F	F	O	O	O	O	\dot{E}
<i>opt4</i>	O	F	F	O	O	O	O	$C_{\dot{E}}$

Legend: F - fixed, O - optimized, CS - constant speed, VS - variable speed, ES - extra solar, stored, NA - not applicable, OF - objective function.

TABLE 4.1: Base and optimization cases used in case studies.

No.	Objective function	Description
1	\dot{E}	<i>bc1</i> vs <i>bc2</i> vs <i>opt1</i> . Comparison of the energy performance of distribution pumps under three operating strategies - constant speed, variable speed, and when the setpoint pressure is optimized for a given demand.
2	$C_{\dot{E}}$	<i>bc3</i> vs <i>opt2</i> . Cost comparison between the optimized battery operation considering hourly electricity pricing as opposed to store electricity only when there is excess from the BIPVs.
3	\dot{E}	<i>bc3</i> vs <i>opt3</i> . Hybridization of the GCHP system through the addition of a theoretical water-to-air heat exchanger. Comparison of the energy performance of the optimized hybrid system against the current one.
4	\dot{E} and $C_{\dot{E}}$	<i>opt3</i> vs <i>opt4</i> . Cost and energy comparison of the theoretical hybrid GCHP system when holistically optimized for different objectives.

TABLE 4.2: Description of the case-study scenarios.

4.3.2 Management of input data

Ambient and demand conditions are the input data to the optimization problems. Ambient temperature and solar irradiation are needed to determine the amount of usable solar energy. Hourly heating and cooling demands are to be met regardless of the objective function defined.

The building comprises of 36 rooms which are summarized into five zones, grouped by the similarity of their demand profiles. Every month of the year is represented by a single 24-hour-day load profile. These simplifications drastically reduce the resolution time required for the solvers. Since the main purpose of this chapter is to illustrate the benefits of performing holistic optimization on the GCHP system, such approximations are still applicable as they do not mask the important trends (*Section 4.5*). Hourly data was used as input for the case study.

4.3.3 Model selection and abstraction

Table 4.3 documents the list of the abstracted component-level models which are required for representing the case study. The operating cost can be easily determined by multiplying the hourly electricity consumption by the specific unit cost of electricity for the given hour (\dot{E}_{ele_rate}). All model variables which were held as parameters for the sake of linearization will be addressed in *Section 4.5*.

Model description	Section
Heat pump	3.3.1
Evaporator pump-network	3.3.3.4
Condenser pump-network	3.3.3.4
Distribution pump-network	3.3.3.5
GHE	3.3.5.3
WAHX	3.3.4
BIPV	3.3.5.1

TABLE 4.3: Component-level models required for this case study.

4.4 Problem formulation

This section deals with the mathematical formulation of the optimization problem. Inequalities are introduced to enable the component-level models to interact. Depending on the optimization cases defined in *Table 4.1* the objective function could either be the minimization of total operating cost ($C_{\dot{E}}$) or electricity consumption (\dot{E}).

In the following two subsections, the treatment of parameters and variables of the GCHP system are first determined before the formulation of the optimization

problem. Subsequently, the error incurred in the models is discussed, before simulating the defined base cases. The error discussed here pertains to the use of the case-study specific data to calibrate the abstracted models discussed in *Chapter 3*.

4.4.1 Parameters and variables

The fidelity of the component models selected enables a degree of freedom higher than required for the GCHP system. Simplification of the problem formulation is done by only considering the tuneable variables of the system. *Table 4.4* details the treatment of the model variables which were held as parameters for the sake of linearization. This, however, is only specific to the case study.

	Treatment
T_g , η_{ESS}	Discretized to a set of fixed values.
\dot{m}_{nwk} , \dot{m}_w	Fixed values - Evaporator and condenser pumps operate at fixed speeds.
T_c^{in}	Correspondingly discretized due to T_g
T_e^{in}	Fixed value, based on a conservative estimate of the highest possible return temperature which will not compromise on comfort temperatures.

TABLE 4.4: Treatment of temporary parameters in the selected component models.

Three identical heat pumps, coupled with non-adjustable flowrates on the evaporator and condenser sides allow the further simplification of the optimization problem by exploiting the equal-load distribution operating strategy (ELD) [164]. The exploitation of the ELD strategy and the treatment of the parameters enabled the optimization problem to be reduced entirely to a MILP. Variables and parameters of a single time-step (1-hour), before the abstraction procedures, are detailed in *Table 4.5*.

4.4.2 Mathematical formulation

In the case-study scenarios, the GCHP system ie either optimized with respect to the total electricity consumed (\dot{E}) or total operating cost ($C_{\dot{E}}$). The two objective functions are:

Variables	Type	Description
T_e^{in}	Discretized	Return water temperature to the evaporator. Discretized if in heating mode.
T_c^{in}	Discretized	Return water temperature to the condenser. Discretized if in cooling mode.
$T_{e,i}^{out}$	Continuous	Heat pump evaporator setpoint temperature, cooling mode only.
$T_{c,i}^{out}$	Continuous	Heat pump condenser setpoint temperature, heating mode only.
$\dot{m}_{z,i}$	Continuous	Flowrate to each zone.
$\Delta T_{z,i}$	Continuous	Temperature difference of each zone.
$\Delta P_{z,i}$	Continuous	Pressure difference of each zone.
T_g	Discretized	Ground temperature.
η_{ESS}	Discretized	Battery efficiency.
\dot{m}_a	Continuous	Air flowrate for WAHX.
\dot{E}_{ESS}	Continuous	Battery charge/discharge.
\dot{E}_{grid}	Continuous	Grid electricity draw.
Y_{hp}, Y_{WAHX} , etc.	Binary	Binary variables to enable activation and deactivation of each component.
Parameters	Description	
\dot{E}_{pv}	Available solar energy.	
$E_{ele_rate,t}$	Hourly electricity unit cost.	
$\dot{m}_{c,i}$	Condenser flowrate.	
$\dot{m}_{e,i}$	Evaporator flowrate.	
T_{amb}	Ambient temperature.	
$T_{g,init}$	Initial ground temperature.	
T_{app}	Approach temperature for the WAHX.	
$\Delta T_{limit,z,i}$	Temperature difference limit for each zone.	
$\dot{Q}_{d,z,i,cm/hm}$	Cooling/heating demand.	

TABLE 4.5: Variables and parameters of the optimization problem.

$$\begin{aligned}
\text{minimize } \dot{E} = & \sum_{t=1}^m \left[\dot{E}_{WAHX,t} + \dot{E}_{dist,pump,t} + \sum_i^3 \dot{E}_{e,pump,t} + \sum_i^3 \dot{E}_{c,pump,t} + \right. \\
& \left. \sum_{i=1}^3 \dot{E}_{hp,i,t} + \sum_{i=1}^{pwl} (1 - \eta_{ESS,i}) + \dot{E}_{ESS,i,t}^{in} \right] \quad (4.1)
\end{aligned}$$

$$\begin{aligned}
 \text{minimize } C_{\dot{E}} = & \sum_{t=1}^m E_{ele_rate,t} \times \left[\dot{E}_{WAHX,t} + \dot{E}_{dist,pump,t} + \sum_i^3 \dot{E}_{e,pump,t} + \right. \\
 & \sum_i^3 \dot{E}_{c,pump,t} + \sum_{i=1}^3 \dot{E}_{hp,i,t} + \sum_{i=1}^{pwl} (1 - \eta_{ESS,i}) \\
 & \left. + \dot{E}_{ESS,i,t}^{in} \right]
 \end{aligned} \tag{4.2}$$

Equations of the abstracted models discussed in *Section 3*, also serve as constraints in problem formulation. The discretization of T_e^{in} or T_c^{in} and parameterization of \dot{m}_c and \dot{m}_e allows the electricity consumed by the heat pump to be expressed as:

$$\dot{E}_{hp,i} = f(T_{e,i}^{in}, T_{e,i}^{out}, T_{c,i}^{in}) \tag{4.3}$$

Since the flowrate of the evaporator and condenser pumps are constants, $\dot{E}_{e,pump,i}$ and $\dot{E}_{c,pump,i}$ will undertake only constant or null values depending on whether the optimizer chooses to have them activated.

Electricity consumed by the distribution pump is not only dependent on the total flowrate through the hydronic network but also the pressure difference - determined partially by the regulation of valves implicit to the pump and network model. The electricity consumed by the distribution pump is:

$$\dot{E}_{dist,pump} = f(\dot{m}_{z,1}, \dots, \dot{m}_{z,5}) \tag{4.4}$$

Constant \dot{m}_e and \dot{m}_c values result in \dot{m}_w also being a constant. Additionally fixing the approach temperature (T_{app}), allows the following expression:

$$\dot{E}_{WAHX} = f(\dot{m}_a) \tag{4.5}$$

The final term $(1 - \eta_{ESS,i})\dot{E}_{ESS,i,t}^{in}$, is included to account for losses incurred during the charging process of the battery. Additional model-specific constraints listed in *Section 4.5* are not discussed here.

4.4.3 Modeling error and base case definition

75% and 25% of the processed data are used for training and evaluating the models respectively (*Figures 4.4 and 4.5*). The MAEs for the models representing the heat pump and distribution pump are 4.79% and 11.27% respectively. Similar values were posted for the evaporator and condenser pumps. The chief causes of inaccuracies were found to be noise in the sensor readings and data aggregation over the hourly time-horizon. Despite so, the fidelity of the models' performance, in reality, is preserved.

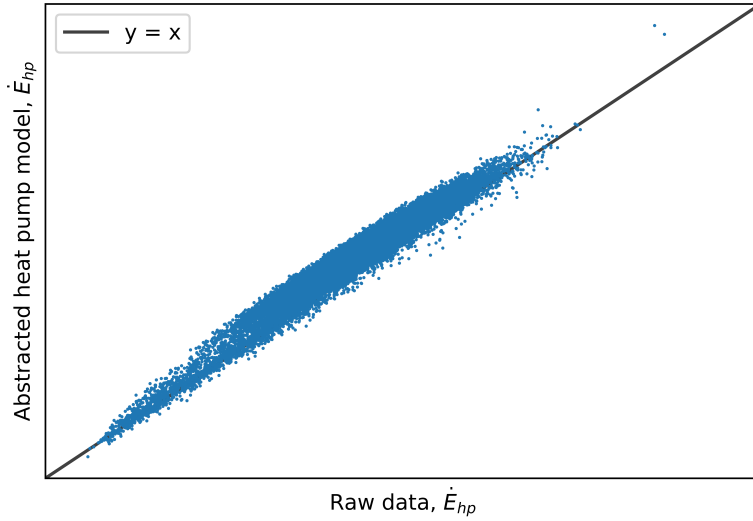


FIGURE 4.4: Heat pump error plots.

The base cases defined in *Section 4.3.1* are also simulated using the models that were chosen. This serves as a fair benchmark for the evaluation of the optimal results obtained.

4.5 Results and discussion

For each of the four case-study scenarios, the comparison of the results of the base and optimization cases for each of the 12 days selected to represent the year is first shown. After this, the findings are explained by using results from a selected representative day as an example.

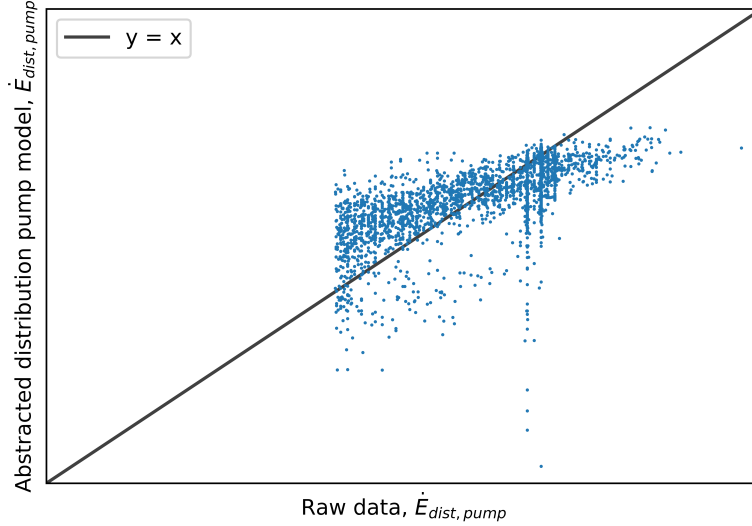


FIGURE 4.5: Distribution pump error plots.

4.5.1 Case-study scenario 1: Energy optimization of the hydronic network.

This case study focuses on the operation of distribution pumps in the hydronic network. *Figure 4.6* illustrates the electricity consumption of the distribution pumps operating under three different control strategies - constant speed, variable speed, and optimized pressure setpoint. *Table 4.6* documents the comparison of electricity saving across the three operating strategies.

The switch from constant speed pumps to variable speed pumps could potentially result in electricity savings of about 19.8%. The bulk of these savings is attributed to the ability for the speed of the pump to be automatically adjusted in tandem with the flowrate demands. However, variable speed pumps are typically operated at a pre-determined pressure setpoint, which is determined through an estimate of a pressure differential which can deliver the required flowrate for the highest demand of a given period. By adapting the pressure setpoint in response to the hourly flowrate requirement, additional electricity savings of 63.16 % could result.

Using a typical day in July as an example (*Figure 4.7*), the pressure setpoint of the variable speed pump is relatively too high for large periods of the day. While it is understandable that the setpoint is determined by the peak demand of a given

period, considerable savings will result if it could be adapted according to demand, especially during the wee hours' of the day.

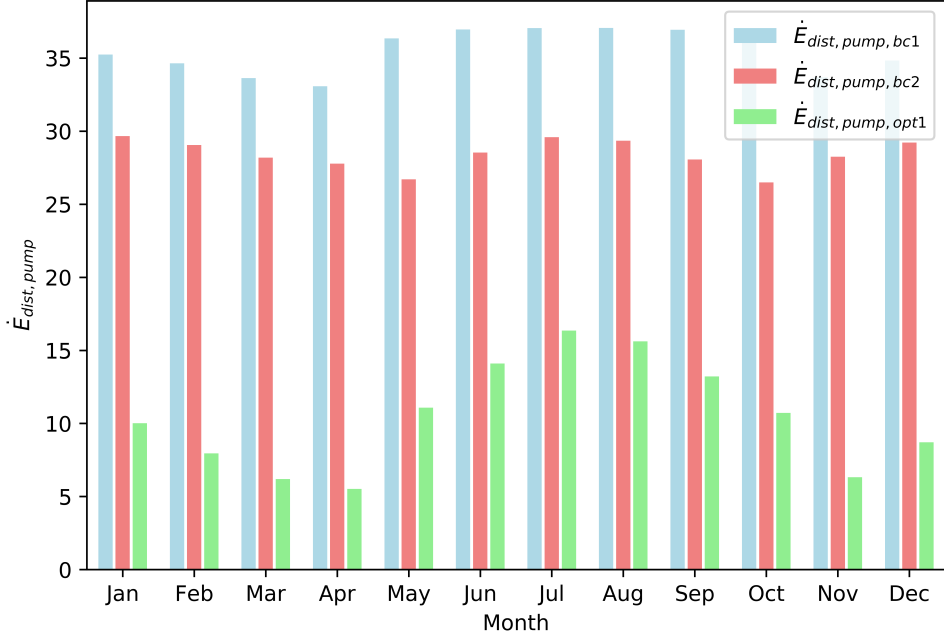


FIGURE 4.6: Approximate distribution pump electricity consumption under three operating strategies.

bc1 vs bc2	bc1 vs opt1	bc2 vs opt1
19.80%	70.79%	63.16%

TABLE 4.6: Comparison of average electricity savings in the distribution pumps across different operating strategies.

4.5.2 Case-study scenario 2: Operation cost optimization.

Batteries in our GCHP system exist for storing excess solar energy which could not be fully utilized. However, more could be done with these batteries - storing electricity from the grid when the price is favorable. The cost-saving potential exists in such a measure. The optimizer has the option of storing electricity from the grid when the price becomes favorable, to optimize operating costs. *Figure 4.8* illustrates the potential monthly cost savings between the two battery operating strategies - storing only when there is excess solar energy and optimized battery storage which also permits storing electricity from the grid. For a given year, approximately 12.73% of the current operating cost could be reduced.

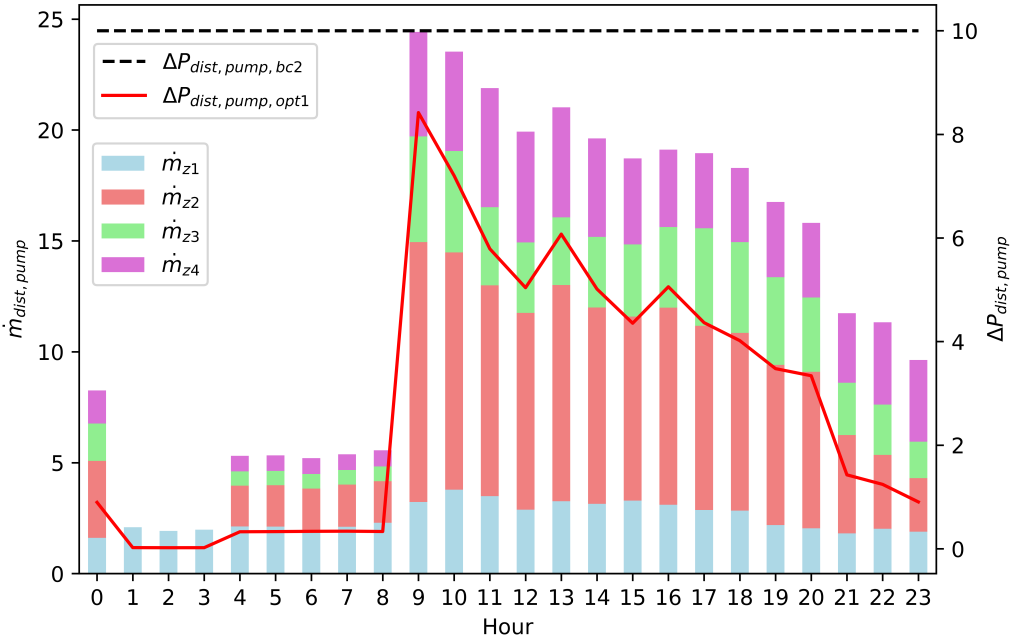


FIGURE 4.7: Comparison of distribution pump pressure setting between *bc2* and *opt3* for a typical day in July.

The difference in battery operation is clearly illustrated in *Figure 4.9*. Electricity was drawn from the grid to be stored in the battery at 0300 and 0700 hours, just before the spike in electricity pricing occurred. This is the primary reason for the cost savings. Other differences in battery operation are inconsequential as they occur when the electricity price remained constant. Storage of electricity from the grid is a difficult decision as it involves determining the trade-off among the losses due to battery charging inefficiencies, cost savings, and future electricity demand, thus, best left to an optimizer.

4.5.3 Case-study scenario 3: Energy optimization including WAHX.

Holistic optimization enabled the identification of key bottlenecks in the GCHP system. It is difficult to significantly improve the energy performance of the GCHP system as the heat pumps are consistently subjected to unfavorable ground temperatures for prolonged periods. This implies a possible under-sizing of the GHE for the system. The only possible way to improve operating temperatures of the heat

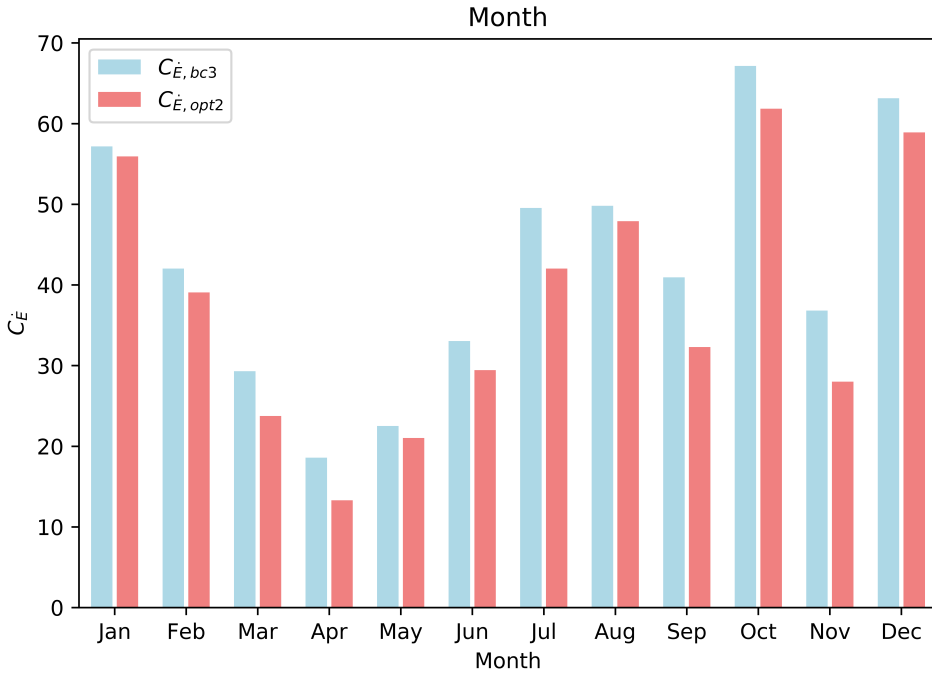


FIGURE 4.8: Comparison of average operating cost between two battery operating strategies.

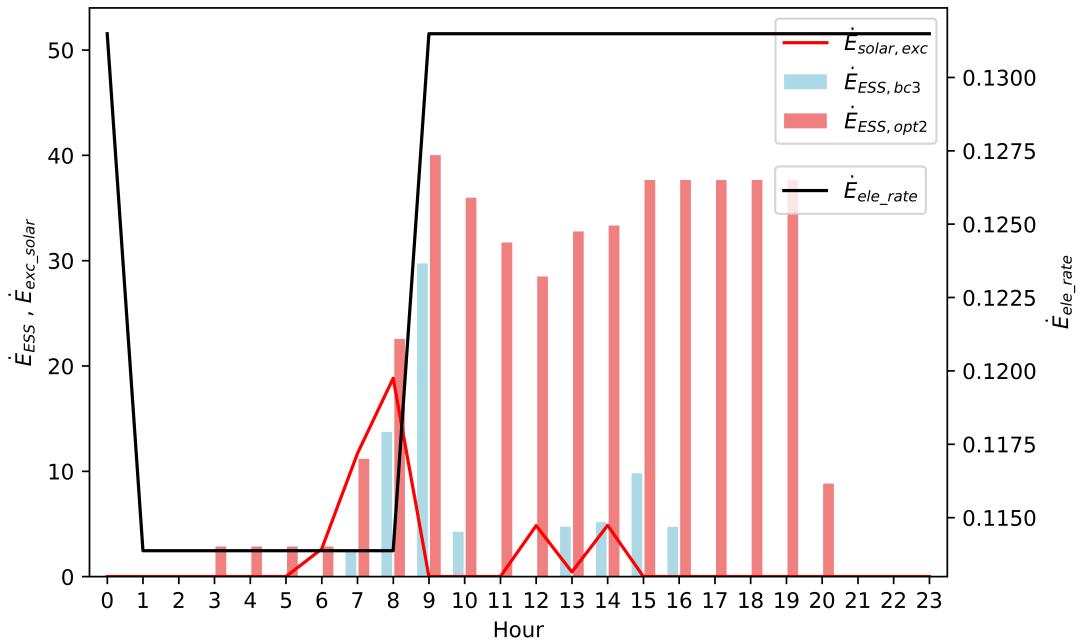


FIGURE 4.9: Difference in battery operation across a 24 hour period in June.

pumps is to provide an alternative to the GHE, hence we introduce a theoretical WAHX to the system.

Figure 4.10 compares the average monthly electricity savings when the operations of the hybrid GCHP system is holistically optimized (*opt3*) as compared to the current operation (*bc3*). Electricity savings across the year averaged at 12.71%. The greatest savings occurred during the months where the thermal (cooling) demand was the highest.

The daily operation of a typical day in July is used as an example to unveil the reasons behind the electricity savings (*Figure 4.11*). Without an alternative for the GHE, recovery of the ground temperatures for *bc3* becomes impossible and begins to rise until it hits a plateau. 33 °C is a relatively high condensing temperature for the heat pumps considering that the ambient air temperature is lower. Under the operating strategy provided by *opt3*, the WAHX is activated whenever the ground temperature starts to rise. By dissipating the condenser heat into the ambient air instead of the ground, it enabled the ground temperature to gradually recover to its initial state.

The WAHX is typically an inferior alternative to the GHE for the two ensuing reasons - additional electrical consumption from fans and less favorable condensing temperatures as they are dependent on ambient air temperatures. This is most evident during 0700, 1400 and 1700 hours where the optimal operation consumed more electricity than current practice. It was a necessary sacrifice for the benefit of the enhanced overall performance of the day. The corresponding system *COP* is plotted in *Figure 4.12*. The limits of the hybrid GCHP system are apparent towards the final hours of the day, where, in spite of superior condensing temperatures, the *COP* of the system only posted marginal improvements due to the heat pumps being operated at extremely low part-load conditions.

4.5.4 Case-study scenario 4: Operation cost optimization including WAHX.

Adding a WAHX to the GCHP system will require monetary investment, and thus should be justified with the savings from operation cost. In this case-study scenario, a comparison between a holistically optimized hybrid GCHP system and the current operating state is done for two objectives - electricity consumption and operating cost. *Figure 4.13* details the monthly average operating cost under three different cases *bc3*, *opt3* and *opt4*. The average cost savings across the three operating cases

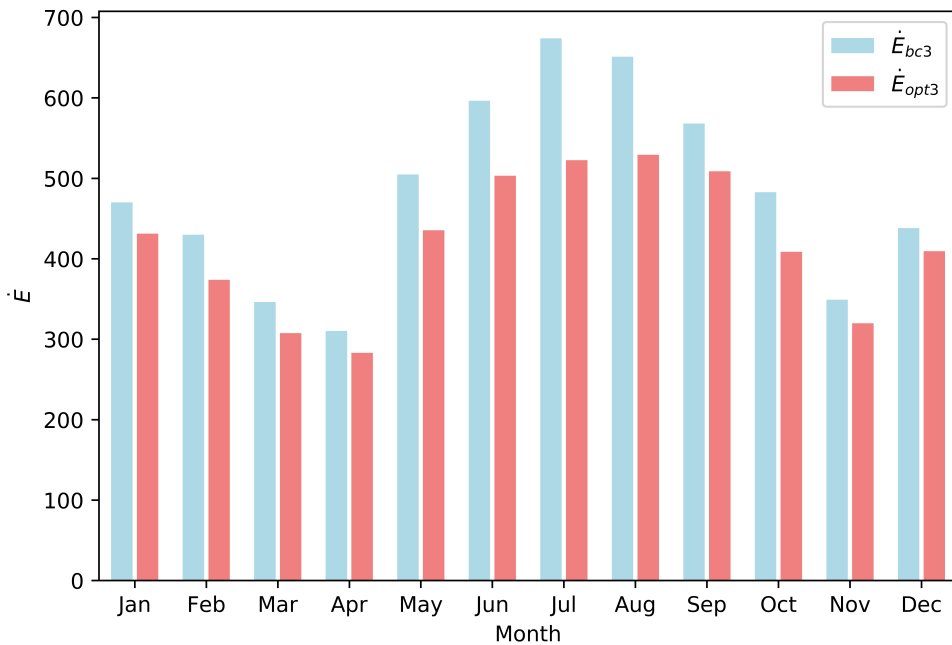


FIGURE 4.10: Comparison of average monthly electricity consumption between current operating practices and optimization with WAHX.

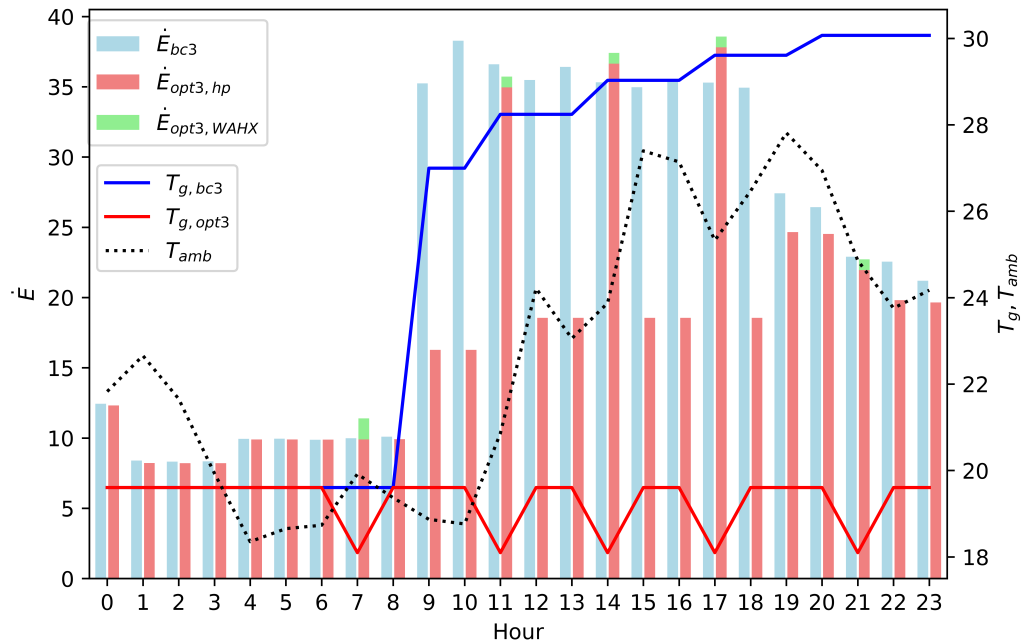


FIGURE 4.11: Plot of electrical consumption and ground temperatures between $bc3$ and $opt3$ for a typical day in July.

are shown in *Table 4.7*. While there exist considerable cost savings when the GCHP system was optimized for electricity consumption, an additional 28.17% could be

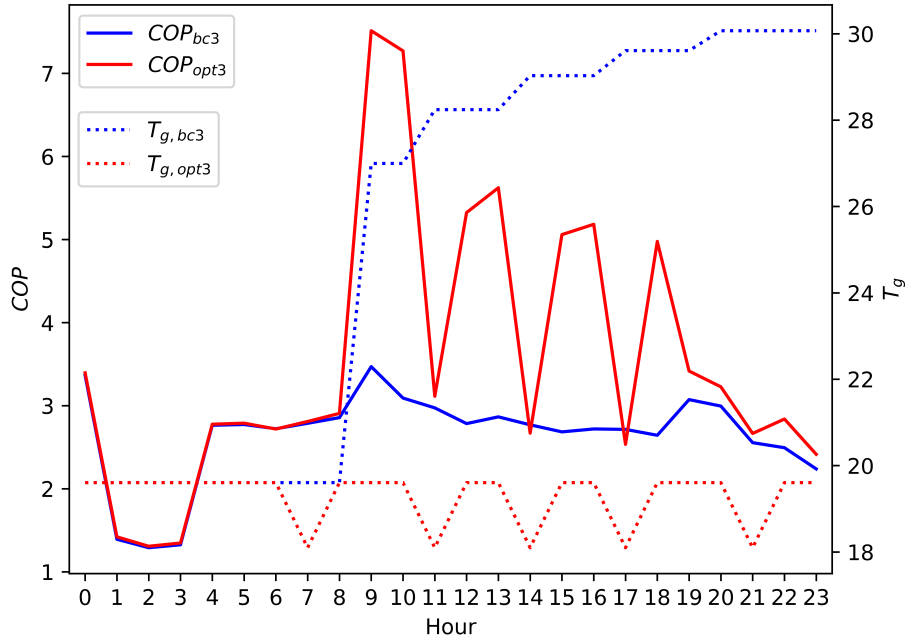


FIGURE 4.12: Comparison of COP and ground temperatures between $bc3$ and $opt3$ for a typical day in July.

realized, when instead the system is optimized for the minimization of operating costs.

The explanation for this additional savings becomes evident when we delve deeply into the optimized results for any given day. A typical day in July is used as an example for discussion purposes. The difference in battery operation could probably explain the difference in operating costs between $opt3$ and $opt4$. As shown in *Figure 4.14*, the excess electricity from solar photovoltaics is never stored in the batteries in $opt3$, when the total electricity consumption is minimized.

Storage of electrical energy in batteries incur losses during the charging process, thus is abstained from, in $opt3$. However, with operating cost as the objective function, it then became necessary to store not only the excess electricity from solar photovoltaics but also electricity from the grid when the price is considerably lower - as it can be used to supplement electrical demands when the price increases. This additional electricity stored, influenced the operation of the hybrid GCHP system in terms of electrical consumption - the inconsequential poorer efficiencies during periods of excess electricity 0400 - 0800 hours, and the considerably better performance during periods where electricity price is high (*Figure 4.15* and

[4.16](#)). There even exist scenarios where the WAHX was activated just before the sharp increase in electricity price as shown in *Figure 4.15* at 1100 hours. This was likely done to improve the *COP* of the heat pumps when the electricity price is higher. Accounting for the trade-off between components of a tightly-coupled system is complex, and non-intuitive, thereby highlighting the benefit of performing mathematical optimization.

From a survey conducted, a typical WAHX suitable for the GCHP system is priced at approximately 25 000 €. Optimization results indicate potential cost savings of about 5600 € when *opt4* is compared to *bc3*. This indicates roughly that the payback period is likely to occur under five years. Finally, a plot of the break down of electricity consumption across all the seven cases in the case study is shown in *Figure 4.17*. The individual components started operating differently as more components are added to the optimization problem, demonstrating the benefit of performing optimization holistically and giving consideration to the tight-coupling between them. Finally, it is important to note that the optimization of operating cost does not correspondingly lead to the best energy performance, as evidenced by *opt3* and *opt4*.

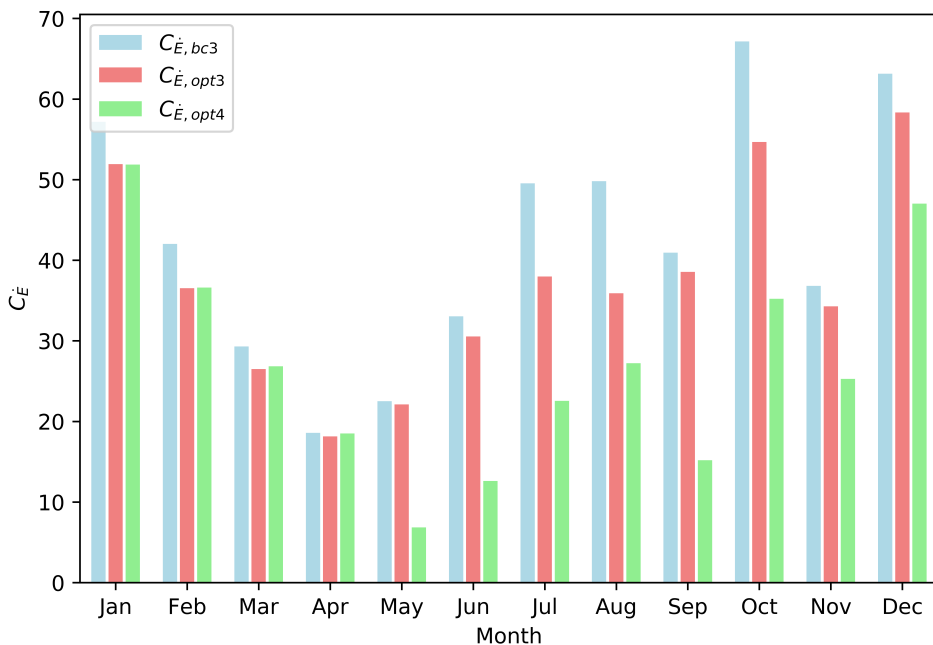


FIGURE 4.13: Comparison of monthly average operating cost amongst *bc3*, *opt3* and *opt4*.

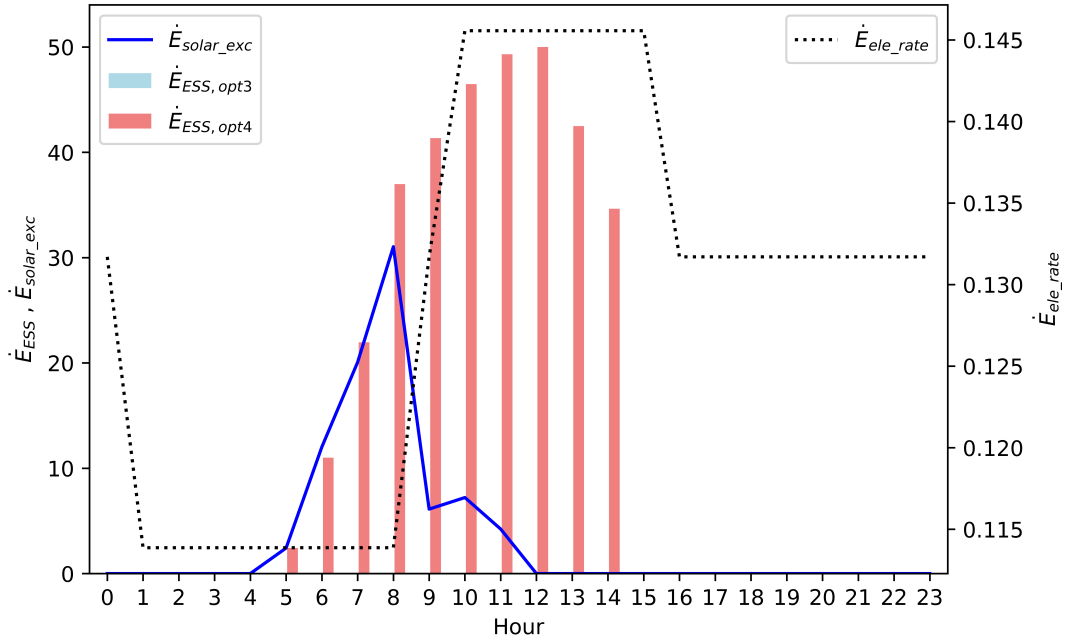


FIGURE 4.14: Comparison of battery operation between *opt3* and *opt4* for a typical day in July.

bc3 vs opt3	bc3 vs opt4	opt3 vs opt4
11.13%	35.79%	28.17%

TABLE 4.7: Comparison of average cost savings across different operating strategies of the GCHP system.

4.6 Conclusion

Abstraction techniques on judiciously selected models can be leveraged to increase compatibility with the commonly deployed MILP format to increase the solvability of holistic system optimization problems. This effect, coupled with the vast benefit of holistic optimization of urban energy systems was highlighted in this chapter through a case study based on an existing GCHP system.

For enhancing the appreciation of holistic optimization, four case-study scenarios were designed to progressively optimize the building-level GCHP system. Through the analysis of the results, two key areas for electricity savings were identified - operation of the hydronic network and the improvement of ground temperatures. The latter was addressed through the hybridization of the GCHP system with a WAHX. Optimized results indicate potential electricity and cost savings of up to 12.7% and 35% respectively. With that, return on investment of the water-to-air

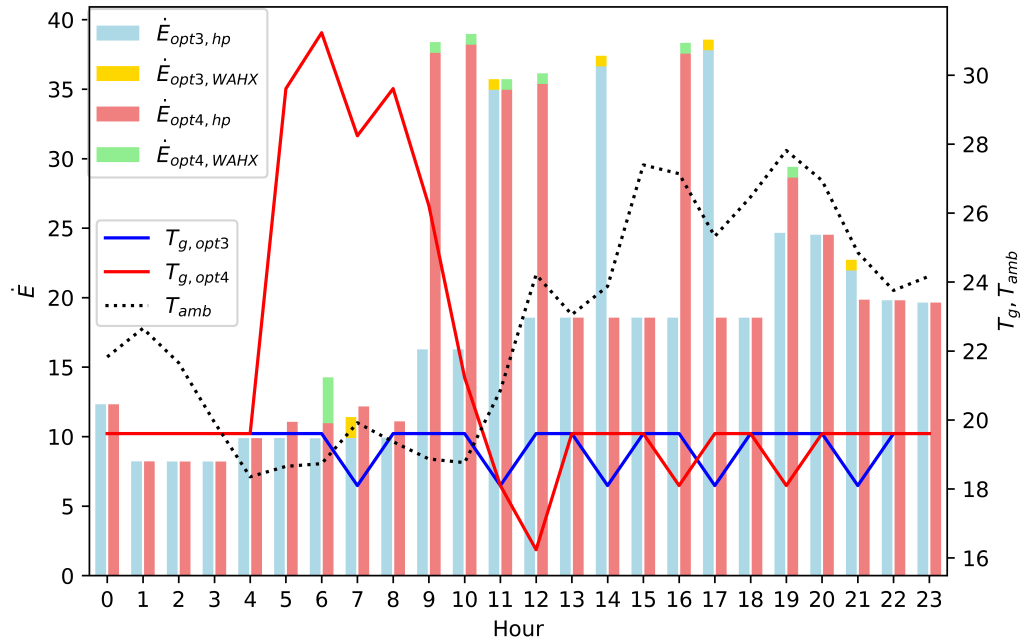


FIGURE 4.15: Comparison of operating strategies among $bc3$, $opt3$ and $opt4$ for a typical day in July.

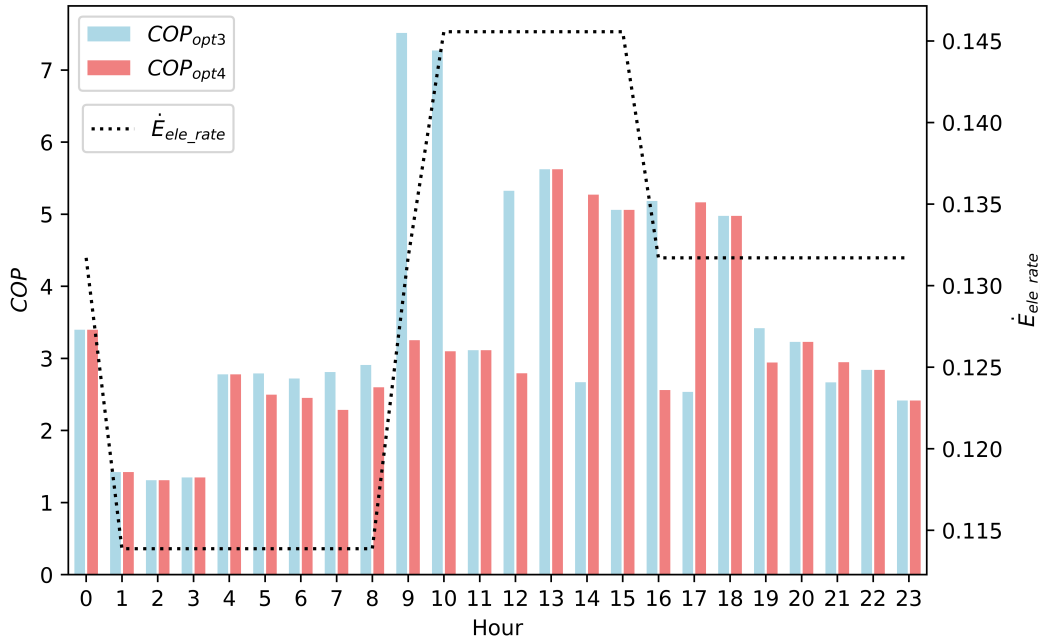


FIGURE 4.16: Comparison of system COP between $opt3$ and $opt4$.

heat exchanger is expected to be under five years. Such levels of savings would not have been possible without consideration of the tight-coupling between the components and holistic optimization.

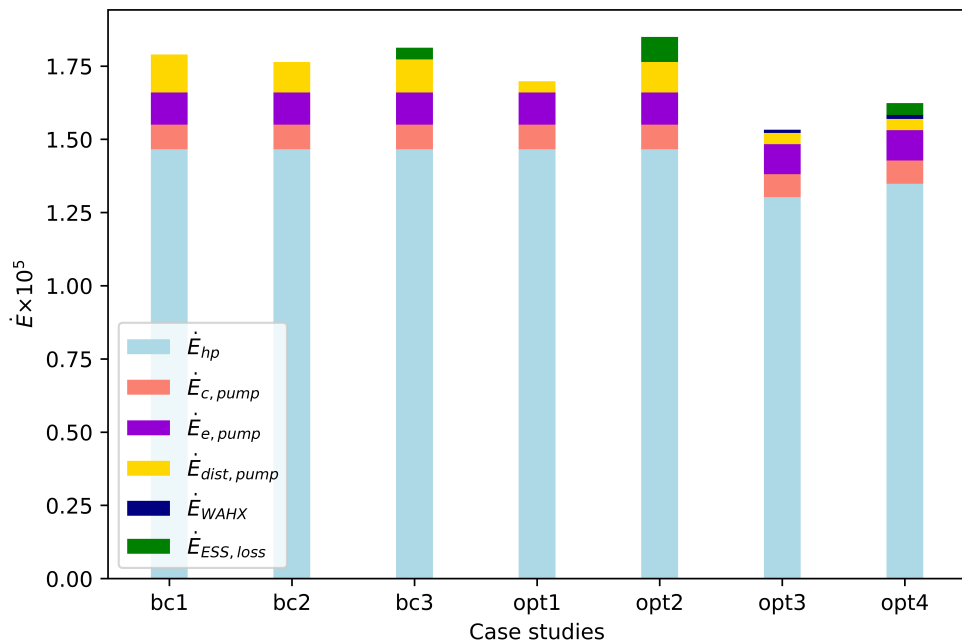


FIGURE 4.17: Plot of electricity annual electricity consumption across all seven cases.

Currently, the scalability of this methodology is limited as it is dependent on case-study specific information to restrict the problem formulation within the realms of MILP. The next chapter addresses this shortcoming through the introduction of a hierarchical optimization framework, which combines a genetic algorithm (GA) with a MILP.

Chapter 5

Hierarchical framework for holistic optimization using genetic algorithm and mixed integer linear program

5.1 Overview

Formulation of an optimization problem that adequately captures the tight-coupling amongst components of urban energy systems and in terms of its tuneable variables often results in a mixed integer non-linear program (MINLP) which is large and difficult to solve. In the previous chapter, while abstraction techniques alone, permitted the GCHP system to be holistically optimized, it depended heavily on case-study specific characteristics to confine the problem within the realms of MILP. Hence, it is unlikely to be scalable for generic urban energy systems.

A hierarchical framework of holistic optimization of the operations of urban energy systems is introduced in this chapter to manage the MINLP. This framework introduces the genetic algorithm (GA) in addition to the MILP which is formulated using abstracted component-level models. The introduction of the GA enables the decision variables which cannot be linearized to be optimized as well. With the

²The work in this chapter has been published in [165]

MILP solver reducing the search space of the GA, the likelihood of achieving global optimality is greatly enhanced. This effect becomes evident when a performance comparison was made between this framework and the sole use of metaheuristics (GA) for operation optimization in a case study based on an existing district-level energy system (DCS) in Europe.

This chapter begins by briefly highlighting the limitations in the existing literature pertaining to the operation optimization of DCS. After this, the hierarchical optimization framework is introduced and applied to the DCS. *Section 5.5* compares the performances of this framework against the sole use of the GA for the same problem, before providing a discussion of the results obtained through holistic optimization of the system. Results indicate electricity reduction of 31%, 27% and 3% across high, moderate and low cooling demand conditions respectively. This methodology has been published in [165].

5.2 Introduction

The demand for space cooling accounts for a significant portion of energy demand. This statistic is even more valid in regions experiencing significant periods of tropical climates [166]. The percentage of energy used for space cooling in Mumbai (40%) is double that of London (20%) [167, 168]. DCS represents one such example of a potentially more efficient means of fulfilling this demand [13]. Thus, DCSs are rapidly becoming a standard feature in new city developments [169, 170]. The performance in reality, however, is uncertain as operating and design conditions differ[5]. The tendency to exercise caution in design often leads to the oversizing of DCS; this results in the underutilization of equipment which is especially detrimental to the overall energy efficiency of the system[171, 172].

Inefficiency is further compounded by control strategies that are either based on predefined setpoints or seek only to achieve optimal performance, local to components [6, 7]. Localized control disregards the cascading effect on the system which inhibits the ability of DCS to adapt well under less-than-ideal operating conditions. The focus of the current work is to introduce an optimization framework which thoroughly explores the solution space mapped by tuneable variables in a DCS, in search of improving energy efficiency holistically at the system-level.

5.2.1 District cooling system

A DCS is a centralized method of cold thermal energy production and distribution for space and process cooling. Chilled water is widely used as the medium for the transportation of thermal energy for cost-effectiveness [12]. The technical description of a typical DCS is comprised of four main components - the central station, distribution network, customers and heat rejection system. *Figure 5.1* illustrates the general components of a typical DCS serving four buildings. Cooling towers often serve as the primary equipment used for heat rejection. The active components of the DCS which consume electricity are the chillers, pumps and cooling towers. The rate at which electricity is consumed depends on the equipment loading, temperature and flowrate setpoints.

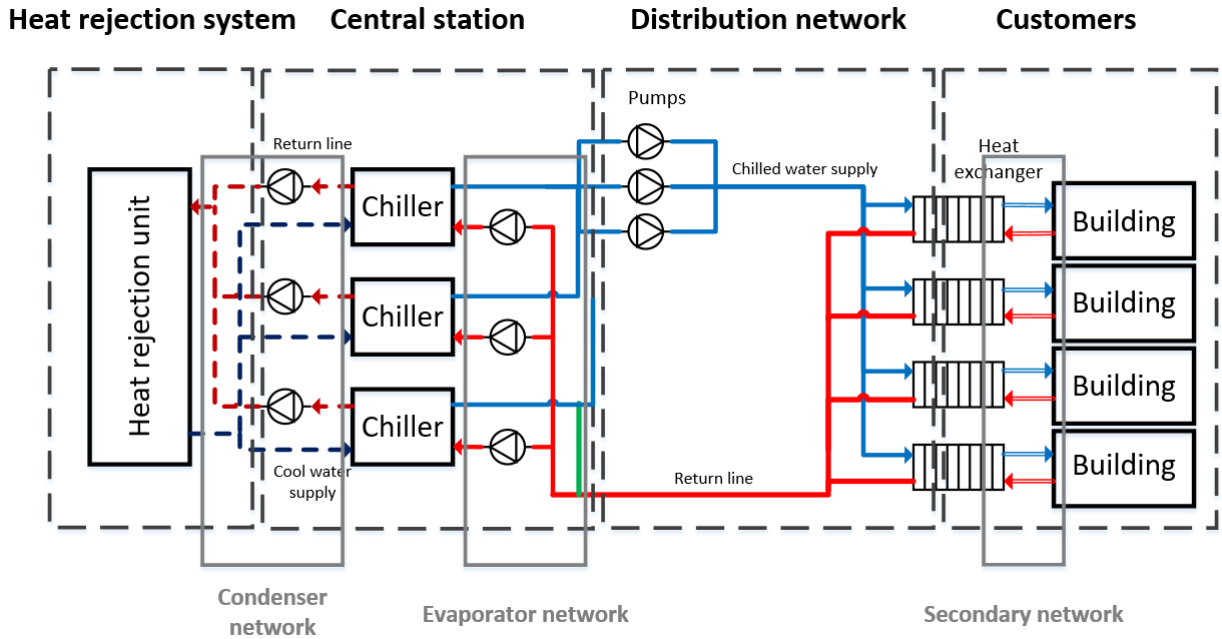


FIGURE 5.1: Overview of the components of a typical DCS.

5.2.2 Literature review

The majority of the optimization work done on DCS and closely related district heating systems (DHS) are focused on presenting solutions to design-related issues [12, 93]. Such problems attempt to determine the optimal configurations of equipment type, primary resource, network layout, and customer configuration. They

employ methods and models which are too abstract for optimizing DCS operations - an example would be the assumption of constant efficiencies, regardless of equipment loading [21, 22]. Conversely, optimization of DCS operation is concerned with determining the most efficient equipment staging, flowrate and temperature settings which fulfills a given cooling demand [19, 20]. Thus, greater modeling detail of components is required.

Component-level optimization is commonplace where DCS operations are concerned. For a given cooling demand, these formulations attempt to determine the optimal operating plan for equipment [19] and the distribution network [20] separately. Detailed modeling of equipment and network hydraulics involved complex equations, which yields MINLP problem formulations making the use of meta-heuristics a popular choice [95, 173].

Several measures were employed to enhance the solvability of the above component-level optimization problems. Sakawa et al. [99] relaxed the cooling demand constraint by reflecting the failure to meet demand as a penalty in the objective function. With the use of appropriate equation-based models, the MINLP could be broken down into simpler quadratic programs (QP), under the assumption that the set of chillers could be aggregated as a single optimal unit [19]. If the distribution network is extensive, the energy expended for pumping could significantly affect the overall system performance. The relatively small working temperature range further compounds the impact for DCS [173]. To simplify the network optimization problem, Schweiger et al. [20] decomposed the MINLP problem into a mixed-integer quadratically-constrained program (MIQCP) and a smaller non-linear program (NLP). This approach reduced the non-convex search space while enabling models of higher detail and physical accuracy to be considered in the problem formulation.

There is no indication that the independent optimization of equipment and network will yield the optimal performance at the system-level. Thus, Jing et al. [95] modeled and optimized the operation of a small-scale district heating and cooling (DHC) system with the consideration of both equipment and network. The formulation enabled the power incurred by the pumps in the network to be reflected in the objective function. However, the direct application of the group search optimizer (GSO) algorithm, does little to ensure the quality of the final solution.

Work on building level optimization of chiller systems is also considered due to their relevance [100, 102]. They, however, tend to mainly focus on solving ‘optimal chiller loading’ (OCL) problems, with little regard for the details of the network, nor the setpoint temperature of chillers. Due to the differences in the scale of a DCS compared to the building level, the energy expended in the network has to be factored. The benefits of holistic system optimization were highlighted in a case study conducted on a building-level chiller plant, where an additional 6.5% of energy savings is possible on top of chiller-only optimization [94].

From the review, it is evident that there is a lack of studies that consider the holistic optimization of DCS operation, much less a systematic framework for this undertaking. Several studies on the closely related topic at the building level, consider fixed temperature setpoints of chillers, effectively misrepresenting the solution space. For a chiller-based system, the concurrent optimization of temperature setpoints and flowrate in response to a given cooling demand proved to be most effective in the minimization of electricity consumption [174]. DCS is also likely to benefit more profoundly from the consideration of temperature variables as it introduces flexibility into an inherently rigid system. Hence, the novelty of the current work lies in the introduction of a framework which can simultaneously optimize all tuneable variables of a DCS for a given cooling load.

5.2.3 Objectives

The hierarchical optimization framework for the holistic optimization of DCS operation is developed for managing the MINLP. It decomposes the optimization problem into two levels - a master and a slave. The key features of the master and slave levels are the GA and MILP solver respectively. This approach functions by having the GA parameterize a subset of variables such that the remaining can be dealt with using the MILP. Given that MILP solvers generally both converge optimally and more quickly than GAs, model abstraction techniques are used to linearize the DCS model as much as possible. Doing so, also reduces the load on the GA, promoting resolution speeds and the likelihood of deriving solutions that are globally optimal.

For illustrative purposes, this framework is applied to a case study based on an existing DCS in Europe. Three scenarios, each with different cooling demand

and weather conditions, are defined to demonstrate and quantify the potential electricity savings through the application of the proposed framework.

5.3 Optimization framework

Taking reference from the approach used by Fazlollahi et al. on district heating/energy systems [91–93], a hierarchical framework for the operational optimization of urban energy systems is proposed. The decomposition method used is the core of the framework. It is introduced to deal with nonlinearities in the optimization problem.

It is apparent from the issues on model abstraction, highlighted in *Chapter 3*, that a method is required to deal with variables held as parameters. MILP can only solve the problem partially (*Chapter 4*). As such, the decomposition approach is employed to couple the MILP formulation with a metaheuristic. It treats the MILP formulation as a larger ‘black-box’ to be optimized. This approach is also beneficial to metaheuristics - having the MILP formulation handle most of the variables reduced the search space, improving solution quality whilst reducing resolution time.

Figure 5.2 illustrates the overview of the proposed optimization framework. The proposed framework improved on the optimization work found in the current literature by considering higher levels of modeling detail. These details (temperature, network operation, the granularity of time-periods, etc.) are critical in the determination of design/operation feasibility. Flexibility was another feature of the framework. New models (equipment, natural resources, etc.) can be easily added without major modifications.

5.3.1 Pre-optimization

The nature of the problem and available data influences the choice of optimization approach and algorithms. This phase accomplishes the preparatory work for the formulation of the optimization problem. The following list details the key steps involved in a general optimization problem related to urban energy systems.

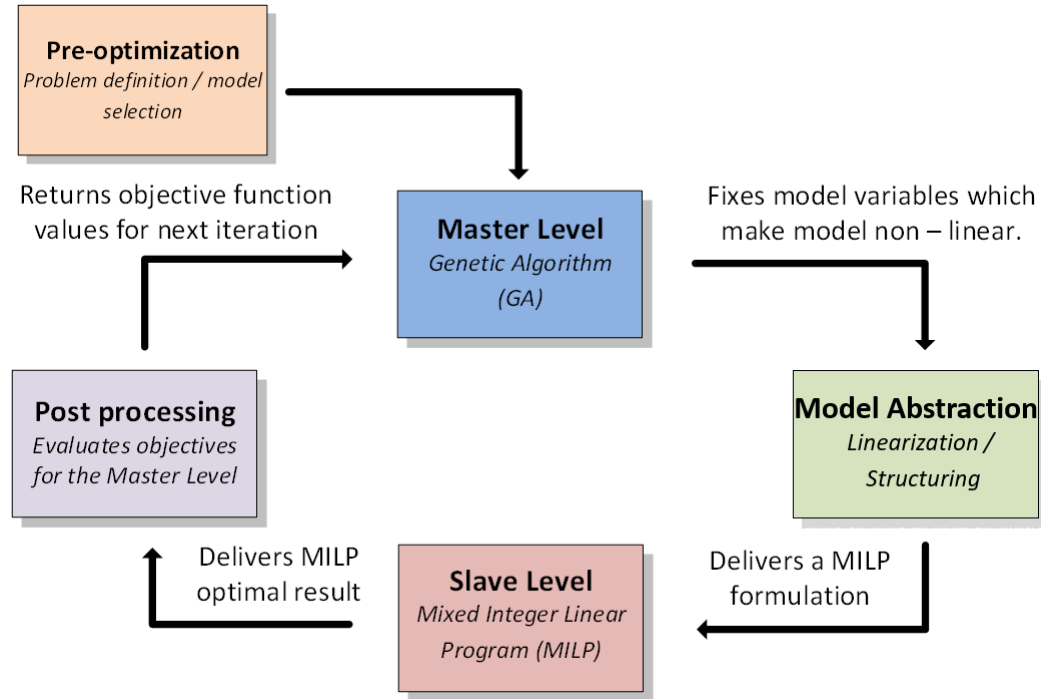


FIGURE 5.2: Overview of the optimization framework.

1. Objective function definition

Minimization of electricity consumption, emissions and cost represent some of the most common choices in literature. Some may be more relevant in design rather than operation problems. The eventual choice will influence the data and models required to reflect it. At times, more than one objective function could be established, and multi-objective optimization could be performed.

2. Data management

The choice of objective function determines the required data. Two types of data are usually required - ‘constraint’, ‘operation’ data. ‘Constraint’ data reflects the physical/geographical constraints in the optimization problem. Minimum and maximum equipment capacities, contractual agreements, infeasible network routes, weather conditions, cooling demand, etc. are examples of these data types. ‘Operation’ data refer to those required to train a selected model. A record of temperature, flowrate, and electricity consumption variation over a period of time for chillers is one such example. The raw data has to undergo cleansing and structuring into usable formats for further use.

3. Model selection, training and algorithm selection

The models are selected and trained with the processed data. Based on the nature of the selected models, the optimization approach is determined. There is a preference for global optimality solvers. The extent of its applicability, however, depends on the selection of the available models.

4. Simulation model

The simulation model comprises of abstracted models. Aside from quick testing of ‘what-if’ scenarios, the model also functions by ‘seeding’ metaheuristics with a starting feasible solution. Doing so ensures that the generated optimal result will always be equal to or better than a certain pre-defined level. For the optimization of operations, the ‘seeded’ value could be derived from the current working conditions. The simulation will also serve as a benchmark for comparison against the ‘optimal’ results generated.

5.3.2 Master level

The GA is used at this level owing to its popularity for solving such problems. This algorithm was utilized to handle non-linear variables, which were to be treated as parameters for the feasibility of MILP formulations. T_e^{in}, T_c^{in} etc. are examples of variables which can be handled by the GA (*Figure 3.3*) such that MILP can handle the remaining ones.

The GA is a population-based global search algorithm. The following list details the steps involved for a generic implementation [175].

1. Parameter definition

Key parameters (population size, generations etc.) and the bounds of the variables are defined.

2. Initialization

An initial population of p sets of variables (agents) is randomly selected and their fitness (objective) function evaluated.

3. Selection

Selection of $n \leq p$ agents are selected for offspring production. Selection is normally based on the fitness function. Probabilistic measures are usually introduced to reduce the likelihood of elitist selection.

4. Crossover

The selected n agents need to mix to produce $(p - n)$ ‘offspring’ agents. The extent of mixing is randomly determined. This is done on the assumption that better parents tend to have better offsprings (fitness function).

5. Mutation

A low percentage (k) of agents within the population are to be subjected to mutation. This means randomly changing the variable values within the agent. Doing so ‘maintains’ the ‘genetic’ diversity of the selected population. This step discourages convergence to local optima.

6. Fitness evaluation / Termination

The fitness function of the new population is evaluated again and steps 3 to 5 will be repeated until a stopping criterion is met. Termination happens after m generations or when the change in optimal value generated is considered to be small.

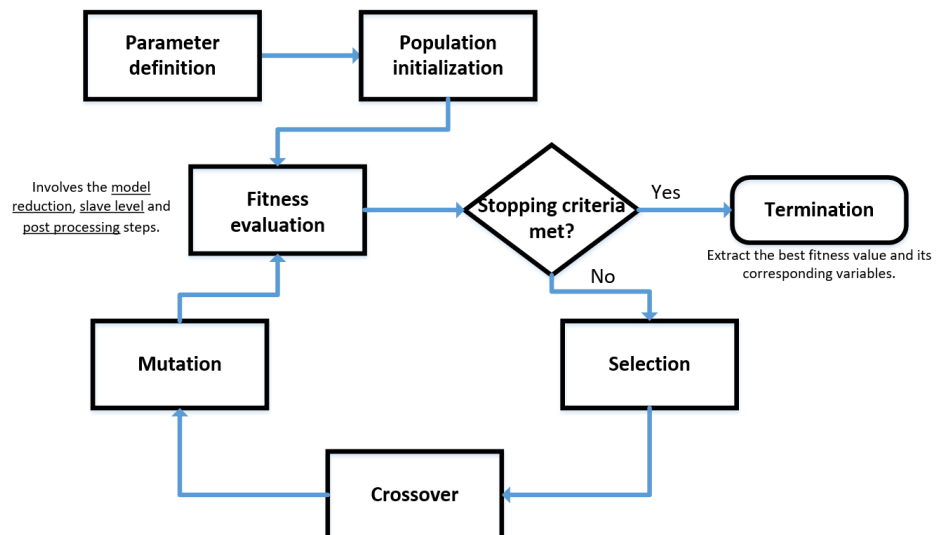


FIGURE 5.3: Overview of a generic genetic algorithm.

Parameters p , n , m , and k have to be properly selected for the algorithm to function well. *Figure 5.3* summarizes this generic genetic algorithm.

5.3.2.1 Current implementation

The GA can be implemented in several ways. The chosen implementation was targeted at improving resolution speeds. Slight modifications are made to the implementation shown in *Figure ??*.

Binary implementation

The implemented GA is coded in binary to facilitate the crossover and mutation process. The reduction of variables to binary enabled a higher level of control over the granularity of change during mixing processes while reducing the search space simultaneously. This implementation is motivated by the original purpose of the GA - to solve combinatorial problems effectively. The following highlights the key changes that were made for this implementation.

1. Parameter definition

Besides the definition of the lower and upper bounds of the variables to be optimized, the precision (decimal points) of the variable and the ‘variable type’ is required as an input. Precision is required to determine the number of binary bits required, while ‘variable type’ determines how the variable is handled. There are three predefined ‘variable types’ - binary, continuous and discrete.

There is no need for binary variables to be treated. For continuous variables, the defined precision effectively determined the number of possible values the variable can take. Consider the variable x such that $0 \leq x \leq 10$ with the precision of 1 decimal place. This effectively means that there are only 101 (0.0 to 10.0) possible values of x . Converting 101 to binary requires 7 bits. Discrete variables are handled in a similar way, where the number of discrete values determines the number of bits required. Since the conversion of decimal to binary is not exact (2^n), some variable values have a slightly higher probability of representation, however, the impact is diminished with longer binary strings.

2. Crossover

Consider the optimization of a three-variable problem - x_1, x_2 and x_3 represented by 3, 4 and 5 bits respectively. Every bit is treated equally, thus the crossover point can occur anywhere between the 1st and 12th bit. As a result, the crossover function can have greater control over offspring generation which is otherwise missing when the variables are treated as though they are continuous (*Figure 5.4*).

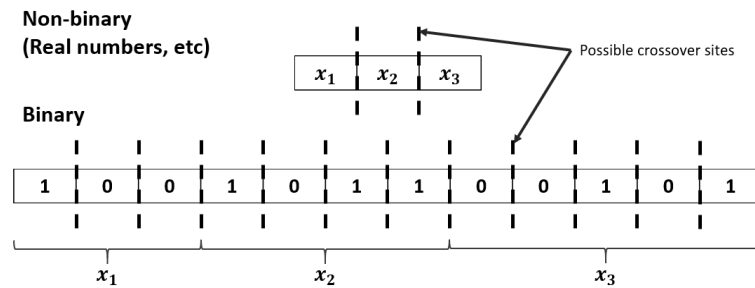


FIGURE 5.4: Crossover sites of continuous and binary implementation.

3. Mutation

The bit length used for each variable is recorded. The probability of a bit being subjected to mutation depends on two factors - the number of variables and its position within the binary string. Using the binary implementation of the three-variable problem illustrated in *Figure 5.4* as an example, the probability of a mutation occurring within the first 3 bits is the same as the next 4 bits and the last 5 bits. This is implemented so that those with shorter bit lengths are not overshadowed. Within each variable, a linearly decreasing probability is implemented. Front bits have a higher chance of selection as they made greater changes to the value of the variable. This ensures the preservation of diversity.

Selection

Tournament selection is used as it is proven to perform relatively well in terms of resolution speed and solution quality [176]. Tournament selection involves selecting the best performing agent(s) from a randomly selected subset (size $j \leq p$) of the original population. This process has to be repeated until the required number

of agents are met (size of crossover pool). Random selection of agents from the subset of size j reduces the risk of premature convergence.

Parallelization

GAs are ‘embarrassingly’ parallel programs. Parallelization can be implemented in many ways and should be taken advantage of especially with today’s computers’ ability to handle multiple concurrent processes. Cantú-Paz reviewed several methods of parallel GA implementations [177]. The global single-population master-slave parallel implementation is selected due to its ease of implementation. Having a single population eliminated the need for the development of communication ‘pipes’ between multiple populations. Thus, better-performing agents are more likely to contribute to offspring production. Such an implementation only involves the parallel evaluation of fitness values. That is very beneficial for this optimization framework as the evaluation of fitness values (solving MILP problems) is the most time-consuming part.

5.3.3 Model abstraction

Inputs from the master level are required for model abstraction to take place. Details of model abstraction techniques are discussed in *Chapter 3*. The focus of this section is to describe the method used for generating a MILP formulation from general bilinear equations. Three building blocks are defined to facilitate the MILP formulation - unit, layer, and constraint. Variables from the master level are treated as parameters in this stage.

5.3.3.1 Unit definition

The unit is modeled to represent a piece of equipment of the DCS (chiller etc.). It comprises of at least 2 continuous variables (up to bilinear), some of which contribute to the objective function value. These 2 variables are constrained by equations describing its capacity, and relationship with other units (streams). *Table 5.1* summarizes the unit definition.

The bilinear equations in *Table 5.1* are linearized using the RLT [137].

Input variables	Description
x_1	First variable.
x_2	Second variable.
Contribution to objective function	
$y = \alpha_0x_1 + \alpha_1x_2 + \alpha_2x_1x_2 + \alpha_3$	y represents the contribution to the objective function (electricity etc.). The objective function is the summation of contribution from all units.
Capacity constraints	
$F^{min}Y \leq \beta_0x_1 + \beta_1x_2 + \beta_2x_1x_2 + \beta_3 \leq F^{max}Y$ $F_{x_1}^{min}Y_{x_1} \leq x_1 \leq F_{x_1}^{max}Y_{x_1}$ $F_{x_2}^{min}Y_{x_2} \leq x_2 \leq F_{x_2}^{max}Y_{x_2}$ $Y_{x_1} + Y_{x_2} - 2Y = 0$	$F^{min/max}$ represents the limits on the unit/-variable. Using a chiller as an example, the limits can be used to represent its cooling capacity, flowrate, etc. Binary variables (Y) are introduced to turn the unit on and off.
Streams	
$st_i = \gamma_{0,i}x_1 + \gamma_{1,i}x_2 + \gamma_{2,i}x_1x_2 + \gamma_{3,i}$	Streams represent inflow and outflows of material (fluid, energy, temperature, etc.). These streams are used to interact with other units. A positive value of sr represents an inflow and vice-versa. There can be as many streams ($n = \sum i$) defined as required.

TABLE 5.1: A general unit description

5.3.3.2 Layer definition

Layers are introduced to ‘connect’ the ‘streams’ flowing in and out of units. For DCS specifically, three stream-types are defined - fluid, temperature, and pressure flows. Ideally, equality constraints in the form of $st_{unit,1}^{out} = st_{unit,2}^{in}$ should be used to respect continuity equations. However such constraints resulted in difficulty for the GA to find feasible solutions.

To rectify the issue, inequalities are used instead. If the inequalities are used correctly, the optimal solution will never violate continuity equations. This is so as violating the equations will result in a sub-optimal solution.

There are occasions where the variables in the GA result in a feasible MILP formulation that violate continuity laws. A penalty function is imposed to reflect the extent of violation to the objective function of the GA. This penalty function is selected to be smaller than the penalty of infeasibility and acts as a guide for the GA to eventually converge to a feasible solution.

Table 5.2 describes the three layer types defined in the hierarchical framework.

Layer type	Example equation	Description
Temperature	$T_1^{out} + \dots + T_n^{out} \leq T_1^{in} + \dots + T_m^{in}$	For DCS, the lower the supply temperature from the cooling source (chillers, etc.), the greater the electricity expended. As such, any optimal solution will try to raise the outlet temperatures as much as possible.
Fluid flowrate	$\dot{m}_1^{out} + \dots + \dot{m}_n^{out} \geq \dot{m}_1^{in} + \dots + \dot{m}_m^{in}$	Should greater fluid flow be supplied than required, more electricity will be expended by pumps and chillers leading to sub-optimal solutions.
Pressure	$\Delta P_1^{out} + \dots + \Delta P_n^{out} \geq \Delta P_1^{in} + \dots + \Delta P_m^{in}$	It is sub-optimal for a pump to supply greater pressure than required.

TABLE 5.2: Layers description

5.3.3.3 Constraint definition

This feature is added to accommodate the need for additional constraints onto the problem formulation. Constraints can be of any form. The two commonly used ones are loosely termed as ‘unit-use’ and ‘stream-limit’ constraints.

Piecewise linearization breaks up a single model into several sub-models. That results in the need for multiple ‘units’ (*Section 5.3.3.1*) to be defined. However, only one sub-model can be activated at any given point, thus the ‘unit-use’ constraint is required. The constraint is placed on the Y variable of the defined units (*Table 5.1*) such that $\sum_{i=1}^n Y_{unit,i} = 1$ where n represents the number of linear pieces.

‘Stream-limit’ constraints place a limit on the in and outflows of ‘units’. For instance, should the temperature of chilled water supply to a substation be required to be under T , this constraint can be used to achieve that.

5.3.4 Slave level

The MILP sub-problem is to be solved at this level. The general format of a typical DCS sub-problem involving the minimization of total electricity consumption comprising of electric chillers, pumps, and cooling towers should look as follows.

minimize

$$\dot{E} = \sum_{i=1}^{n_{ch}} \dot{E}_{ch} + \sum_{j=1}^{n_{pump}} \dot{E}_{pump} + \sum_{k=1}^{n_{ct}} \dot{E}_{ct}$$

subject to

Capacity constraints (*Table 5.1*)

Layer constraints (*Table 5.2*)

Additional constraints (*Section 5.3.3.3*)

The output of the slave will be the optimal solution to the sub-problem based on variables selected at the master level. Due to the use of RLT, the corresponding variable values (u and v , etc.) of the optimal solution may not be in their original form and will need to be converted for readability in the next step.

5.3.5 Post processing

This section is included to process the results of the slave level. It is responsible for converting the optimal values of variables (u and v etc.) back to their original forms (T , m etc.) for the sake of readability. It is also responsible for communicating the levels of infeasibilities back to the final objective function value (master level, GA). Currently, infeasibilities in the slave get an objective function value of 5 orders of magnitude higher than feasible ones violating continuity laws (*Section 5.3.3.2*). The purely feasible solutions get reflected to the master level as they are.

The difference in objective function values is meant to guide the selection of variable values of algorithms at the master level.

5.3.6 Summary

Figure 5.5 summarizes the hierarchical optimization framework which is designed to solve mono-objective MINLP. The decomposition method employed split the workload to the master and slave levels such that convergence can occur within a reasonable time. On average, it takes approximately 4 to 5 seconds to solve a sub-problem at the slave level. The majority of the computational time is spent on the preparation of data in the ‘model abstraction’ stage (*Figure 5.2*).

The modular design of the optimization framework can easily accommodate changes in algorithms, models, and solvers. For instance, slight modifications to the algorithms at the master and post-processing stage levels can be done to accommodate multi-objective optimizations - the GA could be replaced with the second version of the non-dominated sorting genetic algorithm (NSGA-II) and the post processing module can be configured to evaluate two objectives instead of one [178].

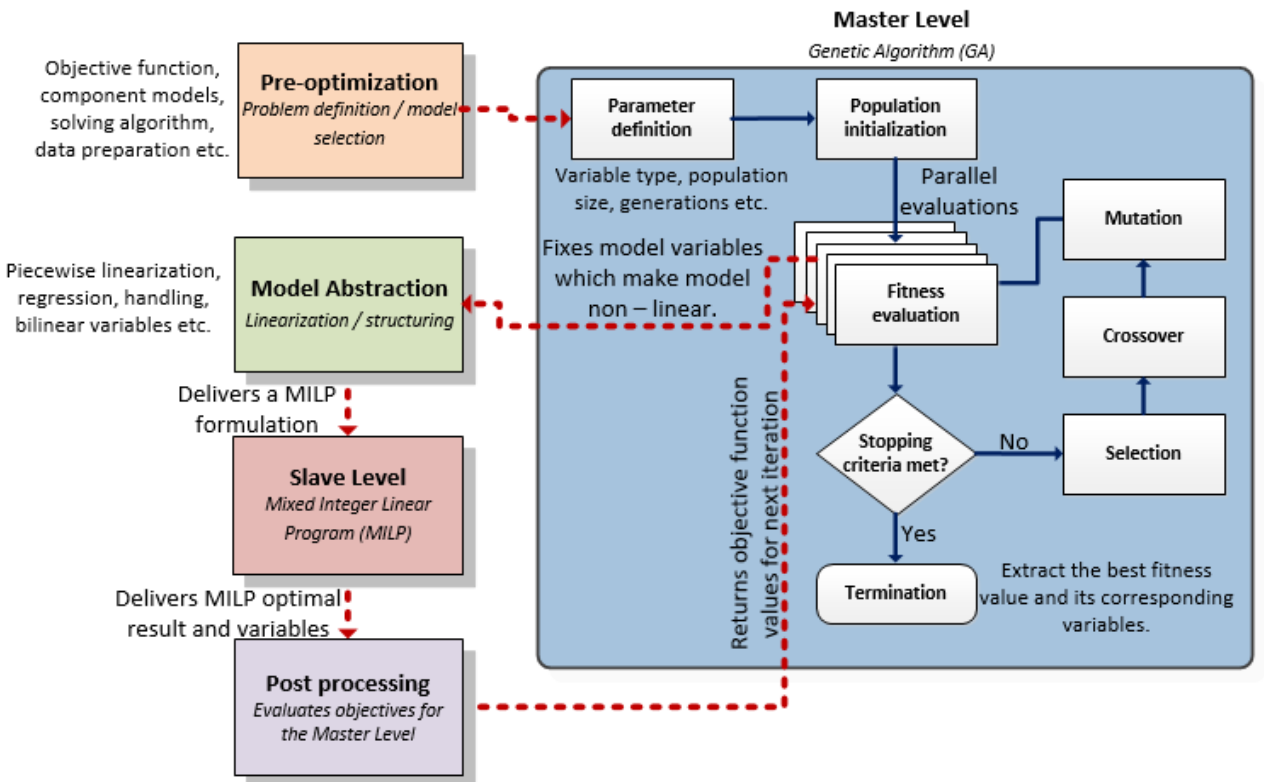


FIGURE 5.5: Complete parallelized hierarchical optimization framework

5.4 Problem formulation

The case study discussed in this section is based on a functioning DCS located in Europe. The expected performance of a DCS is usually entirely different from reality owing to the limited information available during the design phase. Various factors could have contributed to the degraded performance of DCS; the lack of cooling demand and less than ideal system design are two common reasons for this occurrence. Development at the site of the DCS was slower than projected due to economic reasons. Without sufficient demand, the DCS cannot operate as efficiently as intended. Therefore, the purpose of this case study is to identify possible changes in operating practices that could potentially improve energy efficiency. The hierarchical optimization framework is employed for the undertaking.

The DCS of interest comprises of a single central station serving four customers of different load profiles (commercial, retail, office). The central station houses three water-cooled chillers - one small and two large ones, cooled by an array of 5 cooling towers (*Figure 5.6*).

Current operating practices, coupled with low demand, often results in the infamous ‘low ΔT ’ syndrome’, where the pumps operate at near maximum capacity while chillers operate inefficiently at low part-load conditions. The purpose of this study is to investigate the extent to which operating practices can be tuned to improve energy usage. This is not a trivial task as it involves the adjustment of many dependent variables with unclear implications, resulting in the need for optimization to be done.

The objective is to optimize the operation of DCS at the hourly level using the framework discussed in *Section 5.3*. Models discussed in *Chapter 3* are used to detail the DCS at the component level before the application of the optimization strategy. Demand conditions for three representative days with low, medium and high cooling demands were selected to illustrate the benefits of performing optimization on the system.

The input conditions such as the cumulative cooling demand profile and the ambient conditions are shown in *Figures 5.7* and *5.8* respectively.

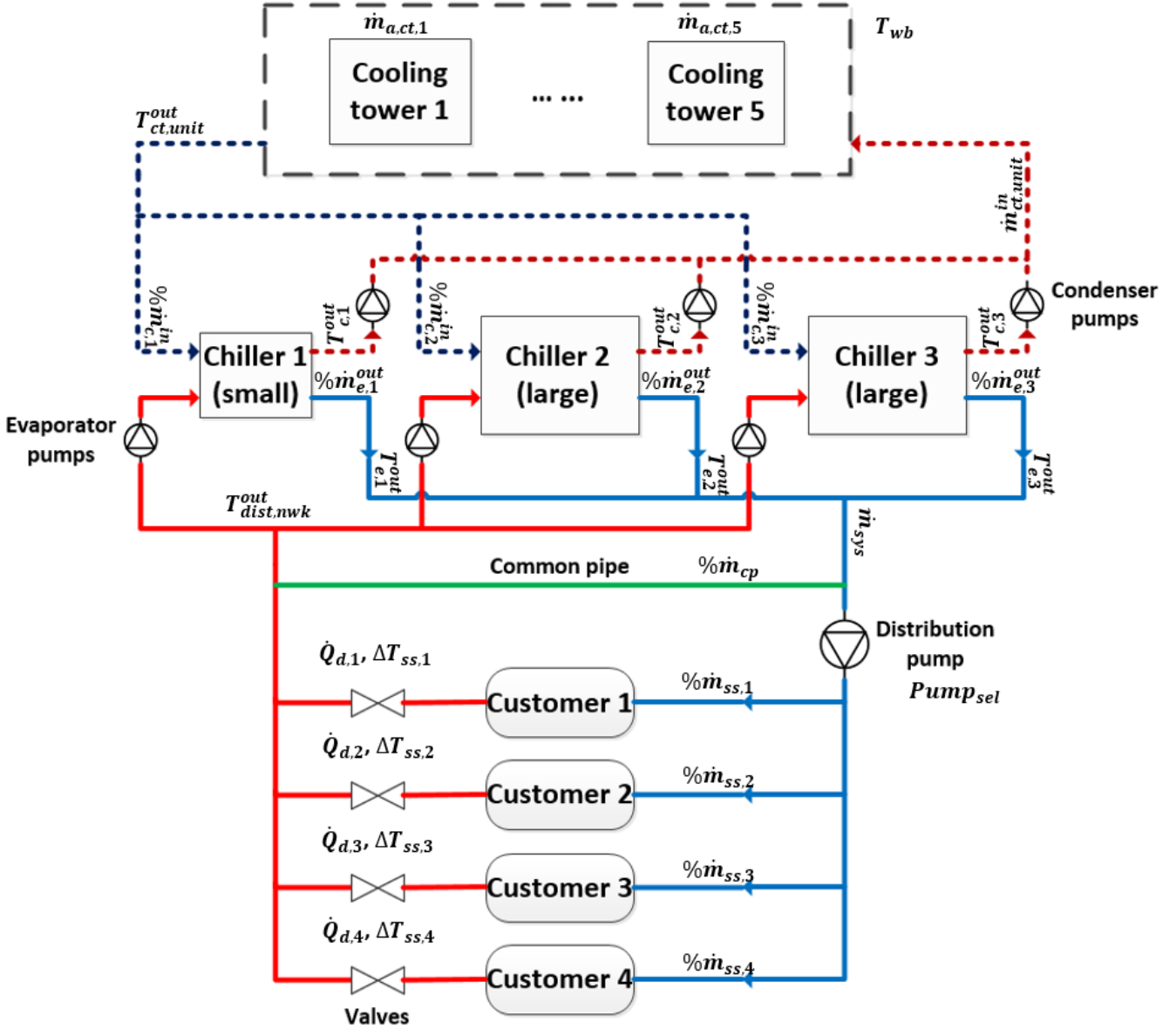


FIGURE 5.6: Schematic of DCS in case study.

5.4.1 Model selection and abstraction

Table 5.3 documents the list of abstract component-level models which are required for representing the DCS in this case study. All model variables which were held as parameters for the sake of linearization are optimized by the GA in the hierarchical optimization framework.

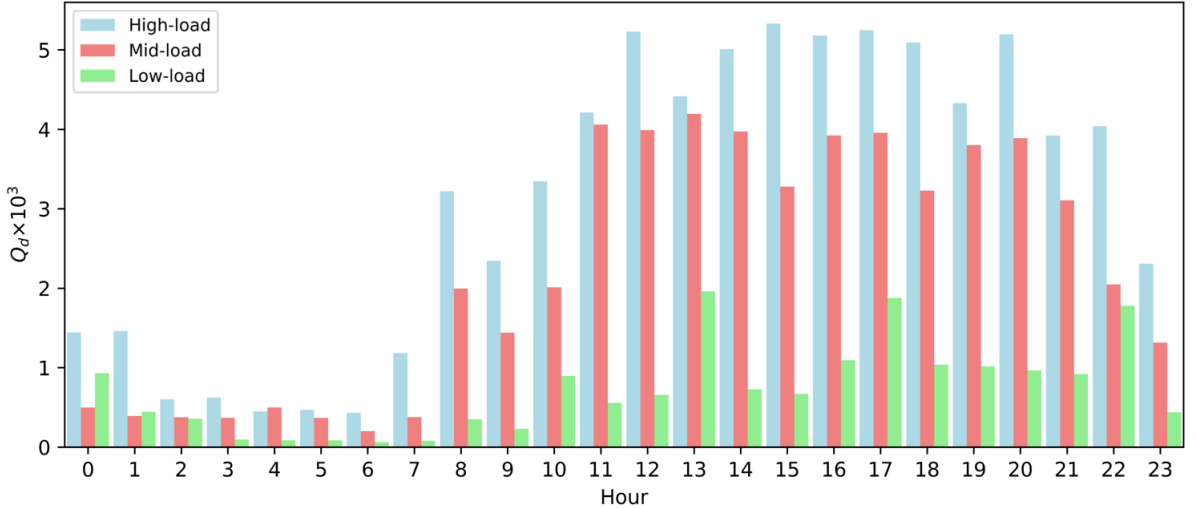


FIGURE 5.7: Customer demand profiles of the three chosen periods.

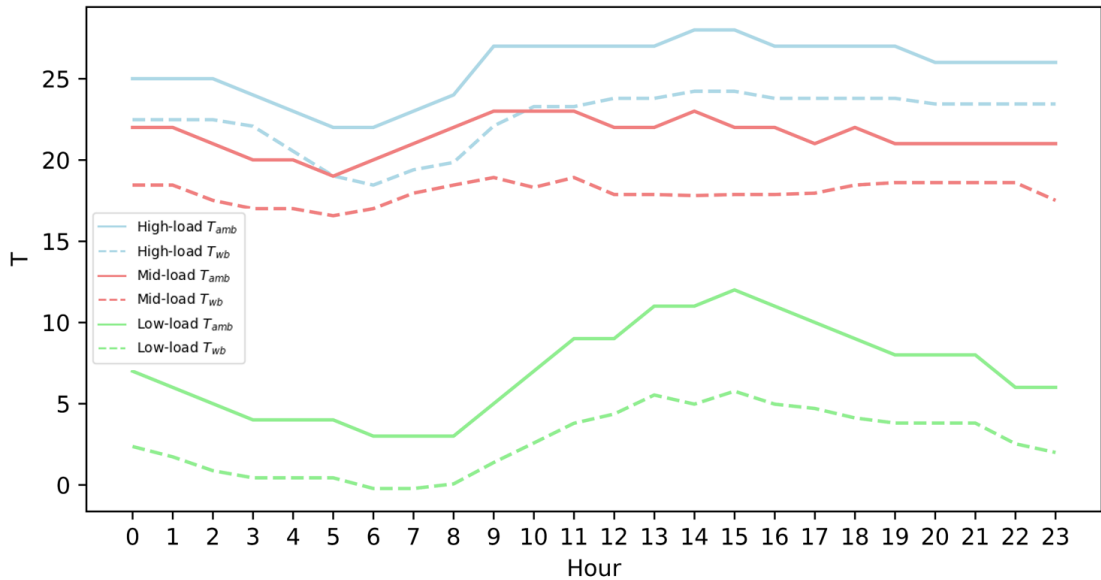


FIGURE 5.8: Ambient condition profiles of the three chosen periods.

5.4.2 Implementation of optimization framework

Table 5.4 describes the variables and parameters involved at each time-period. The variables are separated into master and slave level variables. These variables are handled separately in different phases of the optimization framework. Optimization of electricity over a 24-hour period involved 684 variables. The problem was simplified using the assumption that every time-period, comprising a 1-hour duration, is independent. The overall ‘optimal’ value, therefore, is the summation of

Model description	Section
Chiller	3.3.1
Evaporator pump-network	3.3.3.4
Condenser pump-network	3.3.3.4
Distribution pump-network	3.3.3.5
Cooling tower	3.3.2

TABLE 5.3: Component-level models required for the DCS case study.

‘optimal’ values of each time-period.

Master level variables	Description
$T_{ct,unit}^{out}$	temperature of fluid exiting the cooling tower array and entering the condenser side of chillers.
$\dot{m}_{ct,unit}^{in}$	total condenser network flowrate.
$T_{dist,nwk}^{out}$	temperature of return fluid from the distribution network entering the evaporator side of chillers.
\dot{m}_{sys}	total evaporator/distribution network flowrate.
Slave level variables	
$\% \dot{m}_{e,i}^{out}$	percentage of total flowrate through the i th chiller evaporator.
$T_{e,i}^{out}$	fluid temperature exiting i th chiller evaporator.
$T_{c,i}^{out}(K)$	fluid temperature exiting i th chiller condenser.
$\% \dot{m}_{c,i}^{in}$	percentage of total flowrate through the i th chiller condenser.
$\% \dot{m}_{cp}$	percentage of total flowrate through the common pipe.
$\% \dot{m}_{ss,i}$	percentage of total flowrate through the i th customer’s substation.
$\dot{m}_{a,ct,i}$	inducted air flowrate through each cooling tower.
$Pump_{sel}$	the choice/combinations of distribution pump(s).
Parameters	
$\dot{Q}_{d,i}$	cooling demand of the i th customer substation.
T_{wb}	thermodynamic wet-bulb temperature.
$\Delta T_{ss,i}^{max}$	maximum temperature difference on the cold-side of the heat-exchanger at the substation.

TABLE 5.4: Parameters and variables associated with the case study.

5.4.2.1 Mathematical formulation

This section illustrates the mathematical formulation of the decomposition approach. The objective function is defined as the minimization of hourly electricity consumption of the DCS.

Master level

The overall objective function for each hour is defined as:

$$\text{minimize } \dot{E}_{DCS} = f(\mathbf{T}_{ct,unit}^{out}, \dot{\mathbf{m}}_{ct,unit}^{in}, \mathbf{T}_{dist,nwk}^{out}, \dot{\mathbf{m}}_{sys}) \quad (5.1)$$

Variables at the master level are treated as parameters at the slave level and used for the computation of various coefficients which ensures that the slave is a MILP. For each set of master level variables, the slave returns an optimal solution. The process is iterated until a convergence criterion is met.

Slave level

The objective function at the slave level is:

$$\text{minimize } \dot{E}_{slave} = \sum_{i=1}^{n=3} \dot{E}_{ch,i} + \sum_{i=1}^{n=3} \dot{E}_{e,nwk,pump,i} + \sum_{i=1}^{n=3} \dot{E}_{c,nwk,pump,i} + \sum_{i=1}^{n=7} \dot{E}_{dist,nwk,pump,i} + \sum_{i=1}^{n=5} \dot{E}_{ct,i} \quad (5.2)$$

With $\mathbf{T}_{ct,unit}^{out}$, $\dot{\mathbf{m}}_{ct,unit}^{in}$, $\mathbf{T}_{dist,nwk}^{out}$ and $\dot{\mathbf{m}}_{sys}$ treated as parameters, the electricity consumed by the chiller and the associated constraints are defined as:

$$\dot{E}_{ch,i} = f(\% \dot{m}_{e,i}^{out}, T_{e,i}^{out}, \% \dot{m}_{c,i}^{in}) \quad (5.3)$$

The flowrate percentages and temperatures are required for the calculation of electricity consumption of the chiller.

With the total network flowrates ($\dot{\mathbf{m}}_{ct,unit}^{in}$ and $\dot{\mathbf{m}}_{sys}$) fixed as parameters, the electricity consumed by the evaporator and condenser pumps could be expressed as follows.

$$\dot{E}_{e,nwk,pump,i} = f(\% \dot{m}_{e,i}^{out}) \quad (5.4)$$

$$\dot{E}_{c,nwk,pump,i} = f(\% \dot{m}_{c,i}^{in}) \quad (5.5)$$

The following equations are involved in the computation of the electricity consumed by the distribution pump given that \dot{m}_{sys} is a parameter.

$$\sum_{i=1}^{n=7} \dot{E}_{dist,nwk,pump,i} = Y_{dist,nwk,pump,i} f(\% \dot{m}_{ss,1}, \dots, \% \dot{m}_{ss,4}) \quad (5.6)$$

$$\sum_{i=1}^{n=7} Y_{dist,nwk,pump,i} \leq 1 \quad (5.7)$$

Eq. 5.6 captures the impact of flowrate distribution in the parallel network on the pressure difference and hence the electricity consumed by the distribution pump. *Eq. 5.7* ensures that only one pump or pump combinations are selected for serving the distribution network. The selected pump is described by the variable P_{sel} .

Given $T_{ct,unit}^{out}$, $\dot{m}_{ct,unit}^{in}$ and T_{wb} as parameters, the electricity consumed by the cooling tower is,

$$\dot{E}_{ct,i} = f(\% \dot{m}_{c,1}^{in}, T_{c,1}^{out}, \dots, \% \dot{m}_{c,3}^{in}, T_{c,3}^{out}, \dot{m}_{a,ct,i}) \quad (5.8)$$

where $T_{c,i}^{out}$ is an output of the chiller model.

An heat-exchanger model was excluded due to the lack of control over the 'hot-side' of the substation as described in *Section 3.3.3.5*. The temperature difference at each substation is,

$$\Delta T_{ss,i} = \frac{\dot{Q}_{d,i}}{\dot{m}_{ss,i} \dot{m}_{sys} Cp_w} \quad (5.9)$$

$$\Delta T_{ss,i} \leq \Delta T_{ss,i}^{max} \quad (5.10)$$

Several additional constraints are needed to model the dependence between the equipment in the DCS. These are captured using the layer definition (*Section 5.3.3.2*). The flowrates in the DCS could be described by,

$$\sum_{i=1}^{n=3} \% \dot{m}_{e,i}^{out} \geq [\% \dot{m}_{cp} + \sum_{i=1}^{n=4} \% \dot{m}_{ss,i}] \geq 1 \quad (5.11)$$

$$\sum_{i=1}^{n=3} \% \dot{m}_{c,i}^{in} \geq 1 \quad (5.12)$$

The temperatures in the DCS could be described by:

$$\sum_{i=1}^{n=4} T_{e,nwk}^{out} + \Delta T_{ss,i} \leq \mathbf{T}_{dist,nwk}^{out} \quad (5.13)$$

$$\sum_{i=1}^{n=5} T_{c,nwk}^{out} + \Delta T_{ct,i} \leq \mathbf{T}_{ct,unit}^{out} \quad (5.14)$$

where $T_{e,nwk}^{out}$, $T_{c,nwk}^{out}$ and $\Delta T_{ct,i}$ could be calculated using the following equations,

$$T_{e,nwk}^{out} = f(\dot{m}_{e,1}^{out}, T_{e,1}^{out}, \dots, \dot{m}_{e,3}^{out}, T_{e,3}^{out}) \quad (5.15)$$

$$T_{c,nwk}^{out} = f(\dot{m}_{c,1}^{in}, T_{c,1}^{out}, \dots, \dot{m}_{c,3}^{in}, T_{c,3}^{out}) \quad (5.16)$$

$$\Delta T_{ct,i} = f(\dot{\mathbf{m}}_{ct,unit}^{in}, \dot{m}_{a,ct,i}, T_{c,nwk}^{out}) \quad (5.17)$$

The linearization process of the original models was described in *Chapter 3*. After the linearization process, the equations are structured in the form described in *Section 5.3.3*.

5.4.2.2 Modeling error

75% and 25% of the processed data were used for training and the evaluation of the models respectively (*Figure 5.9*). The MAE for the models representing the chiller, distribution pumps and cooling towers are 11.3%, 6.9%, and 1.8% respectively. The evaporator and condenser pumps report similar values to the distribution pumps. The aggregation of data over hourly time-horizon coupled with inaccuracies in the sensor readings was likely causes to the noise in the data. Nevertheless, the models can capture the performance of the equipment as evidenced by the plots.

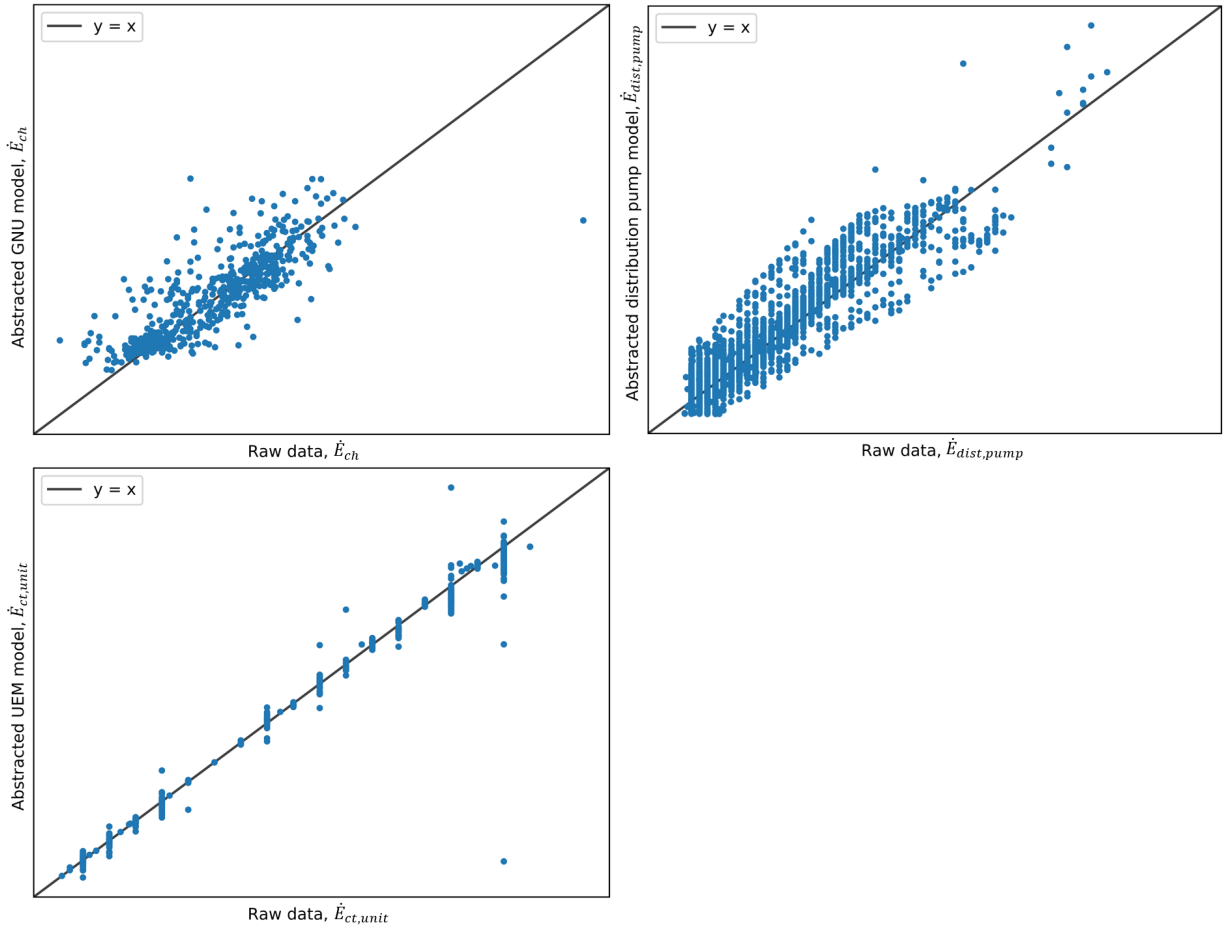


FIGURE 5.9: Error plots of the chosen models used in the case study.

5.4.2.3 Definition of base-cases and algorithm parameters

Simulation of the current operating practices using the chosen models is used as a benchmark for the evaluation of the results derived from the optimization strategy. These operating practices were a mixture of commonly employed control strategies for chiller plants [6, 7]. Results of the simulation are also used for ‘seeding’ the GA to eliminate any chance of the optimal value being worse-off than the ‘base-case’.

Additionally, chiller-only optimization was also defined to highlight the benefits of performing holistic optimization on the DCS. For this scenario, each chiller is permitted to optimize independent variables of the unit, while respecting the constraints of other units. This is done to illustrate the additional benefits of holistic optimization to chiller-only optimization - a practice which is commonplace in the literature. *Table 5.5* lists the treatment of key variables in both cases.

		'Base-case'	'Chiller optimization'	'Holistically optimized'
Decision variables	ΔT_{app}	Fixed	Fixed	Variable
	$\dot{m}_{c,i}$	Fixed	Fixed	Variable
	$\dot{m}_{e,i}$	Fixed	Variable	Variable
	$T_{e,i}^{out}$	Fixed	Variable	Variable
	$\Delta T_{ss,i}$	Averaged from raw data.	Variable	Variable
	$Pump_{sel}$	Staged based on flowrates.		Variable
	$Y_{ch,i}$	Staged based on flowrates.	Variable	Variable

TABLE 5.5: Decision variable settings of the DCS in the three optimization cases defined.

All computations were done on a workstation with 16 GB of RAM, and an i7 4710HQ CPU clocked at 3.5 GHz on all cores. The cumulative time required for a single run of the model reduction to post-processing phases averages at 40 seconds. Solving the slave sub-problem, however, only requires approximately 5 seconds. For the GA, a population size of 100 was defined and evaluated until there is no change in the objective function for 10 generations. For the MILP, the solver was set to terminate should the optimality gap between the lower and upper objective bound is below 10^{-4} .

5.5 Results and discussion

For data confidentiality, all numbers are scaled by a common factor. The order of magnitude is still preserved.

5.5.1 Comparison of approaches: GA-only and the optimization framework

The advantage of using the optimization framework over the direct application of the GA onto the case study is highlighted in *Figure 5.10*. Both methods were used to optimize the electricity consumption for a given demand for a single hour. Hyperparameter settings for the GAs used in both approaches are detailed in *Table 5.6*. The hyperparameters are defined such that the ratio between the variables,

population and tournament sizes are maintained. The six trials were allowed to iterate for the same time duration.

Without the need to execute of MILP solvers, the GA-only approach could complete evaluating more generations than the optimization framework. However, the value of the final objective function from this approach left much to be desired - despite iterating through more generations; it did not deliver the same objective function value for each of the three trials. For the case of the optimization framework, the reduced number of variables that the GA had to deal with, likely allowed it to converge to a superior solution more quickly.

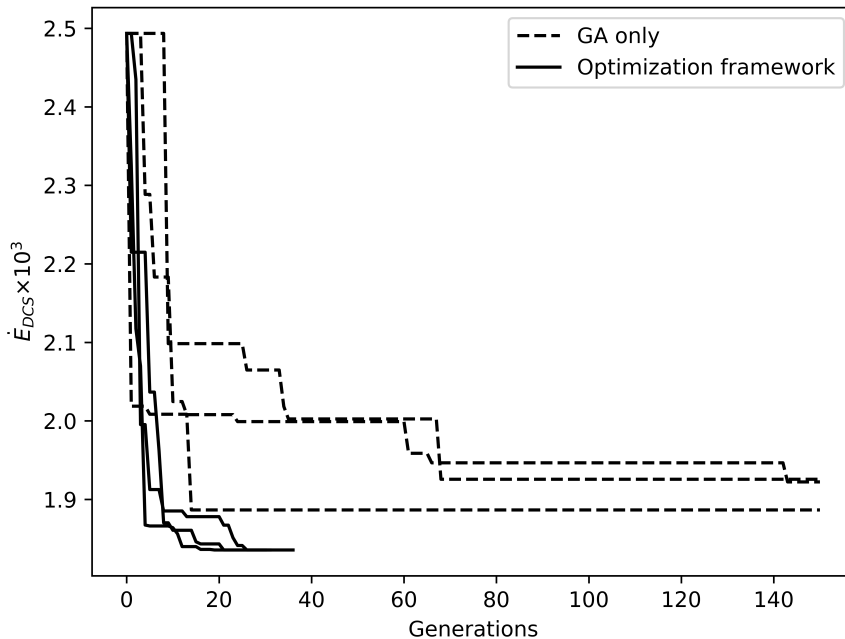


FIGURE 5.10: Performance comparison between the direct application of GA and the optimization framework.

	GA only	Optimization framework
Number of GA variables	4	22
Population size	100	550
Tournament size	30	165
Crossover percentage	0.4	0.4
Mutation percentage	0.1	0.1

TABLE 5.6: GA hyperparameters for both approaches.

5.5.2 Case study results

The cumulative electricity consumption of the DCS for the ‘base’, ‘chiller optimization’ and ‘holistically optimized’ cases are plotted in *Figure 5.11*. A decrease in electricity consumption of 31.93%, 27.38%, and 3.03% is observed across the three 24 hour periods representing high, medium and low cooling demand respectively between the first and third cases. *Table 5.7* details the breakdown of the decrease in electricity consumption by component.

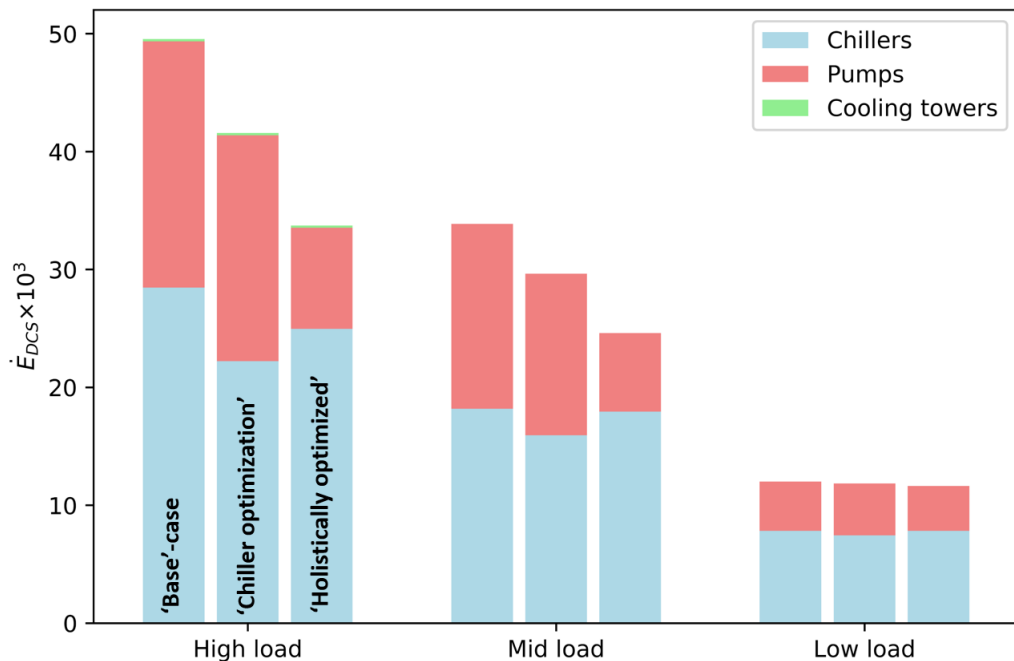


FIGURE 5.11: Result comparison of the three optimization cases over the three representative periods.

Not all components experienced the same rate of decrease in electricity consumption despite the overall figures. This highlights the benefit of performing optimization holistically as compared to the chiller-only approach, as the results are not apparent. Overall, the savings in the operation of the pumps are the most significant contributors to the savings in electricity. Optimization of the chillers, independent of the pump operations neglected this opportunity for added electricity savings. This effect is clearly illustrated when comparing the results of the chiller-only and the holistic approach. At the ‘optimum’ chillers were operated up to 12% less efficiently in the holistic as compared to the chiller-only optimization approach. The slight reduction in chiller efficiencies, enabled the pumps to be operated more efficiently, thereby contributing to greater electricity savings for the entire system.

	'base' vs 'chiller optimization'	'base' vs 'holistically optimized'	'chiller optimization' vs 'holistically optimized'
High load	Percentage decrease in electricity consumed (%)		
Chillers	- 21.94	- 12.28	12.36
Pumps	- 8.24	- 58.95	- 55.26
Cooling towers	0.00	- 5.00	- 5.00
Overall	- 16.07	- 31.93	- 18.89
Mid load			
Chillers	- 12.45	- 1.36	12.66
Pumps	- 12.58	- 57.56	- 51.45
Cooling towers	0.00	0.00	0.00
Overall	- 12.51	- 27.38	- 17.00
Low load			
Chillers	- 4.81	0.06	5.12
Pumps	5.33	- 8.81	- 13.42
Cooling towers	0.00	0.00	0.00
Overall	- 1.28	- 3.03	- 1.77

TABLE 5.7: Percentage change in electricity consumption across the representative periods.

The concurrent changes in chiller and network operation are the main reasons for this occurrence. The following discussions explain the reasons for the electricity savings from the perspective of the chiller and distribution network operation by comparing the results of holistic optimization against the 'base' case. The discussion omits the impact of the cooling towers as they were hardly in operation due to the relatively low ambient temperatures (*Figure 5.8*).

As there exists a minimum flowrate on the evaporator side of every chiller, more chillers in operation generally implied an increase in chilled water flowrate which loaded the pumps more heavily. The cumulative operating hours of the 'holistically optimized' cases are always lower than their corresponding 'base' cases (*Table 5.8*). This means that fewer chillers are activated to meet the cooling demand which results in a reduced load on the pumps.

There could be several explanations for this occurrence. For illustration purposes, the chiller staging strategies and the flowrates in the distribution network for all three load scenarios are plotted in *Figures 5.12* and *5.13*. It can be seen that under the 'holistically optimized' operating strategy, there is a general preference

		Working hours (h)			
		Chiller 1	Chiller 2	Chiller 3	Total
High-load	'Base'- case	14	18	7	39
	'Holistically optimized'	7	8	11	26
Mid-load	'Base'- case	17	15	0	32
	'Holistically optimized'	12	6	8	26
Low-load	'Base'- case	18	9	0	27
	'Holistically optimized'	16	7	2	25

TABLE 5.8: Working hours of chillers in DCS.

for operating as few chillers as possible. For fewer activated chillers with lower flowrates to fulfill the same cooling demand, the chilled water supply temperatures ($T_{e,i}^{out}$) of chillers had to be lowered. These lowered temperatures increased the thermal energy content of the working fluid which enabled the cooling demand to be met. The impact of such an action is usually unclear; lower chilled water supply temperature increases compressor lift which decreases energy efficiency. Conversely, general improvements in loading conditions have the opposite effect. This effect is illustrated in the part-load performance plot of one of the chillers in the case study (*Figure 5.14*). Additional consideration of the impacts on pumps and networks further complicated the outcome.

Scenarios also exist whereby operating a larger chiller is more economical for the entire system. This can be seen from the period spanning from 0100hrs to 0700hrs across all three load scenarios (*Figure 5.12*). Operating a larger chiller means that the criteria for the minimum flowrate have to be raised (*Figure 5.13*). Raising the flowrate negatively impacted the ΔT of the distribution network. However, due to chiller 2 and 3 being dual-compressor systems, having a single compressor activated meant that it had the luxury of utilizing the entire heat-exchange surface area on both the condenser and evaporator sides. That results in a higher *COP* as compared to operating chiller 1 for the given load.

There are uncommon instances where (low-load, *Table 5.7*) where the 'holistically optimized' results suggest that chillers should operate less efficiently for the benefit of the overall system performance.

It is thus, worthwhile to investigate the operation of the distribution network since the pump operations at the 'optimum' are the largest contributors to the overall electricity savings. It has been established that the lower chilled water supply

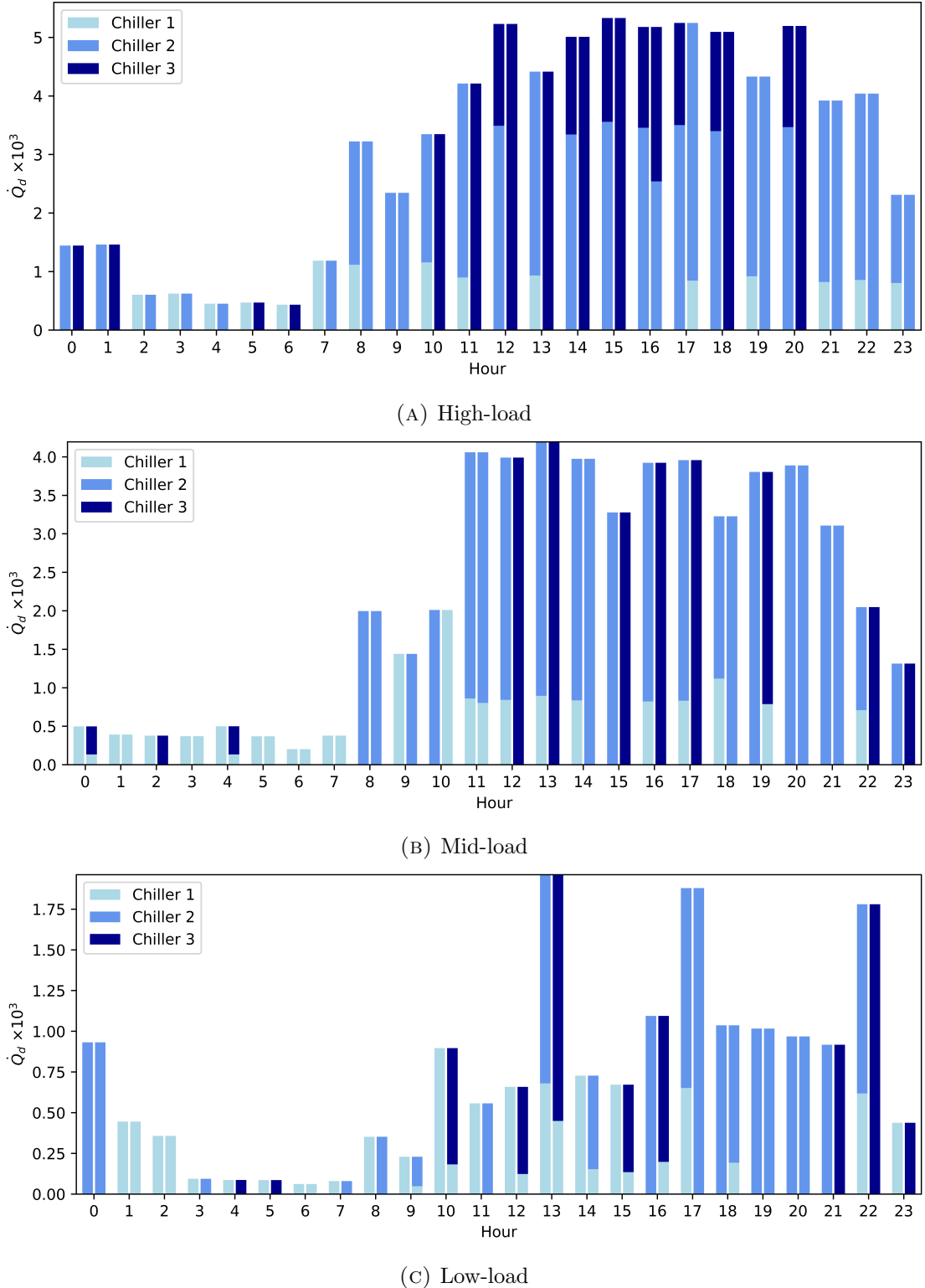


FIGURE 5.12: Comparison of chiller staging strategies between the ‘base’ and ‘holistically optimized’ cases.

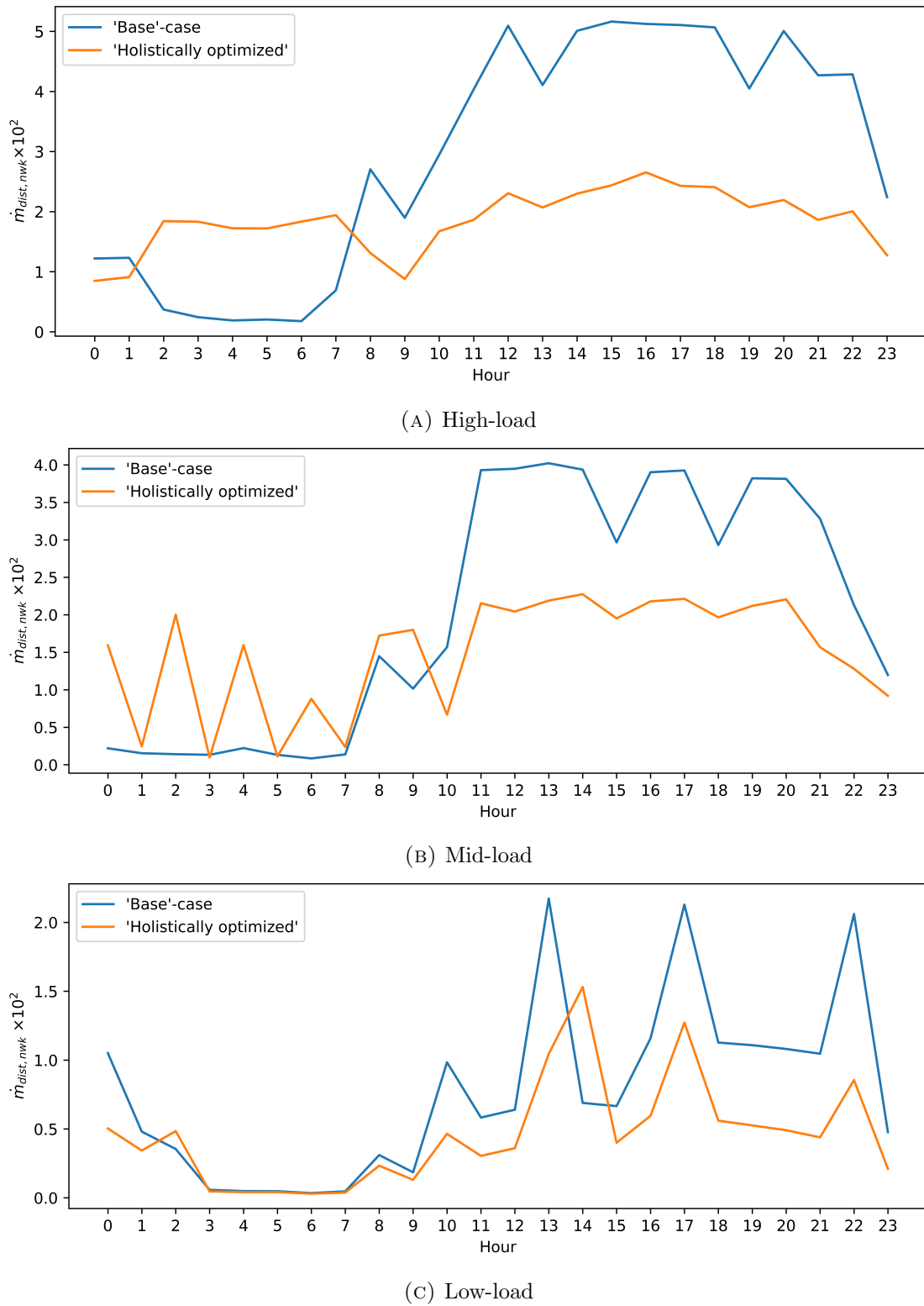


FIGURE 5.13: Comparison of $\dot{m}_{dist,nwk}$ in the distribution network between the 'base' and 'holistically optimized' cases.

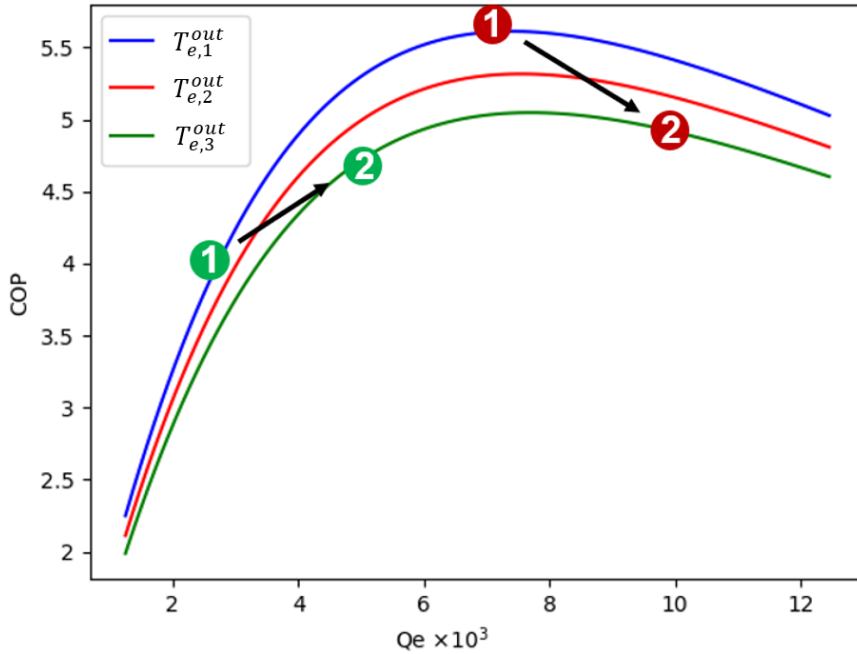


FIGURE 5.14: Impact of lowering chilled water temperatures at various points of the part-load curve.

temperatures ($T_{e,i}^{out}$) reduces the overall flowrate and hence the load on the pumps. That, however, is only just one side of the equation. Comparison of *Figures 5.13* and *5.15* reveals a positive relationship between the flowrate ($\dot{m}_{dist,nwk}$) and the pressure difference ($\Delta P_{dist,nwk}$) in the distribution network. While that is generally true, the reduction of $\Delta P_{dist,nwk}$ could also be explained by another factor - valve regulation at the substation of customers.

Most of the above explanations are focused on how lowering chilled water supply temperatures, reduces the overall flowrate in the distribution network and hence the electricity consumption of the pumps. *Figure 5.16* compares the temperature difference at the substation level ($\Delta T_{ss,i}$) between the ‘base’ and ‘holistically optimized’ cases. A reduction of distribution network flowrate should increase the value of $\Delta T_{ss,i}$ across the board, however, scenarios exist, at the ‘optimum’ where the value of $\Delta T_{ss,i}$ is lower than that of the ‘base’ case. Intuitively, this should not happen as it only serves to degrade the return temperature to the chillers ($T_{dist,nwk}^{out}$), which will adversely impact the efficiency of chillers. The reason for this observation becomes clearer only when analyzing the results from the standpoint of network pressure difference. In a parallel network configuration with each branch independently controlled by a valve, the situation with the lowest flow impedance

occurs when all valves are fully open. Partially closing a valve in any branch will serve to impede flow and subsequently increase the pressure difference of the entire network. Depending on the cooling demand scenario, it is hence, conceivable that some valves regulated such that more chilled water flows through a given substation than required. Doing so, despite compromising on $\Delta T_{dist,nwk}$ saves electricity by reducing $\Delta P_{dist,nwk}$. This effect is most commonly observed in the mid-load condition (*Figure 5.16b*).

The benefits of applying optimization to the DCS are highlighted in the case study. Optimization of DCS at the system level extended beyond the consideration of chillers alone. This was especially true in DCS where considerable energy is used in the distribution of chilled water, a key difference between district and building-level systems. There are even instances where a slight reduction of chiller efficiencies resulted in overall electricity savings at the system level. The reduction of chilled water supply temperatures to prevent another chiller from being activated is one such example. For a system with such tight-coupling between components, the best operating strategy is usually non-trivial.

There are limitations to the extent of improvement, however. At extremely low loads, little can be done to improve the operation of the DCS. This is a design-related issue that has to be dealt with separately. The proposed methods of improving system performance can be used as short-term measures, as well as a guide for further improvements in design. For instance, it may not be ideal to supply chilled water colder than required for prolonged periods. Should the operation of DCS at part-load conditions be expected to prevail, perhaps the addition of a smaller chiller, storage or making changes to heat-exchangers at the substations could prove much more beneficial. Such conclusions can only be reached after conducting proper cost-benefit analyses.

5.6 Conclusion

In this chapter, a hierarchical framework for holistic optimization of the operations of urban energy systems has been introduced. This framework utilizes a combination of GA and MILP to solve MINLP problems in a bid to bridge the deficit between design and operating performance. It could also function as a tool that

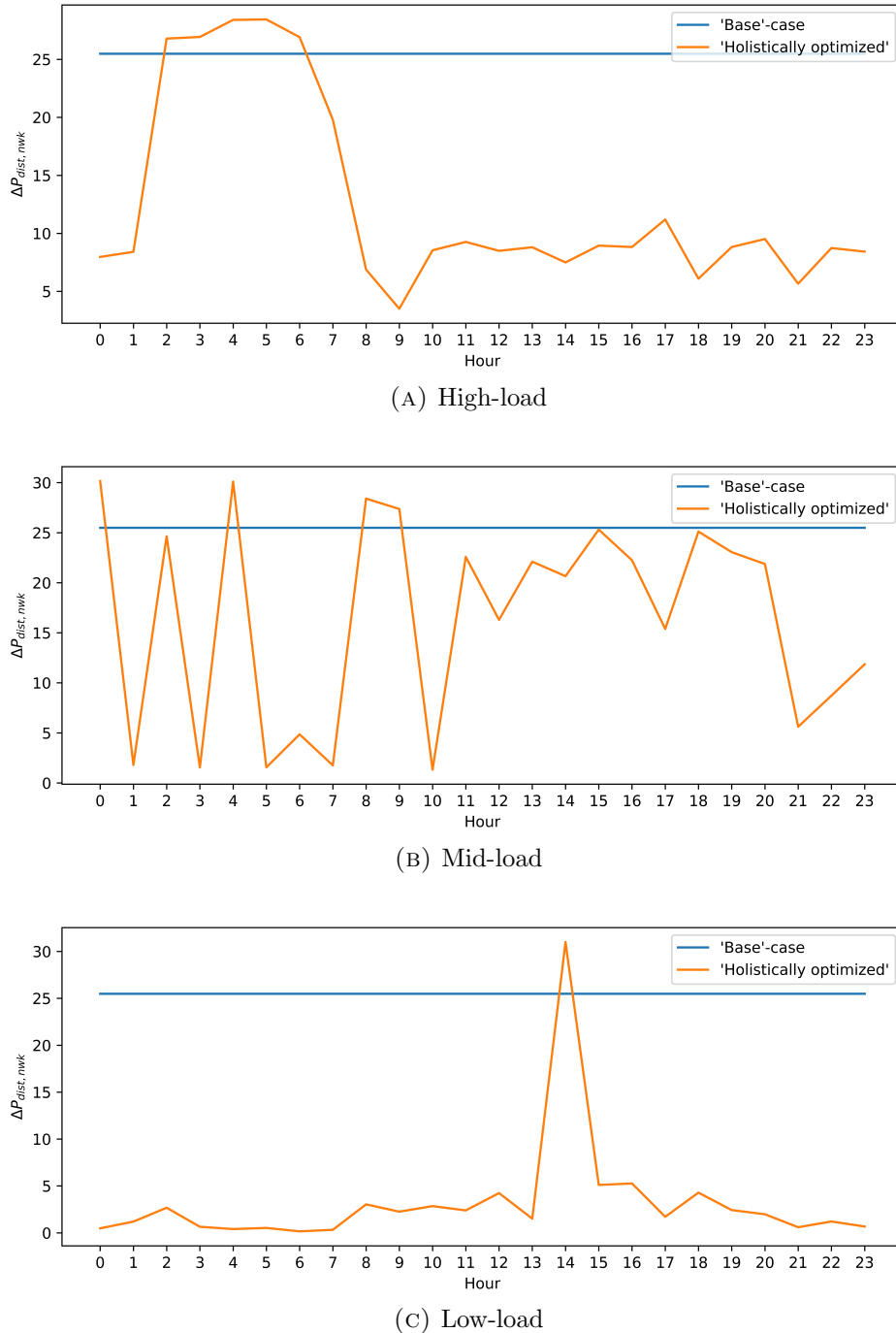


FIGURE 5.15: Comparison of $\Delta P_{dist,nwk}$ between the ‘base’ and ‘holistically optimized’ cases.

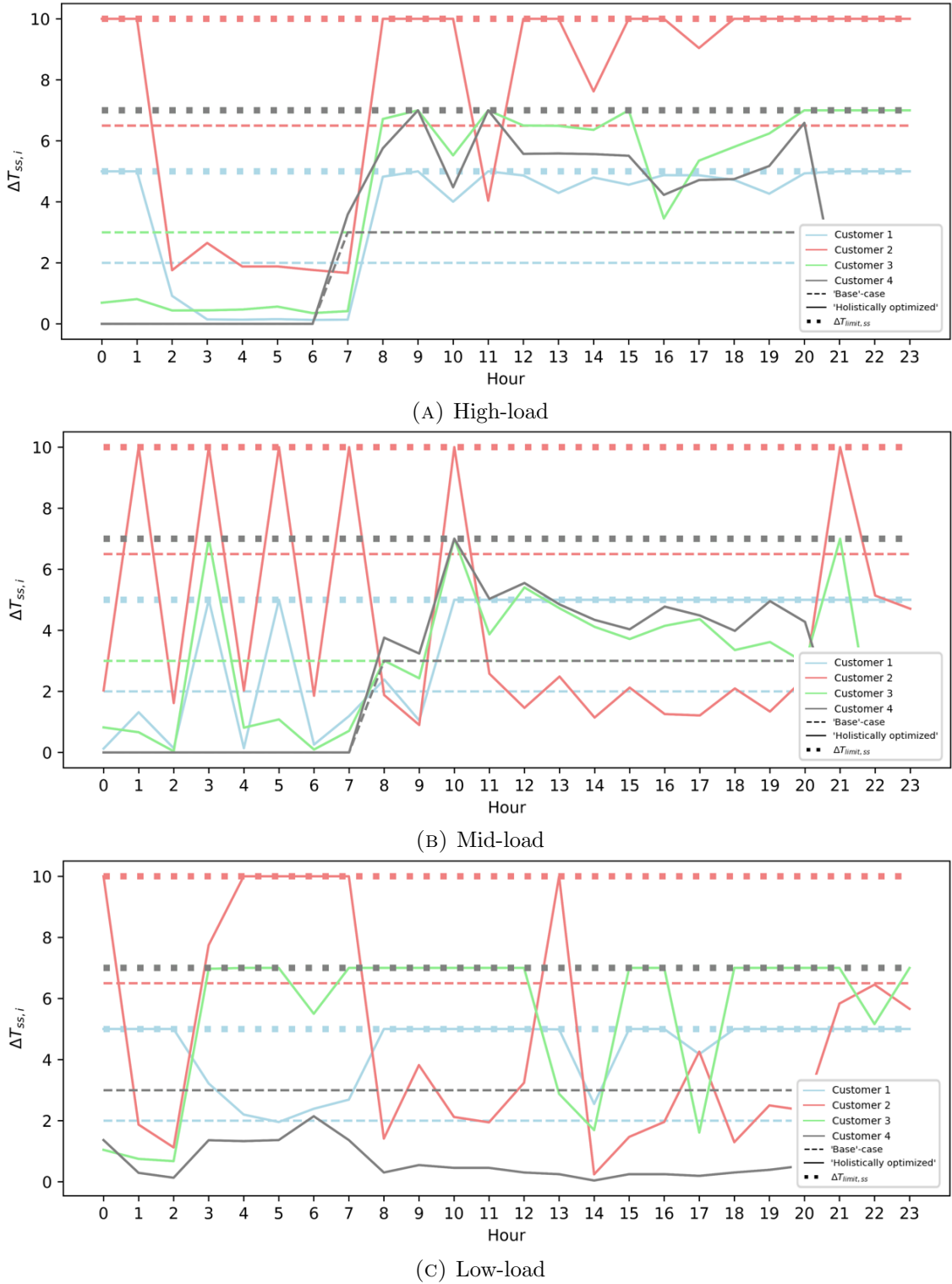


FIGURE 5.16: Comparison of customer substation ΔT between the ‘base’ and ‘holistically optimized’ cases.

aids the decision-making process of operators' of such systems. Compared to the pure application of metaheuristics, the methodical decomposition of the complex MINLP problem in the proposed framework hugely benefited not only solution quality but also resolution time.

Through this framework and its subsequent application on a case study, the holistic-level is once again proven to be superior to component-level optimization. This is primarily derived from the modeling of interdependencies amongst the system-components at the appropriate fidelity. Finally, the limits of operation optimization are also highlighted - operation optimization alone is no solution for an inherently inferior design ('low-load' condition).

The current state of the framework is plagued by one glaring issue, which is brought about by the GA - slow resolution speed. This is inevitable due to the population-based, iterative nature of the algorithm. The impact becomes compounded when the size of the optimization problem gets larger (i.e. energy storage, and resulting coupling across time-periods, etc.). This framework as it is is not yet suitable for real-time deployment. To address these shortcomings, approximations (*Chapter 6*) are introduced together with machine-learning (*Chapter 7*) techniques to hasten the execution of the algorithm in real-time.

Chapter 6

Multi-period, multi-objective, holistic optimization, using the sliding-window approach

6.1 Overview

The inclusion of energy storage in urban energy systems burgeons the size of the optimization problem, making the already computationally intensive task intractable. Intractability occurs when there are just simply too many decision variables for the algorithms to handle, resulting in excruciatingly long resolution times. The need to simultaneously solve for the optimal values across various time-periods for multiple objectives is the primary reason for this occurrence. The hierarchical framework introduced in the previous chapter does not perform satisfactorily for solving large scale problems, especially when there are many decision variables at the master-level. The genetic algorithm's (GA) iterative nature and difficulty of expressing constraints at the master level are the two chief reasons for the inefficiency of *Chapter 5*'s methodology.

To aid the solvability of the complex multi-period, multi-objective mixed-integer non-linear program (MINLP), the hierarchical framework is enhanced with a new feature - the sliding window technique. This new feature permits the limitation of the number of time-periods to be simultaneously solved, hence, benefitting the framework's resolution speed for energy-storage related optimization problems.

This chapter begins with an introduction of the sliding-window technique and the limitations in the existing literature. Subsequently, the demonstration of the new version of the hierarchical framework is done through its application on a case study in *Section 6.3*. Finally, the results of the case study are presented and discussed.

6.2 Introduction

For energy storage to be meaningfully incorporated into optimization problems, two additional features must be included - multi-period and multi-objective considerations. The primary existence of storage systems is to provision for energy to be stored in more favorable periods, which is then made available thereafter. This is mainly done for two reasons - to improve the energy performance or cost-effectiveness of the system. Improvements in energy performance are largely related to how the storages affect the operational efficiency of the system components. There usually exists a narrow bandwidth for peak performance in these components; failing to operate within, results in substantial penalties in efficiencies. Energy storages, thus aid the cause by permitting these components to over/under produce energy irrespective of demand conditions so that efficiency is maintained. Hence, the inclusion of multi-period capabilities is paramount.

Another important reason for storing energy is to take advantage of the ratio of resource prices to energy production. Building-level systems for instance, typically require electricity from the grid for operation. The greatest amount of monetary savings is likely to occur when both system efficiency is balanced with operating costs. To do that, the objective function has to, for example, be changed from the minimization of electricity consumption to that of operating cost. However, the most cost-effective method does not necessitate the implication of the most environmentally friendly one, hence multi-objective features are required to generate Pareto frontiers, where the tradeoff between both objectives becomes explicit.

This chapter explores the use of the sliding-window technique to complement *Chapter 5*'s hierarchical framework for handling the two, above-mentioned features. The applicability of the proposed method is highlighted through a case study based on the same district cooling system (DCS) as in the previous chapter, with the addition of a theoretical cold-water tank thermal energy storage (TES).

6.2.1 Sliding-window technique

The version of the sliding-window technique used in this chapter assumes a fixed window size (m , number of time-periods, considered), which is pre-determined. Once the window size is fixed, the concomitant optimization problem is formulated for the size of the specific window and solved. However, once solved, the solution is only extracted for the first time-period of the window. Subsequently, the window will ‘slide’ - in doing so, it removes the first time-period and adds the next time-period, which was formerly outside, i.e. $t = m + 1$, before repeating the entire process until the full multi-period optimization problem is solved. The sliding-window technique can be better visualized through *Figure 6.1*.

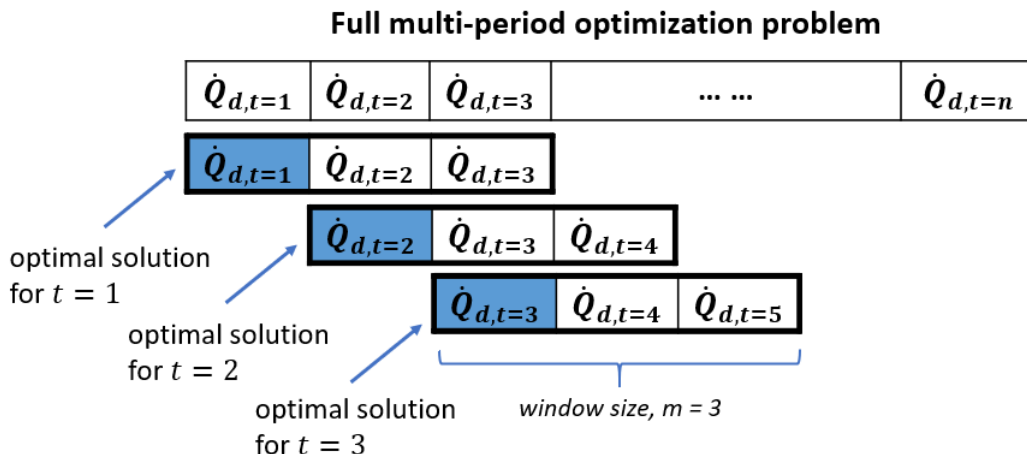


FIGURE 6.1: The sliding-window technique.

The choice of the window size factors future demand conditions, when making decisions in the present, hence it has to be chosen judiciously for results to be satisfactory. Incorporating the sliding-window technique into the hierarchical framework has two primary benefits - increasing the solvability of a large optimization problem and the ability to deliver results for individual time-periods quickly.

6.2.2 Literature review

MILP is commonly deployed to solve for the optimum operation plan of urban energy systems including storages [179–181]. The highly abstract models utilized in these studies, permitted the formulation of the optimization problem as a MILP, hugely promoting solvability. These models are only capable of quantifying the

energy in and out-flows; regardless of how positive the optimal results are, they suggest very little on how the system should be operated. The efficiency of urban thermal systems, in particular, are especially sensitive to temperature changes, hence optimization with respect to thermal energy flows alone is insufficient [63].

For design-related problems, MINLP solvers are deployed to manage the non-linearities which pertain to the sizing of the storage system [182, 183]. These studies, however, pertain to the sizing of the storage system, rather than its operation. Additionally, MINLP solvers, while capable of generating improved solutions, have no guarantee on resolution time and solution quality. For even more complex models, simulation is used [184].

Samira et al. discretized the thermal storage into several temperature bands before using a combination of evolutionary algorithms and MILP to solve for the optimal system design [92]. Despite being a design-related study, the factoring of temperature variables offers a guide on the appropriate temperatures to operate the system. Fang et al. formulated an optimization problem into a linear program for the optimization of thermal storage of a combined heat and power (CHP) plant [185]. Despite, the simplistic modeling of the CHP plant, attempts were made to reduce the complexity of the problem reduced through the use of the sliding-window technique. These findings show that a negligible impact on the objective function is observed, once a window size of five time-periods (days) was chosen. This effectively suggests that solving the problem in its entirety (simultaneous consideration of all time-periods) is an unnecessary endeavor.

It is indicative from this review that besides [185], there is little attempt to improve on the solvability of multi-period optimization besides model simplification. Where the optimization of the operations of urban energy systems is concerned, it is important to express the problem in terms of tuneable variables as the generated solution can be easily translated into actionable improvements. This still holds even with the addition of energy storage systems. Hence, the current work focuses on exploring techniques other than model simplification to improve the solvability of multi-period operation optimization problems.

6.2.3 Objectives

The complexity of the holistic optimization of the operations of urban energy systems is further exacerbated with the addition of storage. In this chapter, the hierarchical optimization framework in *Chapter 5* is augmented with the sliding-window technique before its successive application on a case study based on an existing DCS with a theoretical storage system. The results presented in this study aspires to accomplish two objectives - illustrate the impact of storage systems on the operation of chillers when optimized for different objectives, and discuss the effect of the window size on the objective function value.

6.3 Problem formulation

This section begins with a description of the case study, followed by the augmented optimization framework. Finally, the formulation of the accompanying optimization problem is presented.

6.3.1 Case study description

Figure 6.2 illustrates the schematic of the DCS with a theoretical storage system. It was established in *Chapter 5* that there are scenarios whereby the chilled water temperature (T_e^{out}) was lowered to prevent another chiller from starting. In an attempt to reduce the frequency of this occurrence, the storage system was added to the DCS to bridge the gap between the small and large chillers. A two-level water storage tank is chosen as the storage medium, due to economical and technology maturity reasons. Typically, either the load-leveling or load-shifting methods would have been used for sizing the tank, however, due to physical constraints in the central station of the DCS, only two tanks are considered - one, sized to the maximum tank size which the facility can accommodate, and the other, half the capacity of the former. The smaller tank is included in the case study for illustrative use, i.e., comparing the effects of the window size, etc.

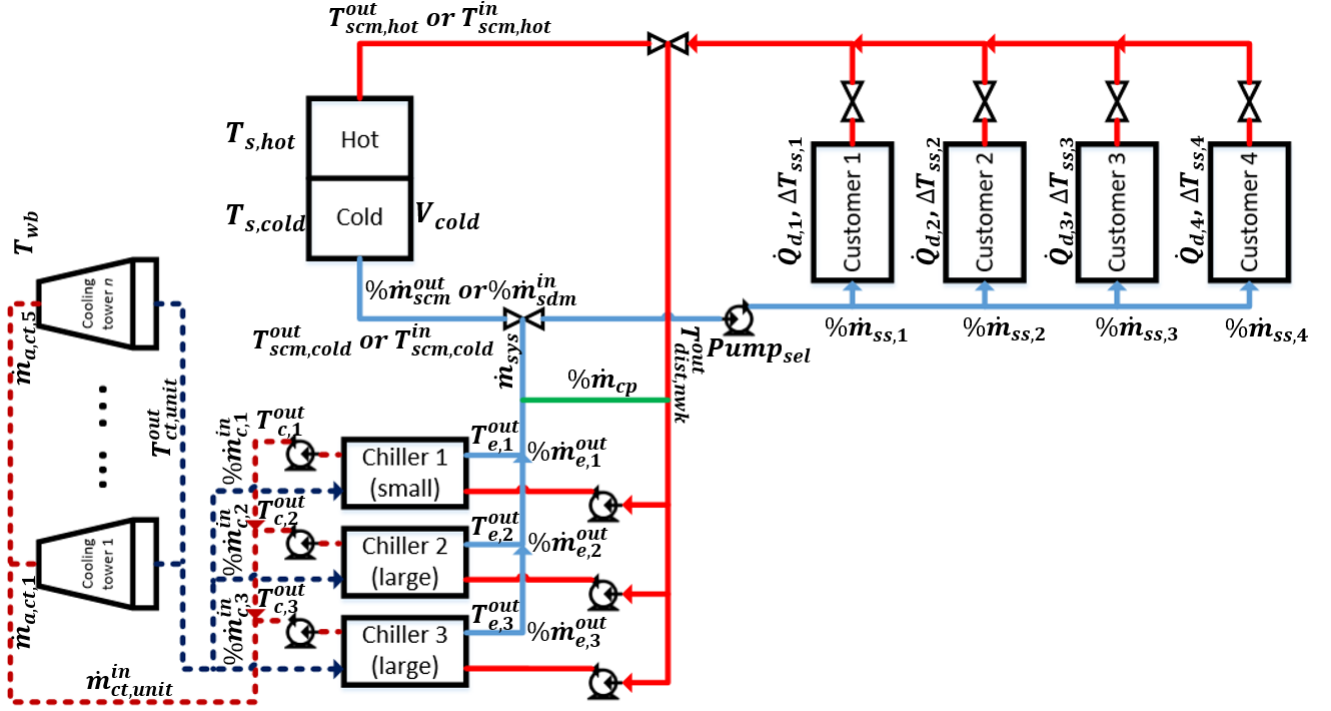


FIGURE 6.2: Schematic of the case study DCS with a theoretical two-layer storage tank.

6.3.2 Sliding-window augmented hierarchical framework

Owing to the sheer size of the optimization problem, when the TES is included, the direct application of the sliding-window technique does little to aid solvability; i.e., even for small window sizes, the GA did not converge to any value better than the seeded one despite the many iterations it had undergone. This is likely due to the difficulty in expressing inter-period constraints at the master-level where the GA resides.

To deal with this issue, the sliding-window technique is first applied to a highly simplified model of the DCS, involving only the chillers, TES, and consumers. Doing so enables the pre-determination of a storage schedule before utilizing the optimization framework. This schedule, when obtained, indicates how much energy to charge and discharge for any given time-period. Finally, the schedule is assimilated as parameters in the hierarchical framework, before solving for the optimal operation plan. The overview of the augmented hierarchical optimization framework is illustrated in *Figure 6.3*.

The chiller and storage models used during the storage scheduling phase have discretized operating temperatures. This is done for enhanced realism; accounting for scenarios whereby more thermal energy may be required to be stored in the tank of fixed volume, even at the expense of current operating efficiencies. Doing so could benefit from the overall electricity consumption over the given period, determined by the window size. Additionally, the operating *COPs* of the chillers can be discretized in this phase, for the same reason. For simplicity, the discretization of *COP* is not presented in this chapter as it can be found in *Section 3.3.1.3*.

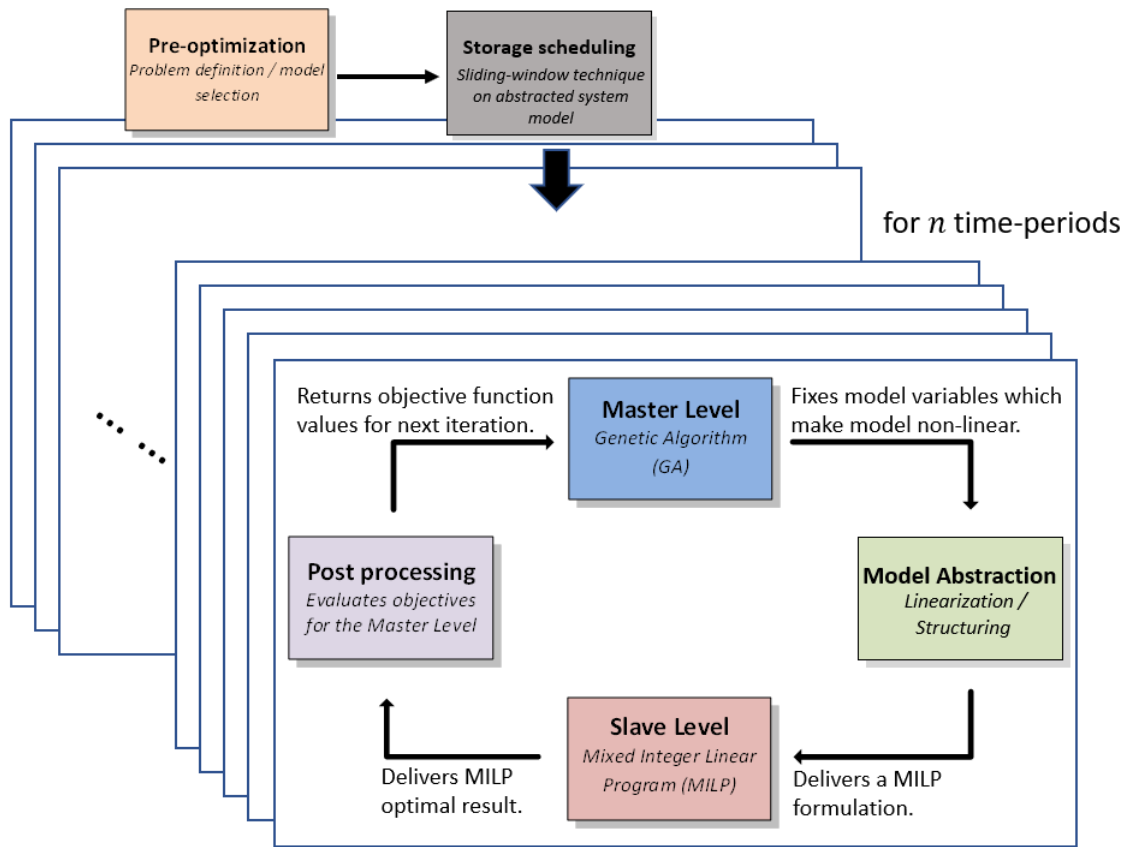


FIGURE 6.3: Overview of the sliding-window augmented hierarchical framework.

6.3.3 Mathematical formulation

This subsection deals with the mathematical formulation of the augmented hierarchical optimization framework. There are three levels in this approach - first the determination of the storage schedule, second, the master-level and lastly, the

slave-level. Detailed description of the component models are not discussed here, as they can be found in *Chapter 3*.

Storage scheduling

The addition of storage systems, inevitably requires multi-objective considerations. For this case, the linear scalarization technique is used to optimize the system either with respect to electricity consumption or operating cost. Both the objectives are first normalized before the application of the linear weights ranging from 0 to 1. *Table 6.1* documents the variables and parameters at the storage scheduling phase.

Variables	Description
\dot{E}	electricity consumed.
\dot{Q}	thermal energy, cooling effect.
Y	binary on/off variable.
Parameters	
C_p	specific heat capacity.
m_{ch}, j, i, t	evaporator flowrate of each discretized chiller.
T_j	discretized temperature.
$\dot{Q}_{min/max}$	upper and lower limits of the chiller capacity.
V	TES volumne.
W	weights
ρ	density
Subscripts	
ch	chiller
d	demand
t	time-period
i, l	chiller index
j, m	discretized temperature index
k	consumer index
li	linear intervals
min	minimum
max	maximum
n	the final index
s	storage
sw	sliding window
w	water
wd	window index within sliding window

TABLE 6.1: Parameters and variables associated with the storage scheduling phase.

The objective functions at the storage scheduling level is defined as:

$$\text{minimize } \dot{E}_{ch} = \sum_{t=1}^{n_t=24} \sum_{i=1}^{n_i=3} \sum_{j=1}^{n_j=3} \dot{E}_{ch,t,i,j} \quad (6.1)$$

$$\text{minimize } C_{\dot{E}_{ch}} = \dot{C}_{ele_rate,t} \sum_{t=1}^{n_t=24} \sum_{i=1}^{n_i=3} \sum_{j=1}^{n_j=3} \dot{E}_{ch,t,i,j} \quad (6.2)$$

where t , i and j represent the current time-period, chiller index and discretized temperature respectively. With T_j and $m_{ch,t,i,j}$, discretized and treated as a parameter respectively, the electricity consumed by each chiller can be defined as:

$$\dot{E}_{ch,t,i,j} = f(\dot{Q}_{ch,t,i,j}, T_j) \quad (6.3)$$

The following equations define the constraints related to the storage scheduling phase of the optimization framework. *Equation 6.4* describes the upper and lower limits of the chiller capacities. The binary variables Y s were added such that the optimizer could choose whether to activate or deactivate the chillers.

$$Y_{ch,t,i,j} \dot{Q}_{ch,i,min} \leq \dot{Q}_{ch,t,i,j} \leq Y_{ch,t,i,j} \dot{Q}_{ch,i,max} \quad (6.4)$$

At every time-period t the following equation ensures that the cooling demand by each substation is always fulfilled, either by the chiller or the stored energy in the current time-period.

$$\sum_{j=1}^{n_j=3} \dot{Q}_{s,j,t} + \sum_{i=1}^{n_i=3} \sum_{j=1}^{n_j=3} \dot{Q}_{ch,i,j,t} \geq \sum_{k=1}^{n_k=4} \dot{Q}_{d,k,t} + \sum_{j=1}^{n_j=3} \dot{Q}_{s,j,t+1} \quad \forall t \quad (6.5)$$

Each discretized TES unit is assigned a different capacity, which is dependent on the discretized temperature. The following equation ensures that the physical capacity of the TES water tank is not exceeded at every time-period.

$$\frac{\dot{Q}_{s,j,t}}{\rho_w C p_w \Delta T j} \leq V_{s,j,max} \quad \forall t \quad (6.6)$$

Finally, the following constraints ensure that only chillers and storages of the same discretized temperatures are activated at any given time-period. This ensures that the ability to store more energy in the TES is only as a result of temperature manipulation.

$$\sum_{j=1}^{n_j} Y_{s,j,t} \leq 1 \quad \forall t \quad (6.7)$$

$$\sum_{j=1}^{n_j} Y_{ch,i,j,t} \leq 1 \quad \forall i, t \quad (6.8)$$

$$Y_{ch,i,j,t} + Y_{ch,l,m,t} \leq 1 \quad \forall t, i \in [1, n_i - 1], l \in [i, n_i], \\ j \in [1, n_j - 1], m \in [j, n_j] \quad (6.9)$$

After defining the objective function and constraints, the sliding window technique is deployed for optimizing the hourly storage schedule. The window size (n_{sw}) and the number of linear intervals (n_{li}) is first determined. Linear intervals serve as weights for the linear combination of both objective functions - (\dot{E}_{ch}) and ($C_{\dot{E}_{ch}}$) to address the need for multi-objective optimization. After the results for each time-period and each linear combination of the objective function is computed, the thermal energy stored in the TES at the discretized temperature t is extracted and used as parameters in the next optimization phase. *Algorithm 1* summarizes the procedure for determining the optimal storage schedule.

Hierarchical framework

Once the storage schedule is determined, the values of $\dot{Q}_{s,j,t}$ and T_j serve as parameters. If the value of $\dot{Q}_{s,j,t}$ is greater than $\dot{Q}_{s,j,t-1}$, this means that the storage was charged, and the reverse will be true if the storage was discharged. In this optimization phase, only one of the two modes (charging/discharging) can be activated at any time-period. During charging mode, the behavior of the storage tank is analogous to a customer, with a cooling demand of $(\dot{Q}_{s,j,t} - \dot{Q}_{s,j,t-1})$ and a requirement that the inflow chilled water temperature of less than equal to T_j . Conversely, in discharging mode, the storage tank assumes the profile of a ‘chiller’

Algorithm 1: The algorithm for determining the storage schedule.

1. Determine the window size (n_{sw}), and the number of linear intervals (n_{li}) to calculate the objective function for. The window size has to be less than the total number of time-periods ($n_{sw} \leq n_t$).
2. **for** $li = 1, \dots, n_{li}$ **do,**
for $t = 1, \dots, n_t$ **do,**

(a)

$$\text{minimize } W_{li} \dot{E}_{li,t} + (1 - W_{li}) C_{\dot{E},li,t} \quad (6.10)$$

where,

$$\dot{E}_{ch,li,t} = \sum_{wd=1}^{n_{sw}} \sum_{i=1}^{n_i} \sum_{j=1}^{n_j} \dot{E}_{ch,i,j,wd} \quad (6.11)$$

and

$$C_{\dot{E},li,t} = \dot{C}_{ele_rate,t} \times \sum_{wd=1}^{n_{sw}} \sum_{i=1}^{n_i} \sum_{j=1}^{n_j} \dot{E}_{ch,i,j,wd} \quad (6.12)$$

where W , and sw refer to the linear weight, and indices within the predefined sliding window respectively.

- (b) extract the optimal levels ($\dot{Q}_{s,j,t}$) at each time-period and the corresponding temperatures T_j for use as parameters later.
-

which consumes no electricity, delivering cold energy of ($\dot{Q}_{s,j,t-1} - \dot{Q}_{s,j,t}$) at temperature T_j . Adding these to the equations presented in *Section 5.4.2.1* allows for the optimal values of the rest of the components to be solved for.

6.4 Results and discussion

The results presented in this section will focus on two key aspects - the impact of TES on the operation of chillers, when optimized with different objectives, and the effect of the sliding-window size on the quality of the final solution. Discussion pertaining to holistic optimization and the effect of storage systems on ancillaries are not included as they revolve around similar explanations as those presented in *Chapter 5*.

6.4.1 Effect of TES on chiller operation

The plots in this subsection are optimized using a window size (n_{sw}) of 24 hours. *Figure 6.4* compares the quantity of cold energy stored in the tank across 24-hours when the DCS with TES is optimized for three different objectives. The system is optimized for minimal electricity consumption and operating cost in the first and third cases respectively. For the second case, it is equally balanced between the first and third objectives. The results shown in the plot are further broken down into three discrete temperature bands for which $T_1 > T_2 > T_3$ and plotted against the prevailing electricity prices.

As seen in the graph, the gradual increase in the importance of operating costs in the objective function results in the optimizer choosing to store more energy in the storage system. This observation becomes more pronounced from 0600 to 0800 hours when the sharp increase in the quantity of cold energy stored in the tank corresponds to the price hike. The optimizer even chose to exceed the design capacity of the tank (at a fixed ΔT), by lowering the temperature of the water stored. This is likely done to make more energy available during periods of high electricity prices. Similar observations are made from 1700 to 1900 hours, although to a smaller extent.

At the opposite end of the spectrum where electricity consumption is minimized, there exists a comparatively low proclivity to utilize the storage system due to losses. Thermal losses, when chilled water is stored for a prolonged period manifests itself in terms of temperature degradation. When chilled water heats up, it loses the capacity to fulfill its task of space cooling. Storage, from a pure energy efficiency perspective, wastes energy in this case.

The reason the storage system is still utilized despite optimizing solely for electricity consumption is shown in *Figure 6.5*. It can be seen from the plots that the larger chillers are never operated; cooling demand is exclusively fulfilled by the small chiller and the storage system. Due to the deficit between the design and operation conditions of the DCS, much of the cooling demand falls between the gap of the small and larger chillers. Operating a large chiller at low part-loads is highly inefficient as it contributes to the infamous ‘low ΔT syndrome’ (*Appendix B*). The choice not to operate the larger chillers suggests that the system is better off operating with storage in spite of thermal losses.

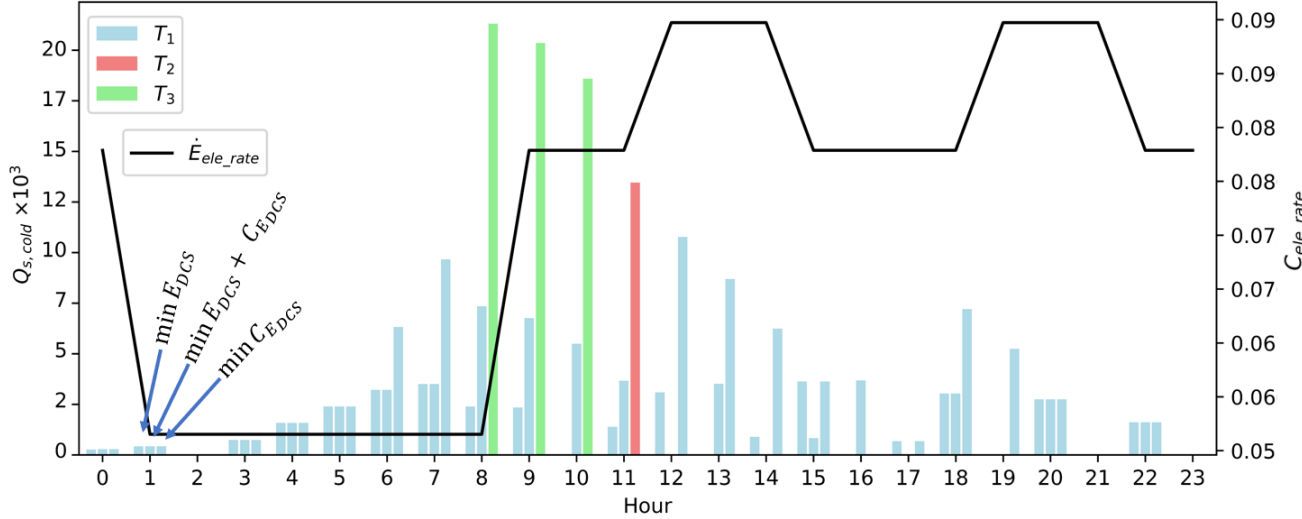


FIGURE 6.4: Comparison of cold energy stored across 24-hours, when optimized for different objectives.

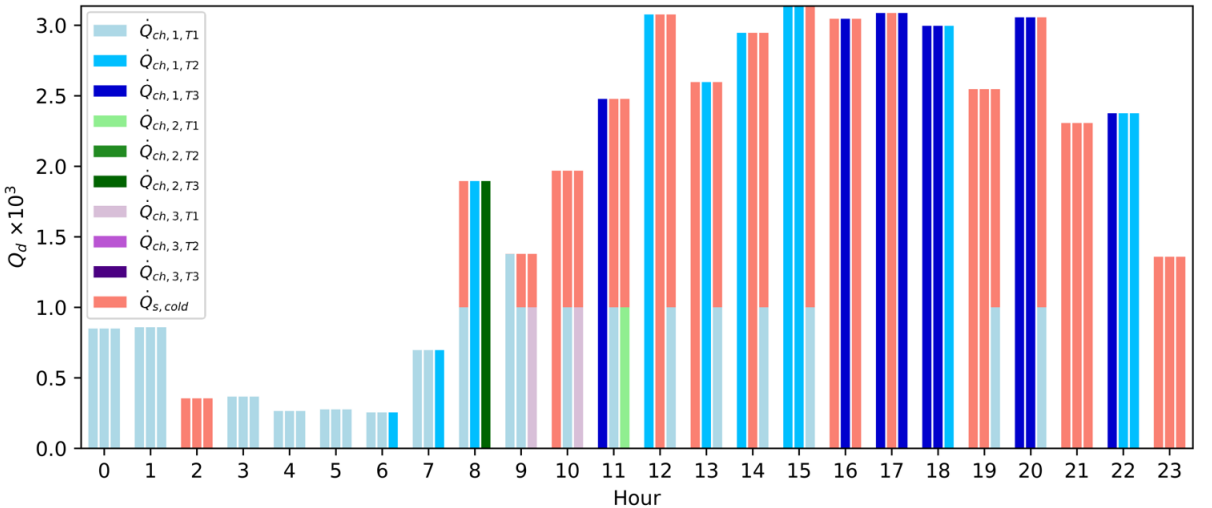


FIGURE 6.5: Comparison of cold energy supply across 24-hours, when optimized for different objectives.

6.4.2 Effect of sliding-window size

Figure 6.6 shows the evolution of the Pareto frontier as the sliding-window size (n_{sw}) is increased. It is no surprise that a larger window size results in a more comprehensive exploration of the solution space. This is evidenced by the length of the frontier growing from a single point as the number of window sizes increases. With the window size of a single time-period, the optimizer is only concerned in determining the best operating condition for the current condition, hence a

single point. The size of the sliding-window enables the optimizer to take into consideration future conditions while optimizing for the current time-period; the greater this consideration, however, also vastly increases the resolution time of the algorithm. For instance, the average resolution time increases exponentially from 2 to 143 seconds as the window size increases from 1 to 24. Depending on the objective, which the system is optimized for, it is unnecessary to utilize any window larger than five as the increase in cost savings falls below 1% thereafter. The same can be said for any window size larger than eight where the minimization of electricity consumption is concerned.

When the size of the storage system is reduced, the corresponding size of the sliding window is also lowered (*Figure 6.7*). This is due to the inability of the storage system to accumulate energy due to capacity constraints.

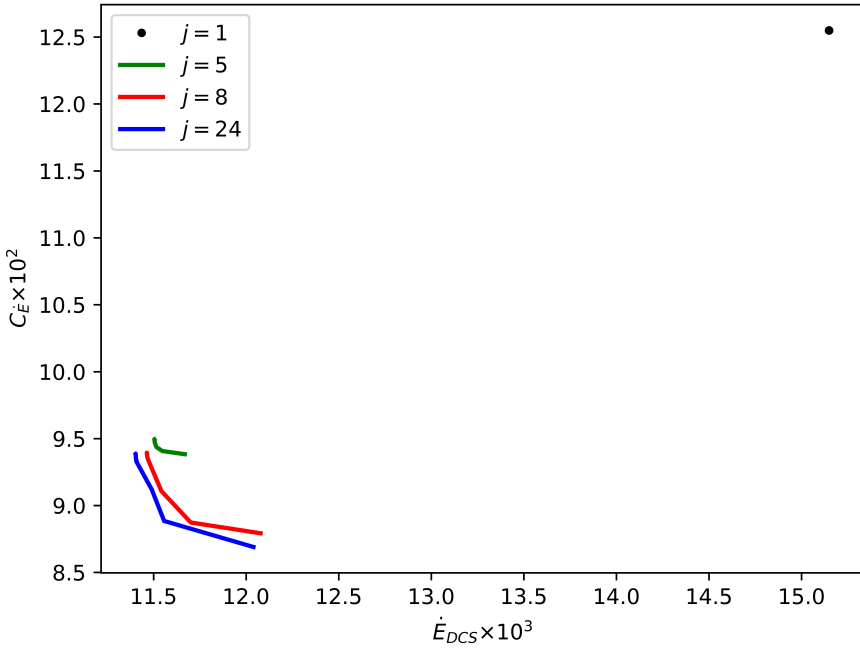


FIGURE 6.6: Pareto frontier evolution with sliding-window size, for large TES.

6.5 Conclusion

The sliding-window technique has been used to augment the hierarchical framework in this chapter. In doing so, the framework is equipped to manage the multi-period

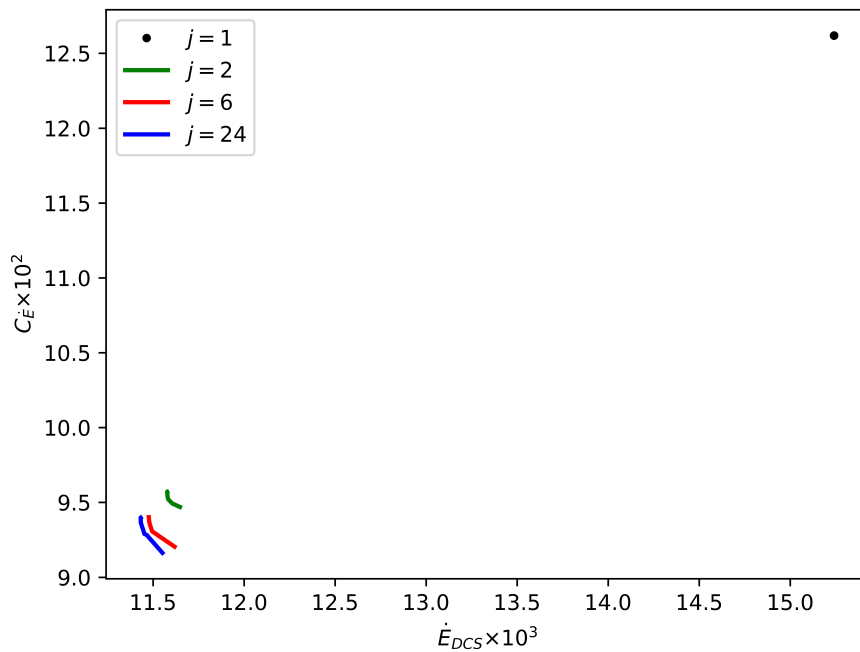


FIGURE 6.7: Pareto frontier evolution with sliding-window size, for small TES.

and multi-objective optimization problems that are presented by the addition of storage systems. The size of the sliding-window is a critical parameter that has to be pre-determined. It is likely to be concurrently affected by a myriad of factors such as storage capacity, hourly electricity price, demand profiles, etc. Currently, it is determined by iterating through all possible combinations until the change in objective functions become negligible. A more systematic method of doing so will add value to this implementation.

Chapter 7

Towards real-time holistic optimization using reinforcement learning and mixed integer linear programming

7.1 Overview

The holistic optimization of an urban energy system is a computationally intensive undertaking, owing to the sheer number of conflicting decision variables and the non-convex nature of the problem. This is the primary reason which inhibits the deployment of optimization algorithms for the real-time optimization of operations. To improve the solvability of the complex mixed-integer non-linear program (MINLP), the hierarchical framework was introduced in *Chapter 5*. However, the framework largely depends on the genetic algorithm (GA) to handle non-linear variables. The GA, being a population-based metaheuristic, required many iterations of the mixed-integer linear program (MILP) sub-problem to converge. This results in pro-longed resolution times, making *Chapter 5*'s implementation of the hierarchical framework unsuitable for real-time deployment.

To overcome this flaw, the GA is replaced by a RL in the framework. This version of the hierarchical framework, by virtue of the RL, enables the heavy computation

³The work in this chapter has been published in [186]

required to optimize the non-linear variables to be shifted offline. Once sufficiently trained, only one iteration of MILP is required to be solved in real-time. The MILP assumes a similar function as it did with the previous version (with the GA) - it drastically reduces the solution space which has to be optimized by the RL, thereby promoting resolution speed and solution quality.

In this chapter, the limitations in the existing literature pertaining to the use of reinforcement learning (RL) for optimization in the domain of urban energy systems are first discussed. Subsequently, the RL-MILP optimization framework is presented. *Section 7.4* compares the results of two versions of the hierarchical framework - RL-MILP and GA-MILP. The case study used in this chapter is a scaled-down version of the DCS that is presented in *Chapter 5*. The methodology presented in this chapter has been published in [186].

7.2 Introduction

This chapter explores the use of RL for the optimization of the operations of a DCS through a case study. The DCS considered in this chapter is a scaled-down version of *Chapter 5*'s. Despite that, the objective of the case study is still met as it only serves as an example for comparison between the RL-MILP and GA-MILP hierarchical frameworks. This chapter seeks to improve the applicability of the hierarchical framework presented in *Chapter 5* by replacing the GA with a RL. Through a case study based on an existing DCS, the results of the RL-MILP and GA-MILP optimization frameworks are compared for their resolution speed and solution qualities.

7.2.1 Reinforcement learning

RL is a generic machine learning technique which involves an agent taking ***actions*** in an ***environment*** and thereby earning a ***reward*** for it. The goal of the agent is to maximize the cumulative reward by iteratively improving on the actions taken. Typically, a neural network (NN) is embedded in the agent, hence, the ***reward***, which the agent receives from taking an ***action*** functions as a pseudo-error which is used to update the weights of the NN. This ***action - reward - state*** loop, thus

progressively improves the predictive ability of the embedded NN, hence resulting in better actions taken each time. The typical implementation of a RL is shown in *Figure 7.1*.

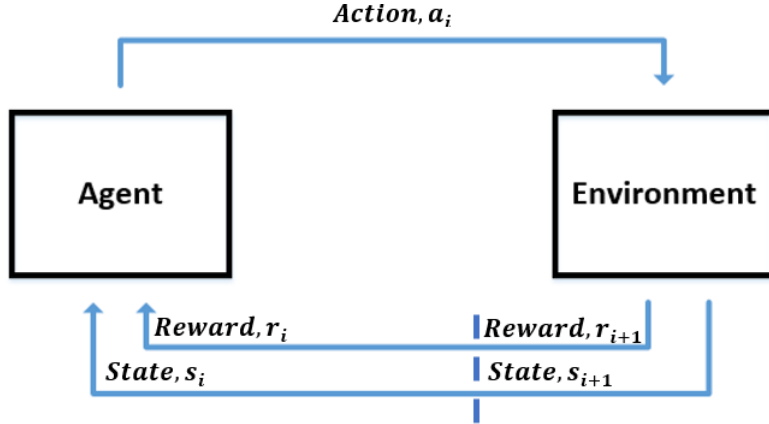


FIGURE 7.1: Typical implementation of a RL.

7.2.2 Literature review

The successful deployment of RL in playing games (Go [187], Atari [188]) and image recognition [189] marks the most significant progress in recent history. Despite the progress, it is essential to note that most of these studies deal with discrete state and action spaces which is not directly compatible with those requiring continuous state and action spaces [190]. Naive discretization of the state or action space leads to the curse of dimensionality that makes the problem intractable. Thus, a class of RL algorithms known as deterministic policy gradients (DPG) has been introduced [191].

As a technique for optimal control, RL is rapidly gaining traction in the closely related field of building energy control [192], [193]. Examples of such applications include the optimization of energy performance or operating cost in HVAC systems, domestic hot water (DHW) and data center cooling, through the manipulation of temperature setpoints. Since these problems mainly involve continuous state and action spaces, deterministic methods have been employed [27]. These implementations typically use end-to-end model-free approaches which only deal with the optimization of a small set of actions (decision variables). There is however no indication that the optimization of the action space will yield optimal performance

of the overall system. Training stability and convergence are other major issues that plague the performance of RL in these domains; hence techniques such as recurrent neural networks, experience replays, pretraining the neural networks with copious buffers of offline traces and guidance through expert-defined policies were some of the measures adopted mitigate these issues [193].

7.3 Problem formulation

The discussion in this section will take the following shape - first, the case study is defined, before the implementation of the RL-MILP optimization framework.

7.3.1 Case study description

The case-study *Figure 7.2* is a scaled-down version of that presented in *Chapter 5*, based on a functioning DCS located in Europe. Cooling towers were omitted, due to their negligible contribution to the objective function. Since the objective of this case study is only to act as a means of comparison between the two versions of the optimization framework, slight deviations from actuality are justified. The objective function defined in this case study is to utilize the RL-MILP and GA-MILP approach to optimize the electricity consumption (\dot{E}_{DCS}) for the given combination of cooling demand $\dot{Q}_{d,j}$ and ambient wet-bulb temperature T_{wb} .

Cooling demand for a single representative day is used to validate the performance of the two versions of the optimization framework. The quality of the optimal objective function and resolution speed will be the metric for measuring the performance of both methods. Additionally, a ‘base’-case which simulates the current operating practices of the DCS is also included for comparison purposes.

7.3.2 GA-MILP approach

In *Chapter 5*, after choosing the appropriate models, the optimization problem was decomposed into two levels - the master (GA) and the slave (MILP). Doing so, leveraged on the capabilities of MILP to increase the likelihood of converging to the globally optimal solution.

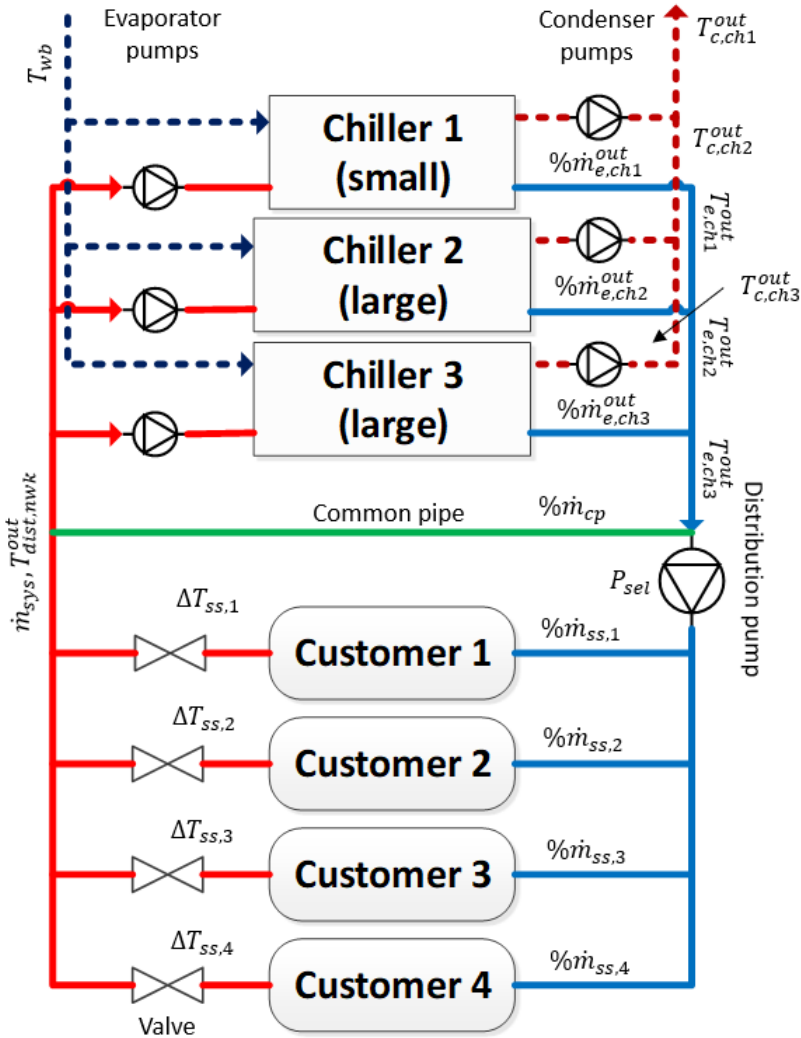


FIGURE 7.2: Schematic of the scaled-down DCS.

Table 7.1 documents the variables and parameters of the case study at each time-period. The variables are separated into master and slave level variables and optimized using the GA and MILP respectively.

7.3.2.1 Mathematical formulation

The objective function for this case study defined as the minimization of the hourly electricity consumption of the DCS. The formulation is almost identical to that found in *Section 5.4.2.1*, without the inclusion of the cooling tower.

Master level

Master level variables	Description
$T_{dist,nwk}^{out}$	temperature of return fluid from the distribution network entering the evaporator side of chillers.
\dot{m}_{sys}	total evaporator/distribution network flowrate.
Slave level variables	
$\% \dot{m}_{e,i}^{out}$	percentage of total flowrate through the i th chiller evaporator.
$T_{e,i}^{out}$	fluid temperature exiting i th chiller evaporator.
$T_{c,i}^{out}(K)$	fluid temperature exiting i th chiller condenser.
$\% \dot{m}_{c,i}^{in}$	percentage of total flowrate through the i th chiller condenser.
$\% \dot{m}_{cp}$	percentage of total flowrate through the common pipe.
$\% \dot{m}_{ss,i}$	percentage of total flowrate through the i th customer's substation.
$\dot{m}_{a,ct,i}$	inducted air flowrate through each cooling tower.
$Pump_{sel}$	the choice/combination of distribution pump(s).
Parameters	
$Q_{d,i}$	cooling demand of the i th customer substation.
T_{wb}	thermodynamic wet-bulb temperature.
$\Delta T_{ss,i}^{max}$	maximum temperature difference on the cold-side of the heat-exchanger at the substation.
$T_{ct,unit}^{out}$	temperature of fluid exiting the cooling tower array and entering the condenser side of chillers.
$\dot{m}_{ct,unit}^{in}$	total condenser network flowrate.

TABLE 7.1: Parameters and variables associated with the case study based on the scaled-down DCS.

The overall objective function for each hour is defined as:

$$\text{minimize } \dot{E}_{DCS} = f(T_{dist,nwk}^{out}, \dot{m}_{sys}) \quad (7.1)$$

Variables ($T_{dist,nwk}^{out}$ and \dot{m}_{sys}) at the master level is hence treated as parameters at the slave level and used for the computation of various coefficients which ensures that the slave is a MILP.

Slave level

The objective function at the slave level is:

$$\text{minimize } \dot{E}_{\text{slave}} = \sum_{i=1}^{n=3} \dot{E}_{ch,i} + \sum_{i=1}^{n=3} \dot{E}_{e,nwk,pump,i} + \sum_{i=1}^{n=3} \dot{E}_{c,nwk,pump,i} + \sum_{i=1}^{n=7} \dot{E}_{dist,nwk,pump,i} \quad (7.2)$$

The detailed equations which describe each element which the slave-level objective function is composed of can be found in [Equations 5.3](#) to [5.16](#), and thus is not reproduced here.

When the case study was formulated, only two decision variables remained as master-level decision variables ($\dot{m}_{sys}, T_{dist,nwk}^{out}$), whilst the rest could be optimized by the MILP. Implementation of the GA meant that numerous iterations of the MILP need to be undergone just for the optimum values of these two variables to be determined. A typical run of the MILP solver takes under 5 seconds to solve, which is considerably rapid, considering that it computes the optimal values to be used over a time-period of an hour. However, coupling the MILP with the GA greatly slows down the entire optimization process. Should the relationship between the two master-level decision variables ($\dot{m}_{sys}, T_{dist,nwk}^{out}$) and the optimal electricity consumption be pre-determined, the feasibility of holistic optimization in real-time will be vastly improved, as only a single iteration of MILP is required. This underpins the motivation for replacing the GA with the RL.

7.3.3 RL-MILP approach

The first step toward utilizing RL is to formulate the problem as a Markov decision process (MDP), with the proper definition of the ***environment***, ***reward***, ***state*** and ***action*** spaces. A MDP is a discrete-time stochastic control process which underpins mathematical framework for RL. In this process, it is assumed that the outcome is partially dependent on both the decision maker and inherent randomness [194]. The probabilistic nature of the MDP enables exploration in the solution space (***reward***) mapped by ***action***.

With the assumption that the ***actions*** taken in each hourly time-period is independent of the next (absence of storage systems), the optimization problem can be formulated in the similar fashion as the classic multi-armed contextual bandit problem [195]. The multi-armed contextual bandit problem, is a classical RL

problem, in which the agent is faced with n slot-machines or ‘bandits’, each with a different ***reward*** distribution. The objective of the actor is to maximize the cumulative ***reward***, by pulling the appropriate ‘arm’, based on the experience gained through conducting various trials. The DCS in the case study could be modeled in a similar fashion - the only difference being continuous state and action spaces [196]. Hence, the GA was replaced with a variant of the deep deterministic policy gradient (DDPG) algorithm [190], however, instead of a ***reward***, a ***penalty*** was introduced to discourage the agent from making poor decisions.

To fully appreciate the DDPG algorithm, two learning approaches that are central to RL must first be introduced - the Q-learning and policy gradient algorithms. In Q-learning, the value-based approach is adopted, whereby the agent seeks to take the best ***action***, given a the present ***state***. It is assumed that by iteratively doing so, the optimal set of ***actions*** (policy) will be eventually determined. The iterative learning process utilizes the Bellman equation to compute the Q-value (value of being a current state). This value is progressively updated after each trial which the actor undertakes. As opposed to the Q-learning, policy gradient algorithms seek to directly determine the ‘set of ***actions***’ (policy) which the actor should take [197]. The policy gradient algorithm utilizes statistical approximations of the gradient of the expected ***reward*** and subsequently updates the policy in that direction. While the policy gradient algorithm is more generic and thus more applicable to a wider range of RL problems, it can suffer from the issue of having high variance which negatively impacts convergence.

Since the ***action*** space are mapped by continuous variables $\mathbf{T}_{dist,nwk}^{out}$ and $\dot{\mathbf{m}}_{sys}$, the DDPG algorithm in the hierarchical framework. This algorithm utilizes NNs to manage the continuous variables and combines both the benefits of the value and policy-based approaches by means of the actor-critic algorithm [190]. By doing so, the Q-value obtained through the value-approach is used to guide the gradient update process in the policy-based approach, thereby reducing the impact of the high variance issue associated with the latter.

Without using the decomposed approach, the subsequent RL problem may be difficult to solve, since the ***action*** space is very large in comparison to the ***state*** space. *Table 7.2* details the definition of the MDP in the proposed RL-MILP approach. In RL, ***state***, ***action*** and ***reward*** is akin to parameters, decision variables and objective function in traditional optimization terms.

State	\dot{Q}_{1-4}, T_{wb}
Action	$\dot{m}_{sys}, T_{dist,nwk}^{out}$
Environment	MILP
Penalty	\dot{E}_{DCS}

TABLE 7.2: Definition of the MDP in the RL-MILP approach.

The actor-critic algorithm in the form of the DDPG is chosen for implementation as the RL design. The actor intakes a ***state*** and outputs an ***action***, for which the critic evaluates the ***state*** and corresponding ***action*** taken by the actor. The policy and value-based approach underpins the workings of the actor and the critic respectively [198]. *Figure 7.3* illustrates the implementation of the forward-feed neural network architecture and *Figure 7.4* summarizes the proposed implementation of the RL-MILP approach. For the actor neural network, the hidden layer is defined to output four values - two mean (μ) and two sigmas (σ) values which were then used with the normal distribution function to generate the values for the output layer. Subsequently, the losses of the neural networks are reduced using the Adaptive moment estimation (Adam) optimizer, with learning rates of 0.001 and 0.0001 for the actor and critic network respectively [199].

75% of the randomly sampled hourly ***state*** data over a period of a month was used for training purposes. The remaining 25% (a week) is then set aside for validation use. Through the use of these ***states***, the initialized NNs can interact with the ***environment*** by taking ***actions*** and receiving ***penalties***. For each episode, the actor NN intakes a ***state*** from the training data-trace and takes an ***action*** in the ***environment***. Concurrently, the critic NN, intakes the current ***state*** and ***action*** from the actor and delivers a Q-value. The Q-value and the ***penalty*** from the ***environment*** is subsequently used to update the weights of the actor and critic NNs respectively. *Algorithm 2* summarizes the training procedure used.

7.4 Results and discussion

In this section, the results of the holistic optimization of DCS operations derived from the GA-MILP and RL-MILP approaches are compared from two perspectives - solution quality and resolution speed.

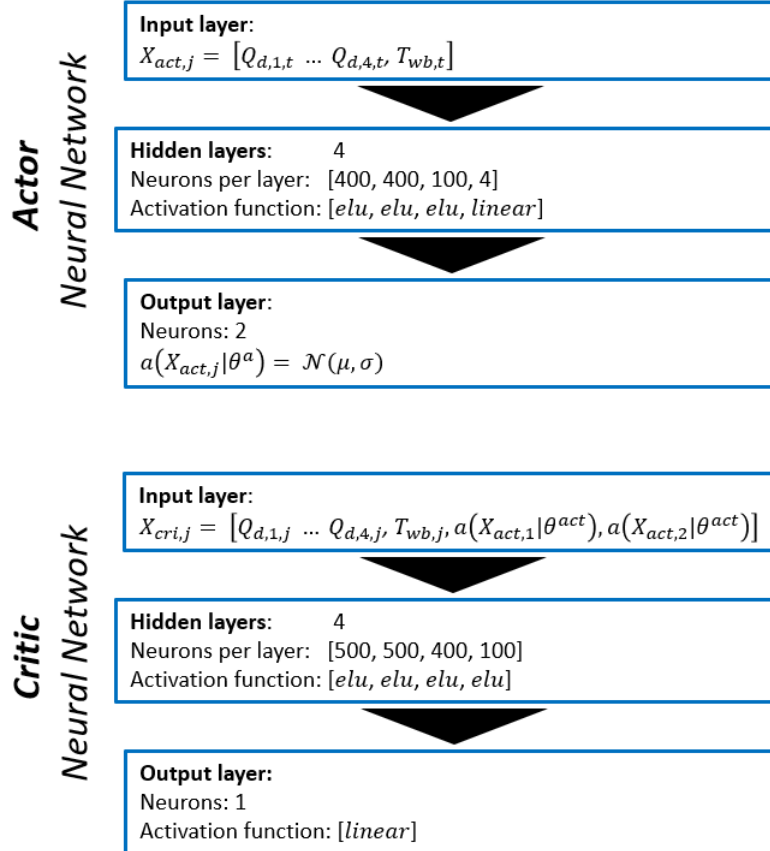


FIGURE 7.3: Neural network architectures.

Algorithm 2: Training algorithm for the actor-critic neural networks.

1. Collect the hourly **state** data over the period of 1 month. The **penalties** refer to \dot{E}_{DCS} which is an output from the **environment**.
2. Select 1 day outside the training data trace to be used for validation.
3. Initialize neural networks $a(X_{act}|\theta^{act})$ and $c(X_{cri}|\theta^{cri})$ with weights initialized using the Kaiming initialization scheme [200].
4. **for** $j = 1, \dots, max\ episodes$ **do**
 - (a) Compute $\delta_{cri,j} = (c(X_{cri,j}|\theta^{cri}) - \dot{E}_{DCS,j})$
 - (b) Update θ^{cri} by minimizing $\delta_{cri,j}^2$
 - (c) Compute $\delta_{act,j} = -\log(\mathcal{N}(a(X_{act,j}|\theta^{act}))) \times \delta_{cri,j}$
 - (d) Update θ^{act} by minimizing $\delta_{act,j}$
- end for**

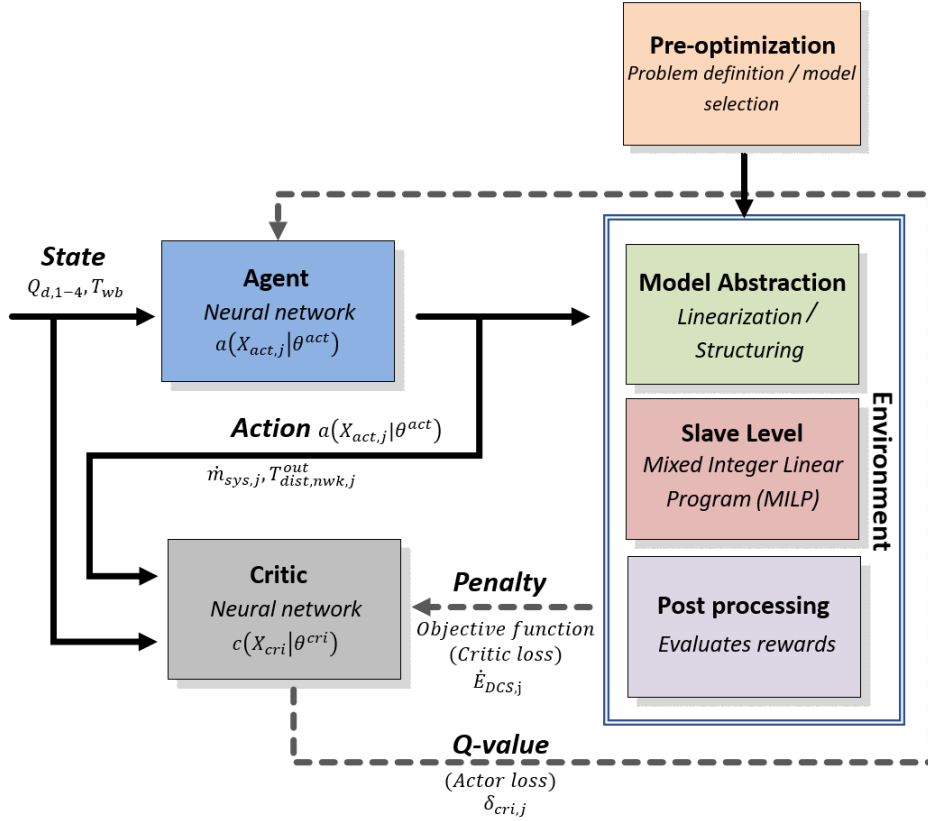


FIGURE 7.4: Summary of the RL-MILP approach.

7.4.1 Solution quality

Figure 7.5 compares the \dot{E}_{DCS} values generated for the validation data-trace using both approaches against the ‘base’-case. After training the RL for 3000 episodes, significant savings in electricity consumption can already be noticed, when compared against the ‘base’-case. Although the GA-MILP approach generally performed better, there exist scenarios whereby it was outperformed by the RL-MILP, such as in the 1st, 5th, and 17th hour. One possible explanation for this observation is the advantage gradient descent optimizers have over the GA when searching for local optima. The converse is true especially in the 12th and 22nd hour where it is likely that the optimizer used to minimize the losses in the NNs (Adam) had trouble escaping local optima.

Table 7.3 documents the percentage difference of \dot{E}_{DCS} of the ‘base’-case, GA-MILP and RL-MILP approaches over 3000 episodes. The accuracy generally improves with the number of training episodes. Beyond 3000 episodes, however, the performance on the validation trace started to degrade. Overfitting to the training data

traces could be a possible reason for this observation. Another explanation could pertain to the inability to fully capture the relationship between the *states* and *actions* within the current size and architecture of the neural networks. Where escaping local optima are concerned, off-policy methods could also be explored. An example would be to generate training data, such as outputs of the GA (independent of the current policy learnt) to further enhance performance.

7.4.2 Resolution speed

This is where the primary benefit of the RL-MILP approach lies. The average time taken to solve the MILP sub-problem ranges from approximately 3-5 seconds. The GA-MILP required about 15 000 evaluations of the MILPs to converge for a single time-period of length one hour. Despite only having undergone 3000 MILP evaluations, the absolute difference in electricity savings between the GA-MILP and RL-MILP approaches is only 7.52%.

Since the RL is trained offline, real-time performance will not be impeded, regardless of the number of training episodes it required to converge to a reasonable value. When properly trained, a single evaluation of the MILP is all that is needed to deliver the optimal values of all the decision variables required to operate the DCS efficiently.

Episodes	Percentage difference (RL-MILP vs 'base'-case)	Percentage difference (GA-MILP vs 'base'-case)
1000	-3.92	
2000	-23.68	
3000	-26.84	
4000	-22.55	-34.36

TABLE 7.3: Comparison of differences in \dot{E}_{DCS} between the 'base'-case, GA-MILP and RL-MILP approach over 3000 episodes.

7.5 Conclusion

Through the use of RL and MILP in the hierarchical optimization framework, the majority of the heavy computation needed to determine the optimal values of the

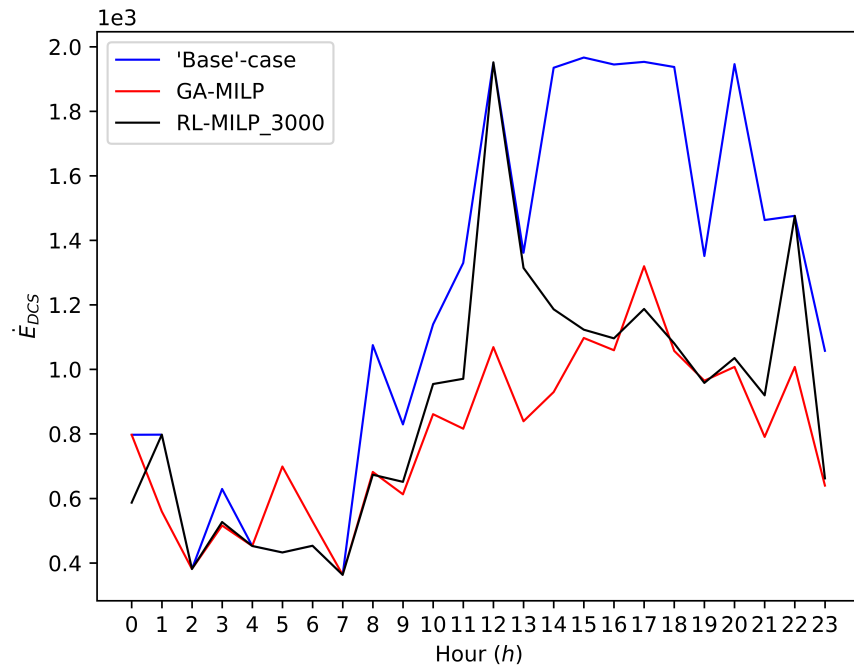


FIGURE 7.5: Plots of \dot{E}_{DCS} for the ‘base’-case, GA-MILP and RL-MILP (after 3000 episodes) approaches.

non-linear decision variables could be shifted offline. This vastly improved the feasibility of the hierarchical framework for real-time holistic optimization applications. When the reinforcement learner was trained, it generated close to optimum solutions almost instantly, a feat which was impossible with the previous version of the framework, involving the GA.

Accounting for stochasticity in demand and improving the optimization capabilities of the RL are two areas that will vastly add value to the current implementation. To function effectively as a decision support tool, the RL-MILP algorithm relies heavily on forecasted demands as input **states**. This is inherently stochastic and is likely to influence the output solutions of the algorithm. Sensitivity analyses could be introduced to influence the training process of the NNs for more robust solutions. Additionally, more advanced NN architectures could also be introduced to increase the learning capabilities of the agent NNs.

Chapter 8

Conclusion

8.1 Overview

The key contributions of this thesis and suggestions for furthering the current work are presented in this chapter. *Section 8.1.1* presents a summary of this thesis. The open problems and short comings of this thesis, which provides directions for futher research on the optimization of urban energy systems, is discussed in *Section 8.1.2*.

8.1.1 Conclusions

The incongruity between design and operating conditions of urban energy systems will always persist due to imperfection in available data for the forecast of future conditions. This results in the potential of urban energy systems being hardly realized. To address this deficit, a framework for the holistic optimization of the operations of urban energy systems has been proposed in this thesis. This framework is comprised of an amalgamation of techniques, ranging from model abstraction to reinforcement learning with the goal of simultaneously achieving two objectives - holistic optimization of the system while maintaining solvability of the concomitant optimization problem. The importance of the former cannot be overstated, due to the high level of interdependence amongst the components of an energy system. Localized optimization categorically denies this, unnecessarily pruning the already restricted solution space for problems concerning operations.

Related studies on the optimization of urban energy systems often deploy highly simplified models, which offer little guidance on the improvement of operations [21, 22]. Two essential criteria have to be met for the results of these studies to be useful - the expression of decision variables that are tuneable and the modeling of the interdependencies amongst system components. These requirements demand for models of higher fidelity; which inevitably complicates the optimization problem. *Chapter 4* addresses this issue through the use of abstraction techniques on judiciously selected component-level models from the existing literature. This endeavor permitted energy systems to be adequately modeled whilst keeping the problem formulation within the realms of a mixed-integer linear program (MILP), thereby ensuring solvability.

Since abstraction techniques alone are insufficient, a hierarchical framework was introduced in *Chapter 5* to complement. This framework utilizes the combination of the genetic algorithm (GA) and MILP solver for the optimization of operations. The GA was introduced to optimize crucial decision variables of the abstracted models which cannot be linearized. The existence of the MILP aids the metaheuristic by reducing the metaheuristic's search space, thereby benefiting resolution speed and the likelihood that global optimality is obtained.

The inclusion of energy storage systems further compounds the problem's complexity, given the necessity for multi-period and multi-objective optimization. Burgeoning sizes and intractability of optimization problems are a consequence when the above-mentioned requirements are simultaneously considered with high-fidelity models. To enhance the solvability of such problems, the hierarchical optimization framework was augmented with the sliding-window technique in *Chapter 6*. The right selection of the window size, drastically improved solvability and gave a good approximation of the optimal solution. This effectively suggests that solving the problem in its entirety is an unnecessary waste of computational resources.

GAs are population-based metaheuristics that utilize iterative methods to derive solutions. Substantial resolution times are a ramification of its use - the primary reason which inhibits the real-time applicability of the proposed optimization framework. To address this issue, the GA was replaced with a reinforcement learner (RL) in *Chapter 7*. This measure enabled the heavy computation required to optimize the non-linear decision variables to be shifted offline. Once sufficiently trained, only a single iteration was required for solving the MILP sub-problem to deliver

close-to-optimal solutions. This version of the hierarchical framework justifies the approximate solutions through drastic improvements in the real-time resolution speeds.

Finally, the use of these techniques across the various chapters has been individually validated through applications on case studies on existing urban energy systems. In *Chapter 4*, system-level optimization of the ground-coupled heat pump (GCHP) system by using abstracted models and MILP revealed significant limitations to the current set-up, prompting the introduction of a theoretical water-to-air heat exchanger (WAHX) and an alternative for thermal exchange with the ground. When operationally optimized, the WAHX prevents the degradation of ground temperatures resulting in significant operating cost and electricity savings of up to 12.7% and 35% respectively.

The GA-MILP hierarchical framework was applied to a district cooling system (DCS) for operational optimization in *Chapter 5*. The benefit of holistic optimization was explicitly highlighted through the comparison of results with chiller-only optimization. An additional 19% of electricity saving was possible when optimization was performed at the system-level. Although chillers undisputedly are responsible for the lion's share of electricity consumption, neglecting the tight-coupling between the ancillary components ignores the possibility of scenarios whereby the efficiency of chillers could be compromised for enhanced overall energy performance of the system. Analysis of the optimal results revealed a myriad of counter-intuitive measures such as the lowering of chilled water temperatures and degrading the temperature difference at the consumer substation level, which were undertaken to significantly improve the energy performance of the DCS. Overall, results indicate energy-saving potential of up to 31 %.

Augmenting the hierarchical framework with the sliding-window technique demonstrated that the problem space could be drastically reduced whilst maintaining the quality of the optimal solution. For the case study considered in *Chapter 6*, raising the number of simultaneously considered time-period above five resulted in less than 1% improvement in the objective function value. This effectively also means improvements in problem tractability, algorithm resolution speed and a reduction in the required computing resources.

The RL-MILP approach was applied a case study based on the same DCS (*Chapter 5*) in *Chapter 6*. Results generated show that when trained, the RL-MILP approach could achieve up to 78% of the optimal results generated by the GA-MILP approach. Shifting the heavy computation offline, meant that the RL-MILP approach could resolve for optimal solutions of approximately 15 000 times faster than the GA-MILP approach in real-time.

Since the proposed methodologies have been verified by case studies, the work in this thesis has thus, successfully addressed the problem statements which were identified in *Chapter 1*.

8.1.2 Suggestions for future work

The contributions of this thesis only address a small part of the inexhaustible list of issues which plague the efficient operation of urban energy systems. Three key issues which have arisen from the shortcomings of the current work are discussed in this subsection, to provide directions for furthering this research.

Modeling Techniques. The applicability of the hierarchical framework developed through the course of this thesis hinges on the quality of the model choice. A model that encapsulates greater details will inevitably also complicate the ensuing optimization problem. Hence, it is paramount to determine and expand on a set of representative models that offer a good balance between fidelity and solvability. It is evident from the review of the state of the art that there exists a knowledge-gap between mathematicians and engineers - through the indiscriminate use of optimization techniques on commercial simulation tools.

The models selected to represent components in the case studies still leaves much to be desired. Network delays, for instance, is one important feature that is absent. This is an especially important aspect for district-level thermal systems as it could take a considerable amount of time for the water from the central station to reach the customer. Not taking that into account risks the possibility of voiding the validity of the ‘optimal’ solution. The likelihood of such an occurrence will only increase when the granularity of time-periods is reduced - a desired feature of fast response real-time control systems. A model that captures this phenomenon

exists in literature, however, research on optimization compatibility has yet to be embarked on [201, 202].

Optimization techniques. This is a closely related topic as a direct consequence of modeling techniques. The deployment of highly abstract models permits the use of better, convex optimization techniques with expeditious resolution times and strong guarantees of global optimality. The heavy reliance on metaheuristics to derive some form of ‘enhanced’ solution on simulation tools is currently, the state-of-the-art. More should be done to address this issue, such as the hybridization of mature optimization techniques with less conventional approaches such as machine learning. One example could be to leverage the modularity of the current framework to include a wider range of convex optimization solvers, such as quadratic programming (QP), geometric programming (GP), etc. This is likely hugely further the work presented in the *Chapter 7* by diversifying the range of problems that the framework can effectively handle.

Another key aspect concerns the assumption that all interacting components within the system have perfect information about each other. This is typically untrue when the complexity of systems present challenges to the relevance of centralized optimization techniques. Additionally, the growing size of urban energy systems poses serious challenges to scalability of centralized optimization techniques. Distributed optimization involves the coordination and solving of problems of smaller sizes, with minimal interaction amongst them. Deployment of these techniques have since gained traction in the field of unit-commitment power generation and should be extended for general energy-related problems [203]. The main challenge resides in the choice of optimization techniques which enable the communication amongst the sub-problems to be minimized [204].

Handling of uncertainties. The overwhelming majority of the optimization studies reviewed in this thesis utilize deterministic methods. This effectively disregards the impact of uncertainties in the derivation of the optimum. Only a handful of preliminary studies forays into the impact of uncertainties in the input parameters at the design level [86–88]. However, these algorithms may not be suitable for real-time operation optimization due to substantial computational requirements. Sensitivity analyses have also been applied to highlight the effect of uncertainties

on the optimal solutions [93]. These methods, however, can only serve as a cautionary role on the viability of the solution in the post-processing phase, as they do nothing to influence the derivation of the optimum.

The tool which this thesis aspires to construct is hugely dependent on input parameters such as energy demands which is by no conceivable means, deterministic in nature. This holds regardless of how accurate predictive algorithms may be. Such considerations threaten to completely transform the optimization landscape - a well-established wisdom in the field of stochastic optimization [205]. The key challenges lie in the development of stochastic models and subsequently deploying appropriate algorithms to solve them. The higher dimensions introduced through the consideration of uncertainties threaten the tractability of the resulting formulation. Determining appropriate relaxations is hence paramount for maintaining the solvability of these problems.

Appendix A

Hydraulically decoupled cooling system

The terms ‘primary’ and ‘secondary’ networks used in this section differ from those used in the report. The term ‘secondary’ network used here is analogous to the ‘distribution’ network in the preceding sections. The nomenclature is as such due to the adaptation of ‘building-level’ concepts for thermal energy systems. *Figure A.1* illustrates a typical piping scheme of this nature, for chilled water systems (heat pump operated as chillers).

The primary-secondary water piping scheme was conceived as a result of heat pumps’ inability to accommodate high flowrate fluctuations at the condenser/e-vaporator side. Control of thermal exchange at the demand side is important and typically done through adjustment of the water flowrates. As a compromise, the common-pipe is introduced to enable the ‘short-circuiting’ of water from the outlet of the condenser/evaporator to the inlet. Older systems cannot control temperature by varying flowrates, thus reheaters, etc., are used instead, resulting in more energy expended. The flexibility of flowrate control despite the limitations of heat pumps is the main benefit of this design [206].

Respective pumps determine the flowrate in each network independently. Flowrate in the common pipe could go either direction, depending on the difference in flowrates in either of the networks. The mixing of water from the common pipe with the supply/return water needs to be managed properly. Excessively low/high

return water temperatures to the heat pumps will impede the heat pumps' capacity to deliver the required cooling/heating and gives rise to a myriad of problems associated with 'low ΔT syndrome'. Recirculation of return water will conversely degrade supply water temperatures in addition to wasting energy.

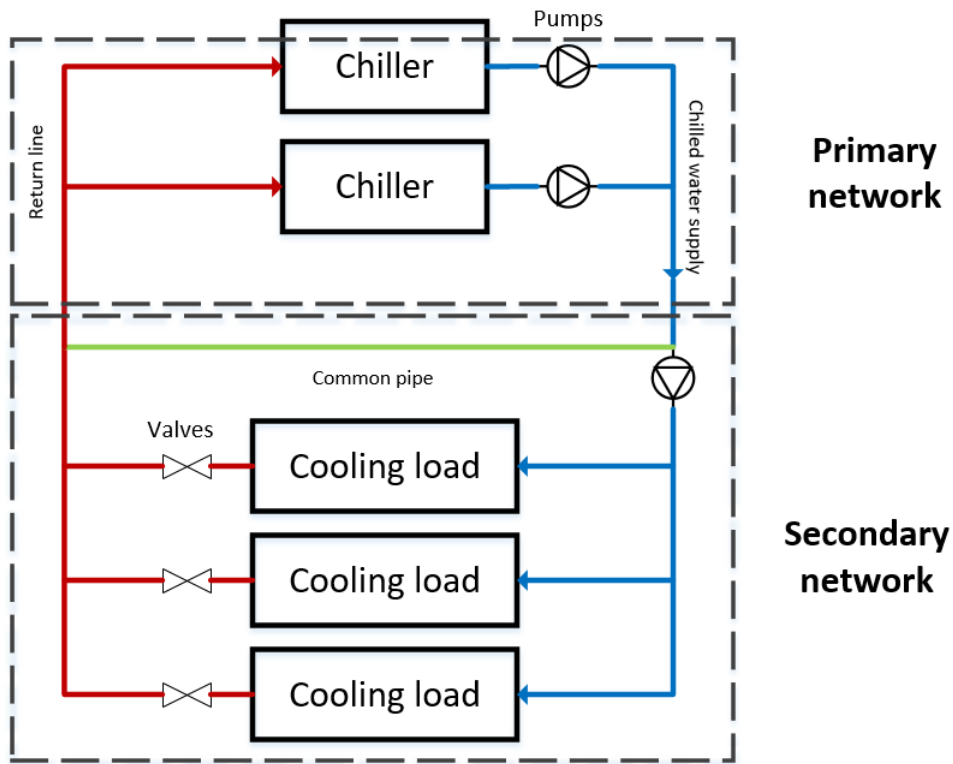


FIGURE A.1: A typical primary-secondary hydronic system, for chilled water distribution.

Appendix B

Low ΔT syndrome

Low ΔT syndrome occurs when the temperature difference across the condenser/e-vaporator side of the heat pump is small.

If the return water temperature to the heat pump is not sufficiently high, the ability of heat pumps to cool down/warm up the water will be impeded. Heat transfer is highly dependent on temperature difference, thus negatively impacting the efficiency of heat pumps. For the same quantity of thermal load required, a small temperature difference would imply high flowrates and increased electricity consumption of pumps.

Changes in thermal loads present a whole new set of issues. Once the system is insensitive to variation of flowrates as a control measure, very large changes in flowrates will have to be made to accommodate small changes in thermal loads. As a result, additional heat pumps (due to flowrate limitation) and pumps will have to be activated. This happens despite not fully loading the currently operating heat pumps [207].

List of Author's Publications¹

Journal Articles

- **Zhonglin Chiam**, Arvind Easwaran, David Mouquet, Samira Fazlollahi and Jaume Villa Millás, “A hierarchical framework for holistic optimization of the operations of district cooling systems,” *Applied Energy*.
- **Zhonglin Chiam**, Ilias Papas, Arvind Easwaran, Corinne Alonso and Bruno Estibals, “Holistic optimization of the operation of a ground-sourced heat pump system: A case study on the ADREAM building in Toulouse, France,” *Energy and Buildings, under review*.

Conference Proceedings

- **Zhonglin Chiam**, Arvind Easwaran, David Mouquet and Mohit Gupta, “Holistic, real-time optimization of the operations of district cooling systems via deep reinforcement learning and mixed integer linear programming” in *international Conference on Applied Energy, 2019*.

¹The superscript * indicates joint first authors

Bibliography

- [1] Whitehouse associates, London. BP statistical review of world energy, 2019. Technical Report 68th Edition, BP statistical review of world energy, 2019. [xxi](#), [1](#), [2](#)
- [2] International Energy Agency. Global energy and *co₂* status report, 2019. URL <https://www.iea.org/geco/emissions>. [1](#)
- [3] International Energy Agency. Energy efficiency: buildings, 2019. URL <https://www.iea.org/topics/energyefficiency/buildings/>. [1](#)
- [4] REN21 Secretariat, Paris. Renewables 2019 global status report. Technical report, REN21, 2019. [1](#)
- [5] N. Deng, G. He, Y. Gao, B. Yang, J. Zhao, S. He, and X. Tian. Comparative analysis of optimal operation strategies for district heating and cooling system based on design and actual load. *Applied Energy*, 205:557–588, 2017. [2](#), [94](#)
- [6] L. Jayamaha. *Energy-efficient building systems green strategies for operation and maintenance*. McGraw-Hill, New York, 2009. [2](#), [94](#), [116](#)
- [7] S. Wang. *Intelligent buildings and building automation*. Taylor and Francis, London and New York, 2010. [2](#), [94](#), [116](#)
- [8] Asia Pacific Urban Energy Association. Introduction to sustainable urban energy systems, 2019. URL <https://www.apuea.org/index.php/urban-energy-systems/introduction-to-urban-energy-systems2>. [3](#), [5](#)
- [9] UN Publications. 2018 revision of world urbanization prospects, 2018. URL <https://www.un.org/development/desa/publications/2018-revision-of-world-urbanization-prospects.html>. [3](#)
- [10] The World Bank, Washington, DC. World development report 2009: Reshaping economic geography. Technical report, The world bank, 2009. [3](#)
- [11] J. Keirstead, M. Jennings, and A. Sivakumar. A review of urban energy system models: Approaches challenges and opportunities. *Renewable and Sustainable Energy Reviews*, 16:3847–3866, 2012. [3](#)

- [12] W. Gang, S. Wang, F. Xiao, and D. Gao. District cooling systems: Technology integration, system optimization challenges and opportunities for applications. *Renewable and Sustainable Energy Reviews*, 53:253–264, 2016. [3](#), [14](#), [17](#), [18](#), [95](#)
- [13] Electrical and Mechanical Services Department, HKSARG. Building: District cooling system, 2019. URL https://www.emsd.gov.hk/energyland/en/building/district_cooling_sys/dcs.html. [3](#), [5](#), [94](#)
- [14] C. Helm and M. Mier. On the efficient market diffusion of intermittent renewable energies. *Energy Economics*, 80:812–830, 2019. [4](#)
- [15] American Council for an Energy-Efficient Economy. Combined heat and power (CHP), 2019. URL <https://aceee.org/topics/combined-heat-and-power-chp>. [4](#)
- [16] Ecoimagination. GE global power plant efficiency analysis. Technical report, General Electric, 2019. [4](#)
- [17] M. Babar, F. Arif, Z. Tan M. A. Jan and, and F. Khan. Urban data management system: Towards big data analytics for Internet of Things based smart urban environment using customized Hadoop. *Future Generation Computer Systems*, 96:395–409, 2019. [5](#)
- [18] M. Sameti and F. Haghishat. Optimization approaches in district heating and cooling thermal network. *Energy and Buildings*, 140:121–130, 2017. [5](#), [30](#)
- [19] K. M. Powell, W. J. Cole, U. F. Ekarika, and T. F. Edgar. Optimal chiller loading in a district cooling system with thermal energy storage. *Energy*, 50: 445–453, 2013. [7](#), [21](#), [96](#)
- [20] G. Schweiger, P. Larsson, F. Magnusson, P. Lauenburg, and S. Velut. District heating and cooling systems - Framework for Modelica-based simulation and dynamic optimization. *Energy*, 137:566–578, 2017. [7](#), [96](#)
- [21] M. Ameri and Z. Besharati. Optimal design and operation of district heating and cooling networks with CCHP systems in a residential complex. *Energy and Buildings*, 110:135–148, 2016. [7](#), [16](#), [20](#), [96](#), [160](#)
- [22] M. Sameti and F. Haghishat. A two-level multi-objective optimization for simultaneous design and scheduling of a district energy system. *Applied Energy*, 208:1053–1070, 2017. [7](#), [96](#), [160](#)
- [23] B. Talebi, F. Haghishat, P. Tuohy, and P. A. Mirzaei. Optimization of hybrid community district heating system integrated with thermal energy storage system. *Journal of Energy Storage*, 23:128–137, 2019. [8](#)
- [24] B. van der Heijde, A. Vandermeulen, R. Salenbien, and L. Helsen. Representative days selection for district energy system optimization: a solar district heating system with seasonal storage. *Applied Energy*, 248:79–94, 2019. [8](#)

- [25] Z. Lee, K. Gupta, K. J. Kircher, and M. Zhang. Mixed-integer model predictive control of variable-speed heat pumps. *Energy & Buildings*, 198:75–83, 2019. [8](#), [22](#), [71](#)
- [26] T. Fang and R. Lahdelma. Optimization of combined heat and power production with heat storage based on sliding time window method. *Applied Energy*, 162:723–732, 2016. [8](#)
- [27] Y. Li, Y. Wen, K. Guan, and D. Tao. Transforming cooling optimization for green data center via deep reinforcement learning. *arVix.org*, pages 1–11, 2018. [9](#), [22](#), [147](#)
- [28] W. Lin, X. Jin, Y. Mu, H. Jia, X. Xu, and X. Yu. Proceedings of the 8th International Conference on Applied Energy. In *Multi-objective optimal hybrid power flow algorithm for integrated community energy system*, Beijing, China, 2016. Energy Procedia. [13](#)
- [29] DHCNews. Chaudes-aigues: France's first heating network, 2015. URL <https://www.dhcnews.co.uk/chaudes-aigues-frances-first-heating-network/>. [14](#)
- [30] D. R. Shiman. Explaining the collapse of the british electrical supply industry in the late 1880s: gas versus electric lighting prices. *Business and Economic History*, 22:318–327, 1993. [14](#)
- [31] Empower. History of district cooling, 2014. URL <http://www.empower.ae/php/history-of-dc.php>. [14](#)
- [32] P. Rutter and J. Keirstead. A brief history and possible future of urban energy systems. *Energy Policy*, 50:72–80, 2012. [14](#)
- [33] G. Masson and I. Kaizuka. Trends 2018, in photovoltaic applications. Technical report, International Energy Agency, 2018. [14](#)
- [34] M. A. Alim, Z. Tao, M. K. Hassan, A. Rahman, B. Wang, C. Zhang, and B. Samali. Is it time to embrace building integrated Photovoltaics? A review with particular focus in Australia. *Solar Energy*, 188:1118–1133, 2019. [14](#)
- [35] M. A. Sayegh, J. Danielewicz, T. Nannou, M. Miniewicz, P. Jadwiszczak, K. Piekarska, and H. Jouhara. Trends of European research and development in district heating technologies. *Renewable and Sustainable Energy Reviews*, 68:1183–1192, 2017. [14](#)
- [36] Forbes. Copenhagen's seawater cooling delivers energy and carbon savings, 2012. URL <https://www.forbes.com/sites/justingerdes/2012/10/24/copenhagens-seawater-cooling-delivers-energy-and-carbon-savings/>. [15](#)
- [37] L. Zhen, D. M. Lin, H. W. Shu, S. J., and Y. X. Zhu. District cooling and heating with seawater as heat source and sink in Dalian, China. *Renewable Energy*, 32:2603–2616, 2007. [15](#)

- [38] H. Shu, D. Lin, C. Zhang, and Y. Zhu. Study on the decision-making of district cooling and heating systems by means of value engineering. *Renewable Energy*, 35:1929–1939, 2010. [15](#)
- [39] U.S. Geological Survey. Aquifers and groundwater, 2016. URL <https://www.usgs.gov/special-topic/water-science-school/science/aquifers-and-groundwater>. [15](#)
- [40] A. Talal. Well & tube well water cold in the summer and warm in the winter, 2012. URL <https://benignblog.com/2012/01/well-water-strange-phenomenon.html>. [15](#)
- [41] G. Eggen and G. Vangnes. Heat pump for district cooling and heating at oslo airport, gardermoen. In *Proceedings of the 8th Heat Pump Conference*, Las Vegas, USA, 2006. [15](#)
- [42] H.O. Paksoy, O. Andersson, S. Abaci, H. Evliya, and B. Turgut. Heating and cooling of a hospital using solar energy coupled with seasonal thermal energy storage in an aquifer. *Renewable Energy*, 19:117–122, 2000. [15](#)
- [43] L. Rybach and B. Sanner. Ground-source heat pump systems - the European experience. *GHC Bulletin*, 2000. [15](#)
- [44] H. Gholami, H. N. Røstvik, and D. Müller-Eie. Holistic economic analysis of building integrated photovoltaics (BIPV) system: Case studies evaluation. *Energy & Buildings*, 203, 2019. [15](#)
- [45] X. G. Casals. Solar absorption cooling in spain: perspectives and outcomes from the simulation of recent installations. *Renewable Energy*, 31:1371–1389, 2006. [15](#)
- [46] D. W. Wu and R.Z. Wang. Combined cooling, heating and power: A review. *Progress in Energy and Combustion Science*, 32:459–495, 2006. [16](#)
- [47] H. Cho, A. D. Smith, and P. Mago. Combined cooling, heating and power: A review of performance improvement and optimization. *Applied Energy*, 136: 168–185, 2014. [16](#)
- [48] M. A. Lozano, J. C. Ramos, and L. M. Serra. Cost optimization of the design of CHCP (combined heat, cooling and power) systems under legal constraints. *Energy*, 35:794–805, 2010. [20](#)
- [49] D. R. Hart and M. A. Rosen. Environmental and health benefits of district cooling using utility-based cogeneration in Ontario, Canada. *Energy*, 21: 1135–1146, 1996.
- [50] B. Yan, S. Xue, Y. Li, J. Duan, and M. Zeng. Gas-fired combined cooling, heating and power (CCHP) in Beijing: A techno-economic analysis. *Renewable and Sustainable Energy Reviews*, 63:118–131, 2016.

- [51] J. Deng, R. Z. Wang, and G. Y. Han. A review of thermally activated cooling technologies for combined cooling, heating and power systems. *Progress in Energy and Combustion Science*, 37:172–203, 2011.
- [52] P. A. Rodriguez-Aumente, M. C. R. Hidalgo, J. I. Nogueira, A. Lecuona, and M. C. Venegas. District heating and cooling for business buildings in madrid. *Applied Thermal Engineering*, 50:1496–1503, 2013.
- [53] T. Zhang, Y. Tan, and L. Bai. Numerical simulation of a new district cooling system in cogeneration plants. In *Proceedings of the 2nd International Conference on Applied Energy*, Perugia, Italy, 2012. Energy Procedia.
- [54] L. Fu, Y. Jiang, W. Yuan, and X. Qin. Influence of supply and return water temperatures on the energy consumption of a district cooling system. *Applied Thermal Engineering*, 21:511–521, 2001.
- [55] H. H. Erdem, A. Dagdas, S. H. Sevilgen, B. Cetin, A. V. Akkaya, B. Sahin, I. Teke, C. Gungor, and S. Atas. Thermodynamic analysis of an existing coal-fired power plant for district heating/cooling application. *Applied Thermal Engineering*, 30:181–187, 2010.
- [56] M. A. Rosen, M. N. Le, and I. Dincer. Efficiency analysis of a cogeneration and district energy system. *Applied Thermal Engineering*, 25:147–159, 2005.
- [57] P. S. Pak and Y. Suzuki. Exergetic evaluation of gas turbine cogeneration systems for district heating and cooling. *International Journal of Energy Research*, 21:209–220, 1997. [16](#)
- [58] S. Udomsri, A. R. Martin, and V. Martin. Thermally driven cooling coupled with municipal solid waste-fired power plant: Application of combined heat, cooling and power in tropical urban areas. *Applied Energy*, 88:1532–1542, 2011. [16](#)
- [59] A. A. Rentizelas, I.P. Tatsiopoulos, and A. Tolis. An optimization model for multi-biomass tri-generation energy supply. *Biomass & Energy*, 33:223–233, 2009. [16](#)
- [60] V. Karlsson and L. Nilsson. Co-production of pyrolysis oil and district cooling in biomass-based CHP plants: Utilizing sequential vapour condensation heat as driving force in an absorption cooling machine. *Applied Thermal Engineering*, 79:9–16, 2015.
- [61] M. Uris, J. I. Linares, and E. Arenas. Size optimization of a biomass-fired cogeneration plant CHP/CCHP (Combined heat and power/Combined heat, cooling and power) based on Organized Rankine Cycle for a district network in Spain. *Energy*, 88:935–945, 2015. [16](#)
- [62] P. Y. Liew, T. G. Walmsley, S. R. W. Alwi, Z. A. Manan, J. Jaromír, Klemeš, and P. S. Varbanov. Integrating district cooling systems in Locally Integrated Energy Sectors through Total Site Heat Integration. *Applied Energy*, 184: 1350–1363, 2016. [16](#)

- [63] A. Volkova, I. Krupenski, H. Pieper, A. Ledvanov, E. Lat ošov, and A. Sirdé. Small low-temperature district heating network development prospects. *Energy*, 178:714–722, 2019. [16](#), [17](#), [132](#)
- [64] W. Tao, W. Lin, and G. Anzhong. Comparison of two schemes for district cooling system utilizing cold energy of liquified natural gas. *Journal of Southeast University*, 26:316–319, 2010. [16](#)
- [65] C. Weng, M. Lin, and M. Huang. A waste cold recovery from the exhausted cryogenic nitrogen by using thermoelectric power generator. *Energy*, 103:385–396, 2016. [16](#)
- [66] A. L. S. Chan, T. Chow, S. K.F. Fong, and J. Z. Lin. Performance evaluation of district cooling plant with ice storage. *Energy*, 31:2750–2762, 2006. [16](#)
- [67] H. Tanaka, T. Tomita, and M. Okumiya. Feasibility study of a district energy system with seasonal water thermal storage. *Solar Energy*, 69:535–547, 2000.
- [68] A. Aktas, K. Erhan, S. Özdemir, and E. Özdemir. Dynamic energy management for photovoltaic power system including hybrid energy storage in smart grid applications. *Energy*, 162:72–82, 2018. [16](#)
- [69] S. M. Hasnain. Review on sustainable thermal energy storage technologie, Part II: Cool thermal storage. *Energy Conversion Management*, 39:1139–1153, 1998. [16](#)
- [70] H. Bo, E. M. Gustafsson, and F. Setterwall. Tetradecane and Hexadecane binary mixtures as phase change materials (PCMs) for cool storage in district cooling systems. *Energy*, 24:1015–1028, 1999. [16](#)
- [71] O. Schmidt, S. Melchior, A. Hawkes, and I. Staffell. Projecting the future of leveled cost of electricity storage technologies. *Joules*, 3:81–100, 2019. [17](#)
- [72] J. Schonekl. How big are power line losses, 2013. URL <https://blog.se.com/energy-management-energy-efficiency/2013/03/25/how-big-are-power-line-losses/>. [17](#)
- [73] M. Vesterlund, J. Sandberg, B. Lindblom, and J. Dahl. Evaluation of losses in district heating system, a case study. In *Proceedings of the 26th International Conference on Efficiency, Cost, Optimization, Simulation and Environmental Impact of Energy Systems*, Gulin, China, 2013. Energy Procedia. [17](#)
- [74] A. Krope and L. C. Lipus. Drag reducing surfactants for district heating. *Applied Thermal Engineering*, 30:833–838, 2010. [17](#)
- [75] N. Nord, E. K. L. Nielsen, H. Kauko, and T. Tereshchenko. Challenges and potentials for low-temperature district heating implementationin Norway. *Energy*, 151:889–902, 2018. [17](#)
- [76] S. Tredinnick and G. Phetteplace. *Advanced District Heating and Cooling (DHC) Systems*. Elsevier, Cambridge, 2016. [17](#)

- [77] S. M. Jayasurya and S. Varun Kumar. Smart grid infrastructure for efficient power consumption using real time pricing algorithm and distributed algorithm. In *Proceedings of the 2018 International Conference on Recent Trends in Electrical Control and Communication*, Chennai, India, 2018. IEEE. 18
- [78] B. Rezaie and M. A. Rosen. District heating and cooling: Review of technology and potential enhancements. *Applied Energy*, 93:2–10, 2012. 18
- [79] T. T. Chow, A. L. S. Chan, and C. L. Song. Building-mix optimization in district-cooling system implementation. *Applied Energy*, 77:1–13, 2004. 19
- [80] X. Feng and W. Long. Applying single parent genetic algorithm to optimize piping network layout of district cooling system. In *Proceedings of the 4th International Conference on Natural Computing*. IEEE, 2008. 19, 27
- [81] J. Söderman. Optimization of structure and operation of district cooling networks in urban regions. *Applied Thermal Engineering*, 27:2665–2676, 2007. 19
- [82] J. Söderman and F. Pettersson. Structural and operational optimization of distributed energy systems. *Applied Thermal Engineering*, 26:1400–1408, 2006. 19
- [83] A. L. S. Chan, V. I. Hanby, and T. T. Chow. Optimization of distribution piping network in district cooling system using genetic algorithm with local search. *Energy Conversion & Management*, 48:2622–2629, 2007. 19, 27
- [84] X. Li, D. Lin, and H. Shu. Optimal design of district heating and cooling pipe network of seawater-source heat pump. *Energy and Buildings*, 42:100–104, 2010. 19, 27
- [85] R. Khir and M. Haouari. Optimization models for a single-plant district cooling system. *European Journal of Operations Research*, 247:648–658, 2015. 20
- [86] W. Gang, S. Wang, G. Augenbroe, and F. Xiao. Robust optimal design of district cooling systems and the impacts of uncertainty and reliability. *Energy and Buildings*, 122:11–22, 2016. 20, 163
- [87] W. Gang, S. Wang, C. Yan, and F. Xiao. Robust optimal design of building cooling systems concerning uncertainties using mini-max regret theory. *Science and Technology for the Built Environment*, 21:789–799, 2015. 20
- [88] W. Gang, G. Augenbroe, S. Wang, C. Fan, and F. Xiao. An uncertainty-based design optimization method for district cooling systems. *Energy*, 102: 516–527, 2016. 20, 163
- [89] J. A. Fonseca, T. Nguyen, A. Schlueter, and F. Marèchal. City energy analyst (CEA): Integrated framework for analysis and optimization of building energy systems in neighborhoods and city districts. *Energy and Buildings*, 113:202–226, 2016. 20

- [90] M. Burer, K. Tanaka, D. Favrat, and K. Yamada. Multi-criteria optimization of a district cogeneration plant integrating a solid oxide fuel cell-gas turbine combined cycle, heat pumps and chillers. *Energy*, 28:497–518, 2003. [20](#)
- [91] S. Fazlollahi, P. Mandel, G. Becker, and F. Marèchal. Methods for multi-objective investment and operating optimization of complex energy systems. *Energy*, 45:12–22, 2012. [20](#), [98](#)
- [92] S. Fazlollahi and F. Marèchal. Multi-objective, multi-period optimization of biomass conversion technologies using evolutionary algorithms and mixed integer linear programming (MILP). *Applied Thermal Engineering*, 50:1504–1513, 2013. [132](#)
- [93] S. Fazlollahi, G. Becker, A. Ashouri, and F. Marèchal. Multi-objective, multi-period optimization of district energy systems: IV - A case study. *Energy*, 84:365–381, 2015. [20](#), [95](#), [98](#), [164](#)
- [94] S. R. Thangavelu, A. Myat, and A. Khambadkone. Energy optimization methodology of a multi-chiller plant in commercial buildings. *Energy*, 123:64–76, 2017. [21](#), [72](#), [97](#)
- [95] Z. X. Jing, X. S. Jiang, Q. H. Wu, W. H. Tang, and B. Hua. Modelling and optimal operation of a small-scale integrated energy based district heating and cooling system. *Energy*, 73:399–415, 2014. [21](#), [96](#)
- [96] J. Ortiga, J. C. Bruno, and A. Coronas. Operational optimization of a complex trigeneration system connected to a district heating and cooling network. *Applied Thermal Engineering*, 50:1536–1542, 2013.
- [97] M. Sakawa, K. Kato, and S. Ushiro. Operational planning of district heating and cooling plants through genetic algorithms for mixed 0-1 linear programming. *European Journal of Operational Research*, 137:677–687, 2002.
- [98] M. Sakawa, K. Kato, S. Ushiro, and M. Inaoka. Operation planning of district heating and cooling plants using genetic algorithms for mixed integer programming. *Applied Soft Computing*, 1:139–150, 2001. [21](#)
- [99] S. Matsuoka, M. Sakawa, H. Katagiri, T. Matsui, K. Ishimaru, and S. Ushiro. Long-term operation planning of district heating and cooling plants considering contract violation penalties. In *Proceedings of the 26th Fuzzy System Symposium*, Hiroshima, Japan, 2010. IEEE. [21](#), [96](#)
- [100] A. Askarzadeh and L. S. Coelho. Using two improved particle swarm optimization variants for optimization of daily electrical power consumption in multi-chiller systems. *Applied Thermal Engineering*, 89:640–646, 2015. [21](#), [97](#)
- [101] A. Beghi, L. Cecchinato, G. Cosi, and M. Rampazzo. A PSO-based algorithm for optimal multiple chiller systems operation. *Applied Thermal Engineering*, 89:640–646, 2015. [21](#)

-
- [102] Y. Chang, T. Chan, and W. Lee. Economic dispatch of chiller plant by gradient method for saving energy. *Applied Energy*, 87:1096–1101, 2010. [22](#), [97](#)
 - [103] B. Mu, Y. Li, J. M. House, and T. I. Salsbury. Real-time optimization of a chilled water plant with parallel chillers based on extremum seeking control. *Applied Energy*, 208:766–781, 2017. [22](#)
 - [104] M. W. Browne and P. K. Bansal. An elemental $NTU - \epsilon$ model for vapour-compression liquid chillers. *International Journal of Refrigeration*, 24:612–627, 2001. [26](#)
 - [105] U. van Houtte and E. van den Bulck. Modelling chiller performance using simultaneous equation-solving procedures. *International Journal of Refrigeration*, 17:191–198, 1992. [26](#)
 - [106] D. J. Swider. A comparison of empirically based steady-state models for vapor-compression liquid chillers. *Applied Thermal Engineering*, 23:539–556, 2003. [27](#), [30](#)
 - [107] F. W. H. Yik and V. K. C. Lam. Chiller models for plant design studies. *Building Services Engineering Research and Technology*, 19:233–242, 1998.
 - [108] T. A. Reddy and K. K. Andersen. An evaluation of classical steady-state off-line linear parameter estimation methods applied to chiller performance data. *HVAC & R Research*, 8:101–124, 2002.
 - [109] T. A. Reddy, D. Niebur, K. K. Andersen, P. P. Pericolo, and G. Cabrera. Evaluation of the suitability of different chiller performance models for on-line training applied to automated fault detection and diagnosis. *HVAC & R Research*, 9:385–414, 2003.
 - [110] D. A. York, F. Eva, and C. C. Cappiello. DOE-2 reference manual. Technical report, Los Alamos: Los Alamos National Laboratory, 1981. [27](#)
 - [111] T. Lee and W. Lu. An evaluation of empirically-based models for predicting energy performance of vapor-compression water chillers. *Applied Energy*, 87:3486–3493, 2010. [27](#), [30](#)
 - [112] J. M. Gordon and K. C. Ng. *Cool Thermodynamics*. Cambridge International Science Publishing, Cambridge, 2000. [27](#)
 - [113] H. R. Khan and S. M. Zubair. Design and performance evaluation of reciprocating refrigeration systems. *International Journal of Refrigeration*, 22:235–243, 1999.
 - [114] K. C. Ng, H. T. Chua, W. Ong, S. S. Lee, and J. M. Gordon. Diagnostics and optimization of reciprocating chillers: Theory and experiment. *Applied Thermal Engineering*, 17:263–276, 1997.

- [115] W. Jiang and T. A. Reddy. Re-evaluation of the gordon-ng performance models for water-cooled chillers. *ASHRAE Transactions*, 109:272–283, 2003.
- [116] P. Sreedharan and P. Haves. Comparison of chiller models for use in model-based fault detection. In *Proceedings of the International Conference for Enhanced Building Operations*, Austin, Texas, 2001.
- [117] J. M. Gordon, K. C. Ng, and H. T. Chua. Centrifugal chillers: Thermodynamic modeling and a diagnostic case study. *International Journal of Refrigeration*, 18:253–257, 1995.
- [118] J. M. Gordon and K. C. Ng. Thermodynamic modeling of reciprocating chillers. *Journal of Applied Physics*, 75:2769–2774, 1994. [30](#)
- [119] T. Lee. Thermodynamic modeling and experimental validation of screw liquid chillers. *ASHRAE Transactions*, 110:206–216, 2004. [27](#)
- [120] D. J. Swider, M. W. Browne, P. K. Bansal, and V. Kecman. Modeling of vapor-compression liquid chillers with neural networks. *Applied Thermal Engineering*, 21:311–329, 2001. [27](#)
- [121] S. Bertagnolio and J. Lebrun. Simulation of a building and its HVAC system with an equation solver: Application to benchmarking. *Building Simulation*, 1:234–250, 2008. [27](#)
- [122] L. Li and W. Cai. A universal engineering model for cooling towers. In *Proceedings of the International refrigeration and air conditioning conference*, Indiana, United States of America, 2002. [27, 37](#)
- [123] P. von Böckh and T. Wetzel. *Heat Transfer (Basics and Practice)*. Springer, New York, 2012. [28](#)
- [124] T. Schütz, R. Streblow, and D. Müller. A comparison of thermal energy storage models for building energy system optimization. *Energy and Buildings*, 93:23–31, 2015. [28](#)
- [125] S. Ikeda, W. Choi, and R. Ooka. Optimization method for multiple heat source including ground source heat pump considering dynamic variation in ground temperature. *Applied Energy*, 193:466–478, 2017. [28, 71, 72](#)
- [126] W. Yang, Bi. Yang, and R. Xu. Experimental study on the heat release operational characteristics of a soil coupled ground heat exchanger with assisted cooling tower. *Energies*, 11:1–17, 2018. [28, 62](#)
- [127] T. Sivasakthivel, K. Murugesan, and H. R. Thomas. Optimization of operating parameters of ground source heat pump system for space heating and cooling by taguchi method and utility concept. *Applied Energy*, 116:76–85, 2014. [28](#)
- [128] Inc. The MathWorks. MATLAB 8.0. Technical report, Natick, Massachusetts, United States, 2018. [28](#)

- [129] E. Almeshiae, A. Al-Habaibeh, and B. Shakmak. Rapid evaluation of micro-scale photovoltaic solar energy systems using empirical methods combined with deep learning neural networks to support systems' manufacturers. *Journal of Cleaner Production*, 2019. [28](#)
- [130] K. Neuhaus, I. Papas, B. Estibals, and C. Alonso. Comparison of electrical energy production using two solar irradiation models of BIPV. In *Proceedings of the 11th International Conference on Modeling and Simulation of Electric Machines, Converters and Systems*, Toulouse, France, 2017. IEEE. [28](#), [59](#)
- [131] A. W. Ling, V. K. Ramachandaramurthy, S. L. Walker, P. Taylor, and M. J. Sanjari. Optimal placement and sizing of battery energy storage system fro losses reduction using whale optimization algorithm. *Journal of Energy Storage*, 26, 2019. [29](#)
- [132] X. Wu, Ye. Liu, J. Du, Z. Song, and G. Wu. Sizing optimization of a wind-energy storage system considering battery life. *Renewable Energy*, 2019. [29](#)
- [133] F. Fodhil, A. Hamidat, and O. Nadjemi. Potential, optimization and sensitivity analysis of photovoltaic-diesel-battery hybrid energy system for rural electrification in algeria. *Energy*, 169:613–624, 2019. [29](#), [60](#)
- [134] M. Jennings, D. Fisk, and N. Shah. Modelling and optimization of retrofitting residential energy systems at the urban scale. *Energy*, 64:220–233, 2014. [29](#)
- [135] S. Fazlollahi, G. Becker, and F. Maréhal. Multi-objectives, multi-period optimization of district energy systems: II - Daily thermal storage. *Computers & Chemical Engineering*, 71:648–662, 2014. [29](#)
- [136] T. Schütz, R. Streblow, and D. Müller. A comparison of thermal energy storage models for building energy system optimization. *Energy and Buildings*, 93:23–31, 2015. [29](#), [65](#)
- [137] H. D. Sherali and A. Alameddine. A new reformulation-linearization technique for bilinear programming problems. *Journal of Global Optimization*, 2: 379–410, 1992. [31](#), [33](#), [48](#), [104](#)
- [138] J. McDonald. Reducing cooling tower operating cost, 2005. URL http://www.veoliawatertech.com/crownsolutions/ressources/documents/2/21849_Issue-16-Reducing-Cooling-Tower-Op.pdf. [39](#)
- [139] F. M. White. *Fluid Mechanics*. McGraw-Hill, New England, United Stated of America, 2009. [43](#), [46](#)
- [140] A. Marchi and A. Simpson. Evaluating the approximation of affinity laws and improving the estimate of the efficiency for variable speed pumping. *Journal of Water Resources Planning and Management*, 139:1314–1317, 2013. [45](#)
- [141] M. Nitsche and R. O. Gbadamosi. *Heat exchanger design guide*. Butterworth-Heinemannl, Oxford, 2016. [56](#), [62](#)

- [142] Z. Chiam, I. Papas, A. Easwaran, C. Alonso, and B. Estibals. Holistic optimization of the operation of a ground-coupled heat pump system: A case study on the ADREAM building in Toulouse, France. *Energy and Buildings*, 2019. [67](#), [68](#)
- [143] H. Yang, P. Cui, and Z. Fang. Vertical-borehole ground-coupled heat pumps: A review of models and systems. *Applied Energy*, 87:16 – 27, 2010. [68](#)
- [144] A. M. Omer. Ground-source heat pumps systems and applications. *Applied Energy*, 12:344 – 371, 2008. [68](#)
- [145] G. Tsilingiridis and K. Papakostas. Investigating the relationship between air and ground temperature variations in shallow depths in northern Greece. *Energy*, 73:1007 – 1016, 2014. [68](#)
- [146] D. Ürge Vorsatz, L. F. Cabeza, S. Serrano, C. Barreneche, and K. Petrichenko. Heating and cooling energy trends and drivers in buildings. *Renewable and Sustainable Energy Reviews*, 41:85 – 98, 2015. [68](#)
- [147] T. You, W. Wu, W. Shi, B. Wang, and X. Li. An overview of the problems and solutions of soil thermal imbalance of ground-coupled heat pumps in cold regions. *Applied Energy*, 177:515 – 536, 2016. [68](#), [71](#)
- [148] J. M. Corberan, D. P. Finn, C. M. Montagud, F. T. Murphy, and K. C. Edwards. A quasi-steady state mathematical model of an integrated ground source heat pump for building space control. *Energy & Buildings*, 43:82 – 92, 2011. [68](#), [71](#)
- [149] LAAS-CNRS. architectures dynamiques reconfigurables pour systèmes embarqués autonomes mobiles, 1999. URL <https://www.laas.fr/public/fr/intelligence-ambiante>. [69](#), [72](#)
- [150] J. R. Cullin, J. D. Spitler, C. Montagud, F. Ruiz-Calvo, S. J. Rees, S. S. Naicker, P. Konecny, and L. E. Southard. Validation of vertical ground heat exchanger design methodologies. *Science and Technology for the Built Environment*, 21:137 – 149, 2015. [71](#)
- [151] Z. Han, B. Li, S. Zhang, C. Bai, and H. Hu. Study on design error of ground source heat pump system and its influencing factors. *Applied Thermal Engineering*, 144:1030 – 1036, 2018. [71](#)
- [152] B. Hénault and M. Kummert P. Pasquier and. Financial optimization and design of hybrid ground-coupled heat pump systems. *Applied Thermal Engineering*, 93:72 – 82, 2016. [71](#)
- [153] I. Grossi, M. Dongellini, A. Piazzi, and G. L. Morini. Dynamic modelling and energy performance analysis of an innovative dual-source heat pump system. *Applied Thermal Engineering*, 142:745 – 759, 2018. [71](#)

- [154] T. Sivasakthivel, K. Murugesan, and P.K. Sahoo. Optimization of ground heat exchanger parameters of ground source heat pump system for space heating applications. *Energy*, 78:573 – 586, 2014. [71](#)
- [155] G. Nouri and H. Yousefi Y. Noorollahi and. Designing and optimization of solar assisted ground source heat pump system to supply heating, cooling and hot water demands. *Geothermics*, 82:212 – 231, 2019. [71](#)
- [156] L. Xia, Z. Ma, G. Kokogiannakis, Z. Wang, and S. Wang. A model-based design optimization strategy for ground source heat pump systems with integrated photovoltaic thermal collectors. *Applied Energy*, 214:178 – 190, 2018. [71](#)
- [157] M. A. Emadi and J. Mahmoudimehr. Modeling and thermo-economic optimization of a new multi-generation system with geothermal heat source and LNG heat sink. *Energy Conversion and Management*, 189:153 – 166, 2019.
- [158] Y. Song, M. Zou, X. Chen, J. Deng, and T. Du. Parameter optimization of passive heat supply tower of ground source heat pump based on NSGA-II. *Solar Energy*, 190:453 – 464, 2019. [71](#)
- [159] J. Deng, Q. Wei, M. Liang, S. He, and H. Zhang. Does heat pumps perform energy efficiently as we expected: Field tests and evaluations on various kinds of heat pump systems for space heating. *Energy & Buildings*, 182:172 – 186, 2019. [71](#)
- [160] Y. Kim, J. S. Lee, and S. W. Jeon. *Advances in ground-source heat pump systems*, chapter 12. Woodhead publishing, 2016. [71](#)
- [161] W. Gang, J. Wang, and S. Wang. Performance analysis of hybrid ground source heat pump systems based on ANN predictive control. *Applied Energy*, 136:1138 – 1144, 2014. [71](#)
- [162] R. Gagnon, L. Gosselin, and S. A. Deckerb. Performance of a sequential versus holistic building design approach using multi-objective optimization. *Journal of Building Engineering*, 26, 2019. unpublished. [71, 72](#)
- [163] I. Papas, B. Estibals, C. Ecrepont, and C. Alonso. Energy consumption optimization through dynamic simulations for an intelligent energy management of a BIPV building. In *Proceedings of the 7th International Conference on Renewable Energy Research and Applications*, Paris, France, 2018. IEEE. [72](#)
- [164] F. W. Yu and K. T. Chan. Optimum load sharing strategy for multiple-chiller systems serving air-conditioned buildings. *Building and Environment*, 42, 2007. [77](#)
- [165] Z. Chiam, A. Easwaran, D. Mouquet, S. Fazlollahi, and J. M. Villás. A hierarchical framework for holistic optimization of the operations of district cooling systems. *Applied Energy*, 239:23–40, 2019. [93, 94](#)

- [166] Colourcoil. Colourcoil Industries Sdn. Bhd., 2011. URL <http://www.colourcoil.com/enewsvol6issue5/enews.htm>. 94
- [167] J. Henley. World set to use more energy for cooling than heating. Technical report, The Guardian, 2015. 94
- [168] S. Cox. Cooling a warming planet: A global air conditioning surge. Technical report, environment360, 2012. 94
- [169] H. J. Uy. District cooling is ganining momentum in asia. Technical report, Climate control middle east, Singapore, 2018. 94
- [170] F. Gulf. Eco-Business, 2014. URL <http://www.eco-business.com/press-releases/understanding-and-unlocking-the-potential-of-district-cooling-in-asia/>. 94
- [171] M. Schwelder. Using low-load chillers to improve system efficiency. *ASHRAE Journal*, pages 14–20, 2017. 94
- [172] C. Yan, W. Gang, X. Niu, X. Peng, and S. Wang. Quantitative evaluation of the impact of building load characteristics on energy performance of district cooling systems. *Applied Energy*, 205:635–643, 2017. 94
- [173] B. Skagestad and P. Mildenstein. *District heating and cooling connection handbook*. International Energy Agency, 1999. 96
- [174] L. Wang, E. W. Lee, and R. K. Yuen. A practical approach to chiller plants' optimization. *Energy & Buildings*, 169:332–343, 2018. 97
- [175] K. Man, K. Tang, and S. Kwong. *Genetic Algorithms*. Springer, Kowloon, Hong Kong, 2001. 100
- [176] K. Jebari. Selection methods for genetic algorithms. *International Journal of Emerging Science*, 3:333–344, 2013. 103
- [177] E. Cantù-Paz. A survey of parallel genetic algorithms. Technical report, University of Illinois at Urbana-Champaign, Illinois, 1995. 104
- [178] K. Deb, A. Pratap, S. Agarwal, and T. Meyarivan. A fast and elitist multiobjective genetic algorithm: NSGA-II. *IEEE transactions on evolutionary computing*, 6:182–197, 2002. 108
- [179] L. Majic, I. Krzelj, and Delimar M. Optimal scheduling of a CHP system with energy storage. In *Proceedings of the 36th International convention on information & communication technology electronics & microelectronics (MIPRO)*. IEEE, 2018. 131
- [180] A. Christidis, C. Koch, L. Pottel, and G. Tsatsaronis. The contribution of heat storage to profitable operation of combined heat and power plants in liberalized electricity markets. *Energy*, 41:75–82, 2012.

- [181] D. Buoro, P. Pinamonti, and M. Reini. Optimization of a distributed co-generation system with solar district heating. *Applied Energy*, 124:298–308, 2014. [131](#)
- [182] H. Ren, W. Gao, and Y. Ren. Optimal sizing for residential CHP system. *Applied Thermal Engineering*, 28:514–523, 2008. [132](#)
- [183] G. Taljan, G. Verbič, M. Pantoš, M. Sakulin, and L. Fickert. Optimal sizing of biomass-fired Organic Rankine Cycle CHP system with heat storage. *Renewable Energy*, 41:29–38, 2012. [132](#)
- [184] M. Noussan, G. C. Abdian, A. Poggio, and R. Roberto. Biomass-fired CHP and heat storage system simulations in existing district heating systems. *Applied Thermal Engineering*, 71:729–735, 2014. [132](#)
- [185] T. Fang and R. Lahdelma. Optimization of combined heat and power production with heat storage based on sliding window method. *Applied Energy*, 162:723–732, 2016. [132](#)
- [186] Z. Chiam, A. Easwaran, D. Mouquet, and M. Gupta. Holistic, real-time optimization of the operations of district cooling systems via deep reinforcement learning and mixed integer linear program. In *Proceedings of the 11th International Conference on Applied Energy*, Västerås, Sweden, 2019. Applied Energy. [145](#), [146](#)
- [187] V. Mnih, K. Kavukcuoglu, D. Silver, A. A. Rusu, J. Veness, M. G. Bellemare, A. Graves, M. Riedmiller, A. K. Fidjeland, G. Ostrovski, S. Petersen, C. Beattie, A. Sadik, I. Antonoglou, H. King, D. Kumaran, D. Wierstra, S. Legg, and D. Hassabis. Human-level control through deep reinforcement learning. *Nature*, 518:529–533, 2015. [147](#)
- [188] D. Silver, A. Huang, C. J. Maddison, A. Guez, L. Sifre, G. van den Driessche, J. Schrittwieser, I. Antonoglou, V. Panneershelvam, M. Lanctot, S. Dieleman, D. Grewe, J. Nham, N. Kalchbrenner, I. Sutskever, T. Lillicrap, M. Leach, K. Kavukcuoglu, T. Graepel, and D. Hassabis. Mastering the game of Go with deep neural networks and tree search. *Nature*, 529:484–489, 2016. [147](#)
- [189] T. P. Lillicrap, J. J. Hunt, A. Pritzel, N. Heess, T. Erez, Y. Tassa, D. Silver, and D. Wierstra. Continuous control with deep reinforcement learning. In *Proceedings of the International Conference on Learning Representations*, San Juan, Puerto Rico, United States of America, 2016. [147](#)
- [190] Y. LeCun, Y. Bengio, and G. Hinton. Deep Learning. *Nature*, 521:436–441, 2015. [147](#), [152](#)
- [191] D. Silver, G. Lever, N. Heess, T. Degris, D. Wierstra, and M. Riedmiller. Deterministic policy gradient algorithms. In *Proceedings of the International Conference on Machine Learning*, Beijing, China, 2016. [147](#)

- [192] R. Jia, M. Jin, K. Sun, T. Hong, and C. Spanos. Advanced building control via deep reinforcement learning. In *Proceedings of the 10th International Conference on Applied Energy*, Hong Kong, China, 2018. Energy Procedia. [147](#)
- [193] J. R. Vázquez-Canteli and Z. Nagy. Reinforcement learning for demand response: A review of algorithms and modeling techniques. *Applied Energy*, 235:1072–1089, 2019. [147](#), [148](#)
- [194] R. Bellman. A Markovian decision process. *Journal of Mathematics and Mechanics*, 6:679–684, 1957. [151](#)
- [195] A. Baños. On pseudo-games. *The Annals of Mathematical Statistics*, 39: 1932–1945, 1968. [151](#)
- [196] R. van Emden and M. Kaptein. contextual: Evaluating Contextual Multi-Armed Bandit Problems in R. *arXiv.org*, 2018. [152](#)
- [197] R. S. Sutton, D. McAllester, S. Singh, and Y. Mansour. Policy gradient methods for reinforcement learning with function approximation. *Advances in Neural Information Processing Systems*, 12:1057–1063, 2000. [152](#)
- [198] V. R. Konda and J. N. Tsitsiklis. Actor-critic algorithms. *Advances in Neural Information Processing Systems*, 12:1008–1014, 2000. [153](#)
- [199] D. P. Kingma and J. L. Ba. Adam: A method for stochastic optimization. *arXiv.org*, 2017. [153](#)
- [200] K. He, X. Zhang, S. Ren, and J. Sun. Delving deep into rectifiers: Surpassing human-level performance on ImageNet classification. *arXiv.org*, pages 1–11, 2015. [154](#)
- [201] L. Laakkonen, T. Korpela, J. Kaivosoja, M. Vilkko, Y. Majanne, and M. Nurmoranta. Predictive supply temperature optimization of district heating networks using delay distributions. In *Proceedings of the 11th International Conference on District Heating and Cooling*, Seoul, South Korea, 2017. Energy Procedia. [163](#)
- [202] A. Vandermeulen, B. Vander Heije, and L. Helsen. Controlling district heating and cooling networks to unlock flexibility: A review. *Energy*, 151:103–115, 2018. [163](#)
- [203] R. Ramanan, M. Yildirim, E. Chow, and N. Gebraeel. Asynchronous decentralized framework for unit commitment in power systems. In *Proceedings of the International Conference on Computer Science*, Zurich, Switzerland, 2017. Procedia Computer Science. [163](#)
- [204] Y. Wang, S. Wang, and L. Wu. Distributed optimization approaches for emerging power systems operation : A review. *Electric Power Systems Research*, 144:127–135, 2017. [163](#)

- [205] A. Zakaria, F. B. Ismail, M. S. H. Lipu, and M. A. Hannan. Uncertainty models for stochastic optimization in renewable energy applications. *Renewable Energy*, 145:1543–1571, 2020. [164](#)
- [206] J. J. Nonnenmann. Chilled water plant pumping schemes. Technical report, Stanley Consultants, Inc., Iowa, United States of America, 2011. [165](#)
- [207] M. Zakeer. Low delta-t syndrome in constant primary and variable secondary water system (linkedin article), 2015. URL <https://www.linkedin.com/pulse/low-delta-syndrome-constant-primary-variable-secondary-zakeer.167>